Dextran Based Polymers Derived Surfaces: Characterization by Attenuated Total Reflection Infrared (ATR-IR) Spectroscopy and Investigation of Protein-Carbohydrate Interactions

Thèse présentée à la Faculté de Science
Institut de Microtechnique
Université de Neuchâtel

Par

Silvia Angeloni Suter

Acceptée sur proposition du Jury:

Prof. Thomas Bürgi[1], directeur de thèse
Prof. Thomas Ward[1], rapporteur
Dr. Hans Sigrist[2], rapporteur
Dr. Guy Voirin[3], rapporteur

Soutenue le 26.10.2007

Université de Neuchâtel
2007

[1] *Université de Neuchâtel, Suisse*
[2] *arrayon biotechnology, Neuchâtel, Suisse*
[3] *Centre Suisse d'Electronique et de Microtechnique, CSEM, Neuchâtel, Suisse*

Blessed be metrical rules that forbid automatic responses, force us to have second thought, free from the fetters of Self.

W.H. AUDEN, *Shorts*

A Francesca. Lei sa.

Université de Neuchâtel

FACULTE DES SCIENCES
Secrétariat-Décanat de la faculté
- Rue Emile-Argand 11
- CP 158
- CH-2009 Neuchâtel

IMPRIMATUR POUR LA THESE

Dextran based polymers derived surfaces: characterization by attenuated total reflection infrared (ATR-IR) spectroscopy and investigation of protein-carbohydrate interactions

Silvia ANGELONI SUTER

UNIVERSITE DE NEUCHATEL

FACULTE DES SCIENCES

La Faculté des sciences de l'Université de Neuchâtel,
sur le rapport des membres du jury

MM. T. Bürgi (directeur de thèse),
T. Ward, H. Sigrist (Arrayon Biotechnology, Neuchâtel)
et G. Voirin (CSEM, Neuchâtel)

autorise l'impression de la présente thèse.

Neuchâtel, le 29 avril 2008

Le doyen :
F. Kessler

UNIVERSITE DE NEUCHATEL
FACULTE DES SCIENCES
Secrétariat - décanat de la faculté
Rue Emile-Argand 11 - CP 158
CH-2009 Neuchâtel
Félix Kessler

Table of Contents

Table of Contents I

Abstract VII

Chapter 1 .....

Introduction 1

1.1. Bioengineering using dextran based polymers 1

1.1.1. Surface glycoengineering 3

1.2. Infrared (IR) spectroscopic investigation of the behavior of dextran based polymers at interfaces 4

1.3. Attenuated Total Reflection Infrared Spectroscopy 5

1.3.1. Theory 6

1.3.1.1. Reflectivity for external and internal reflection 8

1.3.1.2. Penetration depth and effective thickness 12

1.3.2. ATR spectroscopy of thin film 16

1.3.3. Improvement of the ATR spectroscopy technique 16

1.3.3.1. Single-Beam-Sample-Reference technique 18

1.3.4. Note on the use of germanium as internal reflection element 19

1.4. Scope of the thesis 20

1.5. References 21

Chapter 2 .....

Attenuated Total Reflection (ATR) Infrared spectroscopy for dextran based polymer characterization 31

2.1. Physisorption of dextran based polymers at interfaces 31

2.1.1. Experimental section 34

2.1.1.1. Chemicals 34

2.1.1.2. Germanium plate modification 35

2.1.1.3. ATR measurements 37

2.2. Results and discussion 38

2.2.1. Dextran physisorption 38
2.2.1.1. Effect of plasma pre-treatment 41
2.2.1.2. Effect of ionic strength effect 43
2.2.1.3. Effect of concentration 45
2.2.1.4. Competitive antibody-dextran adsorption onto the surface 45
2.2.2. Amino Detran physisorption 47
2.2.2.1. Kinetics of the adsorption process 53
2.2.3. Carboxymethyl dextran physisorption 56
2.2.3.1. Kinetics of the adsorption process 58
2.2.4. OptoDex ® dextran based polymers physisorption. 59
2.2.4.1. OptoDex ® C physisorption 59
2.2.4.2. OptoDex ® B physisorption 59
2.2.4.3. OptoDex ® A physisorption 62
2.2.5. Dextran based polymers covalent immobilization by photobonding 65
2.2.5.1. ATR spectra and discussion 67
2.2.6. Orientation measurements 73
2.2.6.1. Orientation analysis 78
2.2.7. Determination of volume concentration and surface concentration 81
2.3. Charge driven Physisorbtion 87
2.4. Determination of polymer film thickness *at* interface 90
2.5. OptoDex® family's photobonding effectiveness 92
2.6. References 95
Chapter 3 .....
Gold nanoparticles immobilization on surface 103
3.1. Monolayer protected metal nanoparticles 103
3.2. Surface decoration using nanoparticles immobilization 104
3.2.1. Experimental section 106

3.2.1.1. Chemicals....106
3.2.1.2. Germanium plate modification....107
3.2.1.3. Gold nanoparticle immobilization technique....109
3.3. Results and discussion....112
3.3.1. MPNs immobilization via OptoDex A thick film (*layer coating*)....112
3.3.2. MPNs immobilization via OptoDex® A thick film (co-coating)....118
3.3.3. MPNs immobilization *via* OptoDex® A thin film....119
3.3.4. Comparison of the described methods for MPNs immobilization....122
3.4. Exploration of monolayer protected gold nanoparticles behaviour versus aminodextran modified surface....125
3.4.1. Experimental section....125
3.4.1.1. Germanium plate modification....125
3.4.1.2. Surface exposure to MPN solution....126
3.4.2. ATR measurements....126
3.5. Results and discussion....127
3.5.1. Transmission Electron Microscopy....129
3.6. Conclusion and outlook....133
3.7. References....135
Chapter 4....
Dextran-based thin film coated platforms for for glycoprofiling in microarray format....139
4.1. Preface....139
4.2. Abstract....141
4.3. Introduction....141
4.4. Results....144
4.4.1. Exopolysaccharide microarray.....144
4.4.2. Glycoprotein microarray characteristics....147
4.4.3. Application: Glycan profiling of model cell extracts....152

4.4.4. Bacterial challenge..... 154
4.4.5. Lectin microarray. 156
4.5. Discussion 157
4.6. Materials and methods..... 160
4.6.1. Biomolecule preparation. 160
4.6.2. Biomolecule immobilization..... 162
4.6.3. Array probing. 163
4.6.4. Cell culture and bacterial challenge. 164
4.7. Acknowledgements..... 164
4.8. References 165
Chapter 5.....
Conclusions and Outlook..... 169
5.1. References 171
Aknowledgemets 173
Curriculum Vitae 175
List of Publications..... 177

Keywords : Attenuated Total Reflection Spectroscopy (ATR)/ dextran/ phisisorption/ photobonding/ Mono Protected Nanoparticles (MPNs)/ glycoarray/ glycomics/ exopolysaccharides/ glycosylation/ lectins

Abstract

Sensitive surfaces imply responsive elements lodged onto a carrier which eventually allows for reaction, recognition and detention. Interfaces require fine tuning for response performance optimization. Observation needs to be focused on the two media common boundary. Currently, dextran based polymers are still a major class of tunable materials for surface modifications. To simply and simultaneously work as biocompatible spacer, antifouling agent, passivation means, and flexible surface chemistry tailor, they require covalent binding to the support. Besides the well defined chemical methods, photochemical procedures provide straightforward and non invasive protocols to generate reactive intermediates. The latter quickly and indistinctively interact with both the surface and the target, establishing definitive ties. Among photochemical methods, photobonding technology (*arrayon Biotechnology*, Switzerland) still remains an outstanding procedure for sample immobilization on inert material surfaces by light-induced processes. Actinic dextrans (like OptoDex ®) are used as photolinker polymers. The generated intermediate is a carbene, a highly reactive organic molecule with a divalent carbon atom which basically interposes itself into an existing bond. The insertion generally does not affect the 3D structure holding the "docking" point. OptoDex ® functionalized platforms are a specific product issue of this technology, intended for bioarray applications. They are plain glass platforms that become appropriate for biomolecule patterning (micropipetting, nanodispensing) after OptoDex ® conditioning. The technology proved successful for a large protein portfolio immobilization and motivated the progress of investigation in

two directions. First, a deeper characterization of the photolinker behavior at interface was judged worthy of a physico-chemical characterization. One should note that the chemical functionalities were already well-established by the supplier quality control procedures (*arrayon Biotechnology* proprietary). A spectroscopic method (molecular-level, label free) could uphold routine analytical methods and functional screening using indirect detection (like fluorescence labeling). Second, the search for a new cutting-edge application which might also fulfill a new market spot, led to the extension of such technology to the domain of glycomics (carbohydrates decorated biomolecules interaction screening and monitoring *via* middle-high density throughput layout).

Attenuated Total Reflection Infrared (ATR-IR) spectroscopy is a powerful method to investigate liquid-solid interfaces. Simplifying, it can be considered an adaptation of the classical IR spectroscopy in transmission (appropriate for solutions) to investigate reactions at the solid-liquid interfaces. The molecular fingerprint is retained, the sensitivity is higher, and quantification is accessible. The characteristics of this surface-sensitive spectroscopy are useful for examining the interface properties of dextran based photolinker polymers. These characteristics are: a penetration depth of evanescent wavelength beam up to 1 μm, and the chemical detectable entities of interest C-H bonds and –OH groups. The effects of the photoreaction at the interface and the physico-chemical characteristics of the adlayer have been explored and defined on a molecular basis (orientation, kinetic evaluations, film thickness determination). Particular attention was paid to physisorbtion of dextran polymers structurally similar to OptoDex ®. Results differ if chemical immobilization is performed allowing previous spontaneous physisorption. This study defined the role of the physisorption intermediate step and elucidated the role of charge as well. To

further explore the potential of the photoinduced immobilization, 2 nm monodispersed gold nanoparticles were nestled onto the dextran adlayer and covalently grafted to the surface by OptoDex ®. ATR-IR equipment proved a powerful tool to detect organic shell capping gold cores down to a small scale.

The application of the photobonding technology in the field of glycomics resulted in the design and optimization of carbohydrate micro arrays. OptoDex ® A mediated immobilization of low and high molecular weight sugar moieties (glycoproteins and exopolisaccharides, respectively) was achieved while evidencing retained bioactivity by fluorescence labeled probes (lectins, namely specific sugar tether binding proteins). Flexibility of the method was demonstrated permuting the probe/target pair: lectins were microprinted in array format, immobilized onto the surface, and probed by fluorescent labeled sugar moieties (glycoproteins). Such a portfolio of detectable interactions and binding tests in miniaturized format allowed monitoring of the glycoexpression related to the evolution of two different cell lines. Carbohydrate microarrays were manufactured and the relative protocols for glycoprofiling established.

Chapter 1

Introduction

1.1. Bioengineering using dextran based polymers

The hunt for novel biofunctional materials for miniaturized biosensors, bioelectronic devices, and medical equipment boosted bioengineering[1]. One of the major issues for sensing format performance is the tuning of interface's chemical and physical properties. This relates to the flexibility and stability of the interface, while keeping or even enhancing transducer sensitivity. The boundary layers may host recognition elements, which interact selectively with analytes and therefore are often designed to satisfy multiple tasks. In this context, the possibility of tailoring the interface properties using versatile polymers becomes attractive. In surface modification for heterogeneous bioassay, the covalent immobilization of biomolecules while retaining specificity and biological function is a major challenge. In the last decades, the working and cognitive method drifted from an analytical approach to large spectrum screening. This favored the optimization of microarray manufacturing which fulfilled the requirement of increasing information throughput[2-12]. Initially the motivation was speeding up (serial analysis done in parallel), economizing (reactants and supplies), and simplifying the complexity of the operations. This allowed a broader user base to execute the handling protocol. Later the motivation moved towards the awareness that, what was little understood using standard methods, could be specifically made clearer by the microarray approach[13, 14]. Furthermore, this method is implicitly scalable to industrial methods[15, 16]. The demand for interfaces

appropriate for biochemical interaction excited scientists to explore polysaccharides for surface modification[17, 18].

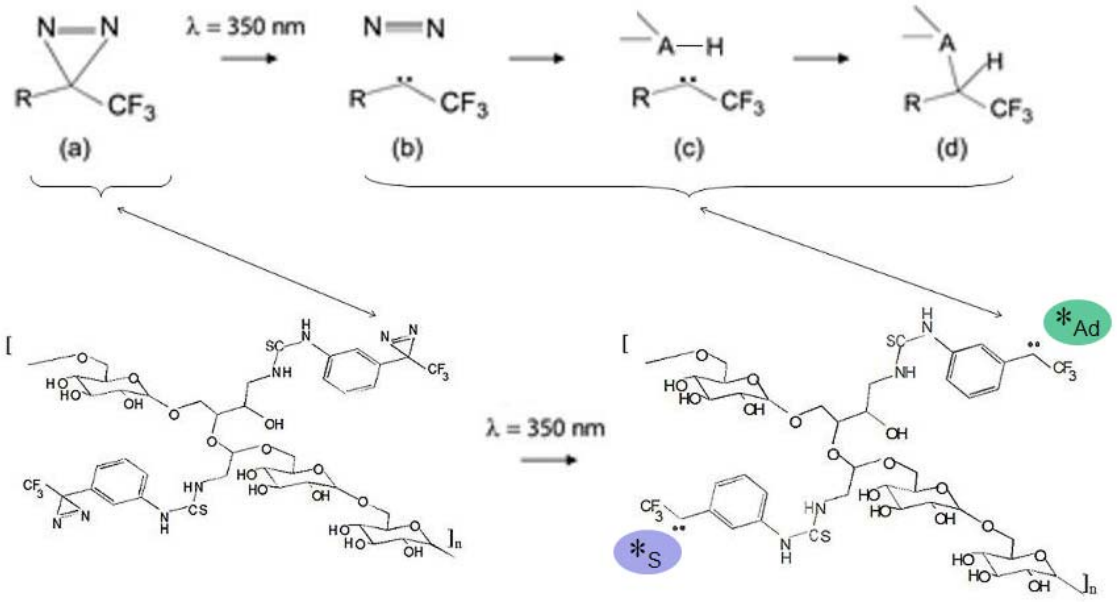

Figure 1-1. Schematic representation of the aryl(trifluromethyl)diazirine (a) photolysis leading to molecular nitrogen release and carbens generation (b). These highly reactive entities inset into almost any existing adjacent chemical bonds (c) establishing covalent links (d) to the surface ($*_S$, lower part) and the adsorbed molecule ($*_{Ad}$, lower part). The dextran backbone is derived by thiocarbomoylation of aminodextran with 3-(trifluoromethyl)-3-(m-isothiocyanophenyl) diazirine (lower part).

Among the plethora of techniques, both chemical[19-29] and photochemical[30-40], photobonding technology[41-43], represents a unique surface engineering method. This method, which is proprietary of arrayon biotechnology (Switzerland, www.arrayon.com), uses actinic dextran based polymers for covalent surface modification and simultaneous covalent (bio)molecules binding[44]. In combination with miniaturized local dispensing, this technique matches with the design of high-density arrays on conventional material surfaces, economic use of reactants, and straightforward customization of device platforms. Surface deposited saccharides (OptoDex®) are modified surfaces containing light sensitive aryldiazirine form

hydrogel-like thin films upon light exposure. The extent of biomolecule immobilization depends on the irradiance and the duration of exposure. The photosensitive dextrans assist in preventing biomolecule denaturation. Moreover, nonspecific binding is suppressed, thereby enhancing the sensing performance[43, 45, 46]. OptoDex® mediated co-immobilization of antibodies on polystyrene or optical waveguide yields a surface density of 1.9 and 4.3 ng antibody per mm^2, respectively. Photobonded enzymes remain catalytically active. The technology fulfills fundamental requirements for the investigation of biological systems. It is applicable in genomics, proteomics, functional proteomics, metabolomics, and cellomics. Figure 1-1 shows the principles of photobonding.

1.1.1. Surface glycoengineering

When the carbohydrate tethers are the bio-sites to be probed, one deals with glycoengineering at the service of glycobiology[47]. The active sites contain sugar featuring molecules such as glycans (simple or complex, low or high molecular weight) which can be attached to proteins or lipids such as glycoproteins or glycoplipids[48]. The attention recently paid to surface glycoengineering stems from the importance of the carbohydrate-protein interactions. Oligosaccharides at cell surfaces regulate bio-recognition, immune response, inflammation, and infection[49]. Carbohydrates guided functionality was recently demonstrated in sequencing the oligosaccharides chain constituting the major blood group antigens[50], in elucidating the anticoagulant activity of heparin (a glucosaminoglycan)[51], and in isolating the sialic acid as binding site for influenza virus[51]. Carbohydrates are known to play a critical role in the regulation of interactions between cells and with artificial surfaces. The carbohydrates abundance and availability is counterbalanced by their complexity which hinders the creation of a unique platform for receptors screening. Immobilization methods either via thin film adsorption or covalent attachment are

complementary. Furthermore, synthetic carbohydrate-based polymers proved a smart solution in the design of biocompatible and renewable materials for water absorbents, chromatographic supports, medical devices, and tissue engineering[52, 53]. Oligosaccharide derivatives of photosensitive diazirine have been utilized for direct covalent attachment of carbohydrates to substrates[54-58]. In this work we explore the application of a photoactiveable dextran-coated analytical platform for one-step irreversible immobilization of a series of bacterial exopolysaccharides, glycans, glycoconjugated, and lectins in microarray formats. Specific detection of oligosaccharides on either glyconjugate or lectin arrays, pertains to receptor binding screening and glycan profiling[59].

1.2. Infrared (IR) spectroscopic investigation of the behavior of dextran based polymers at interfaces

This study aimed to set up a proper apparatus to observe and eventually control the dextran based coating of material surface. Ascertaining whether the intensity of physical adsorption and/or chemical graft would influence the morphology of the adlayer was a major goal. In this perspective, infrared based spectroscopy was chosen to investigate the interaction between surface and dextran-based polymers. Biocompatibility is biased by the spatial organization at the biomaterial interface[60]. The vibrational (IR) spectrum of a molecule or polymer adsorbed on a surface contains detailed information about surface-molecule interaction and intermolecular interaction within the adsorbate itself. Furthermore the technique allows one to obtain information about the orientation of molecules or functional groups[61]. Quantitative analysis of infrared spectra yields surface concentration[62]. The method is fast, which allows one to study the kinetics of adsorption *in situ*. The resulting comprehensive information identifies and defines the adsorbate layer. Thereby, vibrational

spectroscopy, and most prominently Attenuated Total Reflection Infrared (ATR-IR) spectroscopy, revealed to be a powerful tool to get understanding into the behavior of polymers at interfaces.

1.3. Attenuated Total Reflection Infrared Spectroscopy

In the early seventeenth century, Newton already reports of the glass' power of attracting light rays and recalling them just when striking the crossing edge with the vacuum in such a way to bring them entirely back. "Resistance of the Absolute Vacuum" was an unsatisfactory explication. He was aware that, tuning the incident light angle, allowing the glass to enter in contact with optically thinner media (i.e. of lower refractive index and transparent), rays were reflected after striking the interface and going outward slightly beyond the media boundary. The first description of *total internal reflection* was given: a wave propagates in an optical thicker medium and generates an *evanescent* field in the adjacent optical thinner medium, getting totally reflected. Although, total internal reflection became a well defined phenomenon, only in the early twenties Taylor and co-workers used these principles for spectroscopic purposes[63-65]. Three decades later, Fahrenfort developed internal reflection spectroscopy for measuring spectra of bulk material, utilizing a single reflection[66]. Concurrently Harrick proposed and developed internal reflection spectroscopy techniques utilizing multiple reflections, for studying surfaces and thin films[67]. When the reflecting surface is placed in contact with an adsorbing medium, the energy is partially absorbed and then the light beam is attenuated. The name Attenuated Total Reflection refers to this mechanism[67]. Among other findings, Harrick pointed out that the attenuation is greater for parallel polarization than for perpendicular polarization and that the evanescent field might be used to record spectra of adsorbed molecules and for *at* or *near* surface investigation of the rarer medium. The studies of Harrick

and Fahrenfort present the theoretical support for the widely spread utilization of ATR-IR spectroscopy today[68].

1.3.1. Theory

Infrared spectroscopy is usually performed in transmission mode (TM). This means that the IR beam passes through the sample and the transmitted IR intensity is measured according to the Lambert-Beer's law (Eq. **1-1**).

$$I = I_0 \, e^{-kcl} \qquad \textbf{1-1}$$

I_0 stands for the incoming light intensity, k for the molar absorption coefficient of the analyte, c for the concentration of the analyte, and l for the thickness of the sample. If applied to biological systems, due to the high absorptivity of water, IR samples must be very thin, usually displaying an optical path of only few micrometers. At the same time, low water content is a critical condition with respect to biological requirements. An alternative to transmission mode is offered by the Attenuated Total Reflection (ATR) technique. As mentioned above, in this technique, the IR beam propagates in an infrared transparent crystal (IRE, internal reflection element) by total internal reflection. At the position where the IR beam is internally reflected, an electromagnetic field penetrates into the optically thinner medium. This field is called evanescent and the penetration depth is a function of the wavelength of the light, typically from some hundreds nanometers to 1 micron. Although no energy flux can be measured in the range of the evanescent field, its nature of electric field remains. Molecules within this evanescent field can absorb IR light, which leads to an attenuation of the field. These effects form the basis for the spectroscopic investigation of phenomena taking place *at* or *close* to the interface, reducing the influence/interference of the bulk (typically the water absorbtion). In order to describe more quantitatively these effects, it is suitable to have a closer look at the

phenomenon of total internal reflection and later introduce the concepts of penetration depth and effective thickness, which relate ATR spectroscopy to the more familiar transmission spectroscopy.

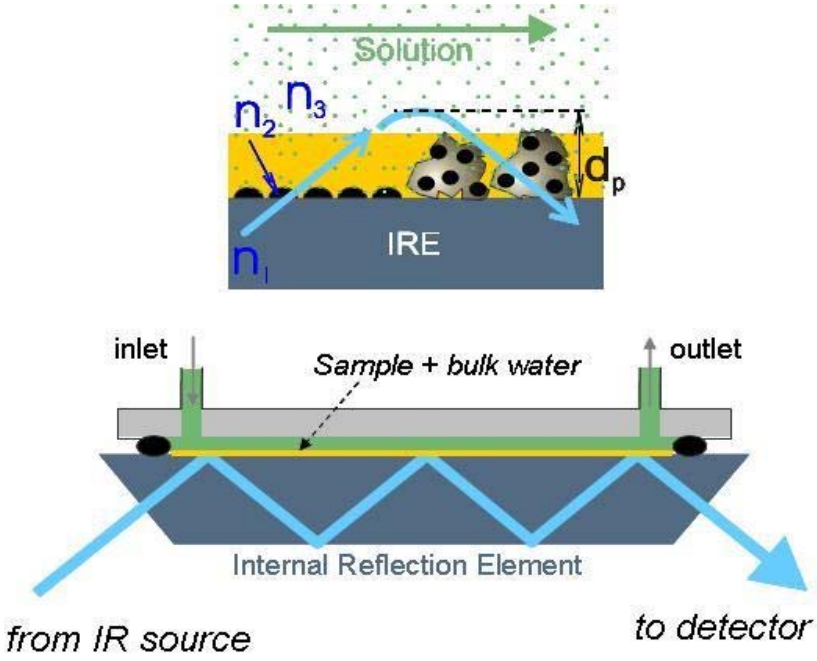

Figure 1-2. Schematic representation of an ATR-IR setup for *in situ* measurements. Infrared light beam enters perpendicularly the denser optical medium through the oblique edge of the trapezoidal Internal Reflection Element (IRE). Incident light crosses firstly the optically denser medium (refractive index $n_1 > n_2, n_3$) and in the same, it propagates by multiple reflections. In the upper part of the figure, a blow-up of the interface is presented. When analytes interact with the surface, they eventually attenuate the intensity of the beam that penetrates slightly in the rarer medium. d_p indicates the penetration depth (typically 1 μm).

1.3.1.1. Reflectivity for external and internal reflection

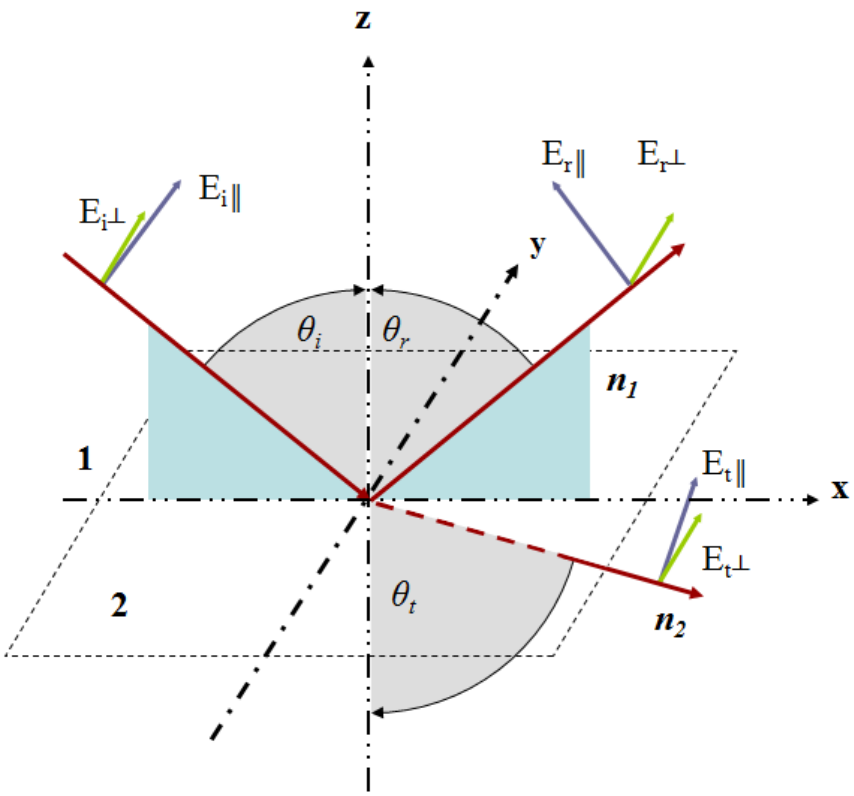

Figure 1-3. Specular reflection and transmission. The angles of incident (i), reflected (r) and transmitted (t) beam are denoted by θ_i, θ_r, θ_t, respectively. The corresponding electric field components are denoted by E. They are split into orthogonal portions, one parallel to the plane of incidence (x, z plane) and the other perpendicular to this plane (parallel to y-axis). Accordingly, electric fields are referred to as parallel ($\parallel$) and perpendicular ($\perp$) polarized; n_1, n_2 denote the refractive indices in the two media**.**

By considering the boundary conditions for the electric and magnetic field at the interface between two transparent media with different refractive index, Fresnel calculated the fraction of a plane wave that is reflected and transmitted. The incident plane wave consists of parallel and perpendicular polarized electric field components $E_{i\parallel}$ and $E_{i\perp}$, respectively (Figure 1-3). The plane of incidence is defined by the incident ray's direction and the normal to the interface. The polarization is called parallel when the electric field vector lies in the plane of incidence. In the other case, the polarization is called perpendicular. Fresnel's equations give the parallel ($r_\parallel$) and

perpendicular component ($r_\perp$) of the ratio of the reflected and transmitted electric field amplitude to the initial electric field amplitude. The equations apply for an electromagnetic radiation incident on a dielectric. This ratio is a function of the angle of incidence (θ_i) and transmission (θ_t), and of the indices of refraction of the two media. The corresponding components of the reflected and refracted (transmitted) electric field are denoted by $E_{r\parallel}$ and $E_{r\perp}$, and $E_{t\parallel}$ and $E_{t\perp}$. Equations **1-2** and **1-3** relate to the parallel ($r_\parallel$) and perpendicular ($r_\perp$) components of the reflected amplitude. Analogously the components for transmitted ratio can be obtained by inserting the corresponding electric field components, $E_{t\parallel}$ and $E_{t\perp}$.

$$r_\parallel = \frac{E_{r\parallel}}{E_{i\parallel}} = \frac{n_1 \cos\theta_t - n_2 \cos\theta_i}{n_2 \cos\theta_i + n_1 \cos\theta_t} \qquad \textbf{1-2}$$

$$r_\perp = \frac{E_{r\perp}}{E_{i\perp}} = \frac{n_1 \cos\theta_i - n_2 \cos\theta_t}{n_1 \cos\theta_i + n_2 \cos\theta_t} \qquad \textbf{1-3}$$

Snell's law (Eq. **1-4**) put in relation the indices of refraction of two media to the direction of propagation of the incident and transmitted beams according to the following formula:

$$n_1 \sin\theta_i = n_2 \sin\theta_t \qquad \textbf{1-4}$$

For internal reflection, the incident medium is the denser one and the angle with the normal is increased by refraction. The denser medium is commonly called the "internal" medium. Air with $n = 1$ is usually the surrounding or "external" medium. Optimal conditions are set placing the sample material in contact with an optically transparent material of higher refractive index whereby light approaches the interface at an angle of incidence greater than the critical angle. Therefore the conditions for total internal reflection can be derived by setting the refracted angle $\theta_t = 90°$ and

calculating the incident angle θ_i. When θ_t reaches *90°*, total internal reflection occurs and θ_i is at the critical angle θ_c as follows from Snell's law:

$$\sin\theta_c = \frac{n_2}{n_1} = n_{21} \qquad \textbf{1-5}$$

Above the critical angle according to Snell's law

$$\sin\theta_t = \frac{\sin\theta_i}{\sin\theta_c} > 1 \qquad \textbf{1-6}$$

and consequently, the corresponding cosine is complex:

$$\cos\theta_t = \pm i\, n_{12}\sqrt{\sin^2\theta_i - n_{21}^2} \qquad \textbf{1-7}$$

Introducing these criteria in Fresnel's equations (Eq. **1-2** and **1-3**), the relation between incident and reflected electric field components is described by:

$$r_{\parallel} = \frac{E_{r\parallel}}{E_{i\parallel}} = \frac{n_{21}^2\cos\theta_i - i\sqrt{\sin^2\theta_i - n_{21}^2}}{n_{21}^2\cos\theta_i + i\sqrt{\sin^2\theta_i - n_{21}^2}} \qquad \textbf{1-8}$$

$$r_{\perp} = \frac{E_{r\perp}}{E_{i\perp}} = \frac{\cos\theta_i - i\sqrt{\sin^2\theta_i - n_{21}^2}}{\cos\theta_i + i\sqrt{\sin^2\theta_i - n_{21}^2}} \qquad \textbf{1-9}$$

It is evident that:

$$\left| r_{\parallel} \right| = \left| r_{\perp} \right| = 1 \qquad \textbf{1-10}$$

indicating that the reflection is total when n_{21} is real. The interpretation, due to Fresnel, of the imaginary angle in Eq. **1-7**, is that no energy is transmitted into the

rarer medium and all of the power is reflected. The percentage of reflected power, i.e. reflectivity, is the measurable physical property and is given by the square of the Fresnel's amplitudes $R = r^2$ for parallel ($R_{\parallel}$) and perpendicular ($R_{\perp}$) component. This holds for both internal and external reflection. In the former (latter) case the light is introduced through the optically denser (rarer) medium. Some qualitative considerations follow from examination of Figure 1-4.

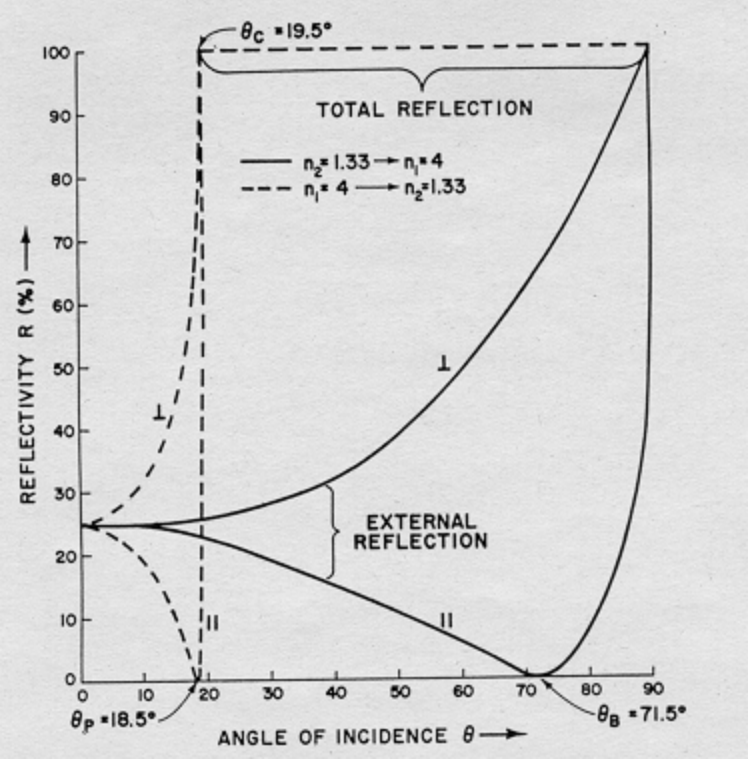

Figure 1-4. Reflectivity versus angle of incidence for an interface between Germanium ($n_1 = 4$) and water ($n_2 = 1.33$) for perpendicular polarized light, $R_{\perp}$, and parallel polarized light, $R_{\parallel}$, for external (solid line) and internal reflection (dashed line). θ_c is the critical angle, θ_B is the Brewster's angle an θ_p is the principal angle defined as $\theta_p = \arctan^{-1} n_{21}$ (internal polarizing angle) and complementary to θ_B. The Brewster's angle is the angle at which the light propagating from the rarer medium (external polarizing angle) with parallel polarization does not reflect while the intensity of the perpendicularly polarized light is not zero. The graphic is a reproduction of Fig.2-2 in Internal Reflection Spectroscopy by N.J. Harrick, 1967[69].

At normal incidence, R is identical for both polarizations and has the same value for internal or external reflection. Therefore the reflectivity has the same value whether light strikes the interface from rarer or denser medium and this value is:

$$R = \frac{(n_{12} - 1)^2}{(n_{12} + 1)^2} \qquad \textbf{1-11}$$

For external reflection, when looked at the perpendicular polarization, reflectivity ($R_\perp$) rises monotonically until 100% at grazing angle. For parallel polarization, reflectivity ($R_\parallel$) decreases at first as the angle of incidence increases, and becomes zero at the Brewster angle (θ_B). For angles greater than θ_B, $R_\parallel$ rises sharply and becomes 100% at grazing incidence. For internal reflection, the reflectivity curves have similar behavior as for external reflection, but the swept incidence angle range is much smaller. At the critical angle, both $R_\perp$ and $R_\parallel$ reach 100%. $R_\parallel$ increases very abruptly from the principal angle (θ_p) to the critical angle (θ_c). These drastic increments result advantageous for index of refraction measurements, for angle sensing, light modulation and deflection. Figure 1-4 shows the high efficiency of internal compared to external reflection. At a glance, it exhibits that, above the critical angle, total internal reflection is achieved for a wide (non critical) range of incident angles. If the rarer medium is absorbing, the complex refractive index has to be inserted in the Fresnel's equations and in this case one has *attenuated* total reflection.

1.3.1.2. Penetration depth and effective thickness

The electric field amplitude as shown in Figure 1-5 is obtained when calculating the behavior of a plane wave at the interface. The electromagnetic field (evanescent field) in the rarer medium is characterized by an exponential decay of the amplitude with increasing distance (z) from the interface (Figure 1-5):

$$E_{x,y,z} = E_{0\,x,y,z} \quad e^{-\frac{z}{d_p}} \qquad \textbf{1-12}$$

E_0 is the electric field amplitude at the interface, which depends on the angle of incidence, the refractive index and the polarization of the field. According to this equation, the penetration depth (d_p) is the distance from the interface at which the electric field amplitude has decayed to *1/e* of its value E_0 at the interface and is given by:

$$d_p = \frac{\lambda_1}{2\pi\sqrt{\sin^2\theta_i - n_{21}^2}} \qquad \textbf{1-13}$$

where $\lambda_1 = \lambda/n_1$ denotes the wavelength in medium 1 (the denser medium). Interestingly, d_p depends on the wavelength of the probing beam, which results in higher absorption intensities at lower frequencies. Typically, this distance is in the order of 1/10 of the probing wavelength, i.e. between several hundred nanometers and a micrometer for the mid-IR. For bulk material, Harrick introduced the concept of the effective thickness. The effective thickness, d_e, stands for the equivalent path in a ideal experiment *in transmission*, that would result in the same absorption signal as recorded *in attenuated total reflection*, under identical conditions (Figure 1-6). d_e is a function of the electric field at the interface E_0, of the refractive index and of the incident beam:

$$d_e = \frac{n_{21}\,E_0^2\,d_p}{2\cos\theta} \qquad \textbf{1-14}$$

This forms the basis for quantitative analysis according to the Lambert-Beer law. For an absorbance signal A, the optical pathway length is replaced by the effective thickness d_e as follows:

$$A = -\log\left(\frac{I}{I_0}\right) = \varepsilon\, c\, d_e \qquad \textbf{1-15}$$

where ε is the molar extinction coefficient and c the analyte concentration. By choosing the appropriate IRE material and the angle of the incident beam θi, the penetration depth can be adjusted to an optimal value with respect to the investigated interface layer.

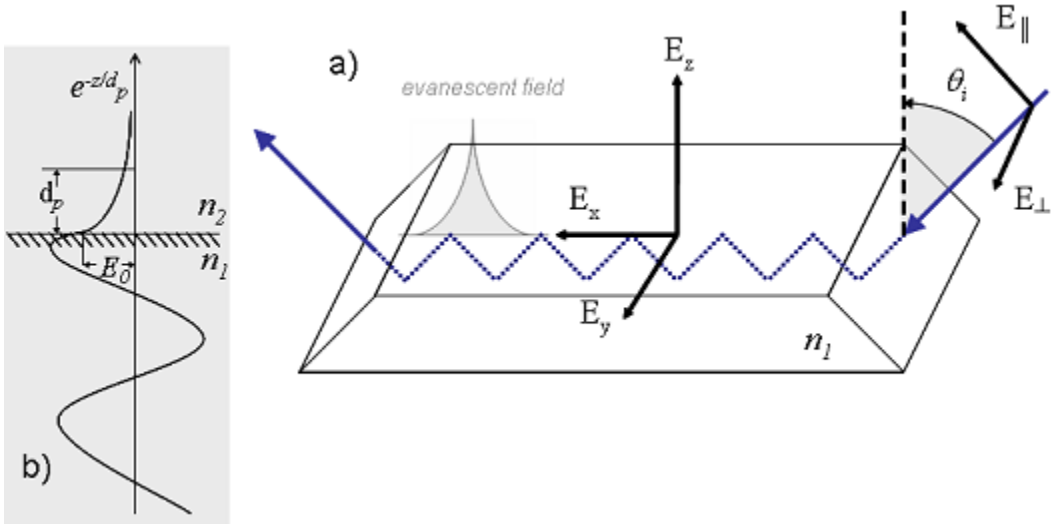

Figure 1-5. An evanescent electromagnetic field penetrates into the optically thinner medium: if this medium is infrared absorbing, the field is attenuated thus producing a spectrum. a) Schematic drawing of an IRE (Internal Reflection Element) with 11 internal reflections for ATR. A coordinate system is fixed to the IRE. $E_\parallel$ and $E_\perp$ denote the parallel and perpendicular polarized electric field components of the light incident to the IRE under the angle θ_i. $E_\parallel$ results in the E_x and E_z components of the evanescent field, while $E_\perp$ results in the E_y component. b) Blow–up of IRE interface with electric field amplitude at both sides of the interface. Evanescent means "tending to vanish" and describes the exponential decay (rather than sinusoidal) with distance from the interface.

Therefore, ATR-IR spectroscopy is a powerful tool to characterize thin films and/or events occurring near or at a surface, *in situ*. The most commonly used IRE materials

are zinc selenide (ZnSe) and germanium (Ge). Several materials and their properties are listed in Table 1-1.

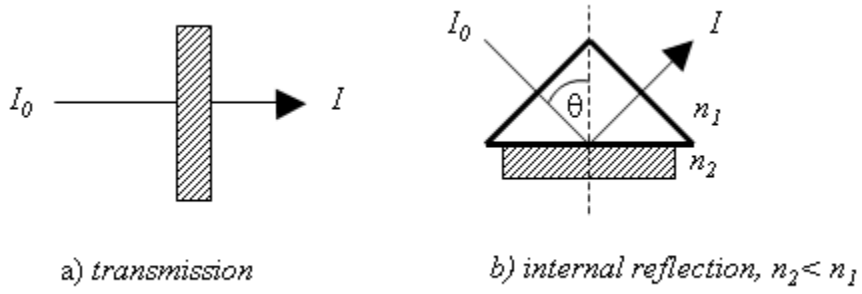

Figure 1-6. Concept of effective thickness d_e (Harrick): equivalent path in a transmission experiment that results in the same absorption signal as the ATR experiment under identical conditions.

For a Ge internal reflection element (IRE, $n_1 = 4$) in contact with water ($n_2 = 1.33$) at an angle of incidence of $\theta_i = 45°$, the effective thickness at $1640\ cm^{-1}$ is $0.44\ \mu m$ for parallel polarized light and $0.22\ \mu m$ for perpendicular polarized light. For a ZnSe IRE the corresponding values are 1.12 and $0.56\ \mu m$.

Material	*Refractive index (n)*[a]	*Usable wavelength range [cm^{-1}]*	*Critical angle (θ_c)*
ZnSe	2.4	20000-450	24,6°
KRS-5[b]	2.37	20000-250	24,6°
Si	3.4	10000-1500	15.6°
Ge	4.0	5500-600	14,5°
AMTIR (As/Se/Ge glass)	2.5	11000-750	23,6°

[a] At 5000 cm^{-1}.
[b] Eutectic mixture of thallium bromide/iodide

Table 1-1. Most common materials used for internal elements (IRE) and their optical properties.

1.3.2. ATR spectroscopy of thin film

Harrick also derived approximate formulas for thin films between the IRE and the optically rarer medium. These formulas rely on the assumption that the thin films are only weakly absorbing and can not be applied in the case of metals, which strongly absorb infrared radiation. Detailed treatment of the various cases (bulk media and thin films, weak and strong absorber) if found in literature.

1.3.3. Improvement of the ATR spectroscopy technique

The sensitivity of an ATR experiment can be increased by using multiple internal reflections. A widely used technique is changing the geometry and size of the IRE in order to increase the number of total reflections in so called multiple internal reflection elements (MIRE). The reflectivity (R) changes with N reflections (according to the Lambert-Beer law):

$$R^N = (1 - \alpha\, d_e)^N \qquad \textbf{1-16}$$

where α is the absorption coefficient. In this way, the effective thickness is amplified with each reflection and the signal to noise (S/N) ratio is increased. Due to low signal intensities at the surface, improvement of the signal to noise (S/N) ratio is an important factor. To further improve the signal to noise ratio, a very promising technique, modulation excitation (ME) spectroscopy and phase-sensitive detection (PSD), has been presented by Baurecht and Fringeli70. If a system is disturbed by periodically varying an external parameter such as temperature, pressure or concentration of a reactant, then all the species in the system, which are affected by this parameter, will also response periodically at the same frequency as the stimulation, or at harmonics thereof. At the beginning of the modulation, the system relaxes to a new quasi steady-state around which it is oscillating at angular frequency

ω. As a consequence, it is possible to separate the signals of the response from the static signals, which are not affected by the periodic perturbation through a phase-sensitive detection (PSD). The response of the system is followed by recording time-resolved spectra, which are converted to phase-resolved spectra by a digital PSD according to the equation 1-17[71].

$$A_k^{\phi_k^{PSD}}(\tilde{\nu}) = \frac{2}{T}\int_0^T A(\tilde{\nu},t)\sin(k\omega t + \phi_k^{PSD})dt \qquad \textbf{1-17}$$

$$k = 1,2,....$$

$A(\tilde{\nu},t)$ is the time dependent absorbance at wave number $\tilde{\nu}$, ω is the stimulation frequency, T is the modulation period and ϕ_k^{PSD} is the demodulation phase-angle[72-75].

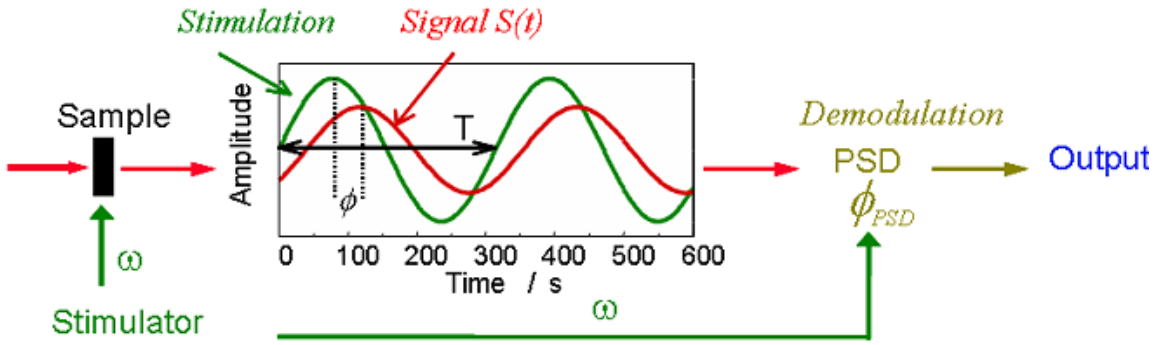

Figure 1-7. Schematic setup for modulated excitation (ME) spectroscopy. Periodic excitation of the system is performed with frequency ω. Detected time-resolved response of the system is transformed by phase-sensitive detection (PSD) to a phase-resolved spectra where static signals are suppressed.

In a simple view, PSD applied to data from a spectroscopic ME experiment results in a kind of difference spectra between excited and non-excited states. PSD is a narrowband technique, i.e. only noise at frequencies close to the stimulation frequency ω contributes to the spectra[76]. Furthermore, if the kinetics of the stimulated process is in the same range as the excitation period, phase lags and damped amplitudes will result, that contain information about the kinetics of the process.

1.3.3.1. Single-Beam-Sample-Reference technique

Another interesting method is changing the spectrometer into a pseudo double-beam mode, which is achieved by mechanically changing the vertical position of the IRE by means of a lift mechanism, so that sample and reference can be measured *quasi* at the same time. This so called single-beam-sample-reference (SBSR) technique was extensively used in this thesis. Most Fourier Transform Infrared (FTIR) spectrometers are working in the single-beam (SB) mode. This implies a time delay between the measurement of reference and sample which are used to calculate transmittance or absorbance spectra. This temporal delay favors instrumental drift, environmental fluctuations and/or sample contaminations in addition to modifications intrinsically linked to the sample and eventually to the supporting crystal.

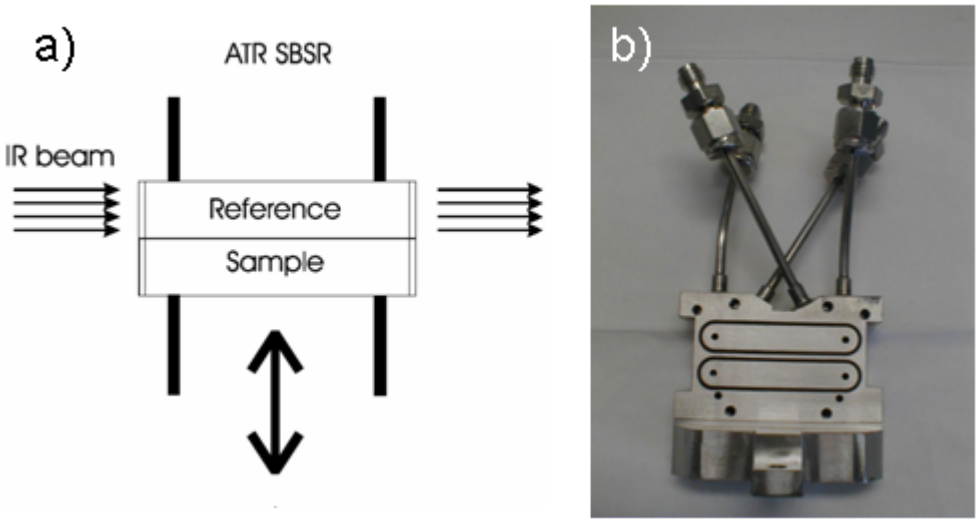

Figure 1-8. a) Single-beam-sample-reference (SBSR) ATR principle. Alternative change from sample to reference and vice-versa is performed by computer-controlled lifting and lowering of the IRE holder; b) double chamber flow-through cell.

To reduce these annoying factors a new type of ATR attachment has been constructed whose design is outlined in Figure 1-8. One half of the IRE is then dedicated to the

sample (S) and the other one to the reference (R). Both sides can be separately addressed with flow-through cells, allowing distinct treatment by liquid or gas flow. A computer-controlled lifting mechanism moves the two compartments up and down, alternatively aligning the sample S or the reference R with the IR beam. Thus absorbance spectra are calculated from single channel spectra registered *quasi-simultaneously*. This implementation is referred to as *single-beam-sample-reference* (SBSR) technique and has been introduced by Fringeli[77]. The conventional SB spectrum reflects the whole history of the sample, whereas the SBSR spectrum reflects the sample state when compared with a reference with the same history. Thus the information that can be extracted is different and in both cases valuable. The SBSR set-up presents clear advantages when looking for signals related to evolving events on the surface, especially if investigated *in situ* during long lasting measurements, as performed, tipically, in this experimental work.

1.3.4. Note on the use of germanium as internal reflection element

The high refractive index, the usable wavelength range (5500-600, cfr. Table 1-1), the available quality of the crystalline structure of the 20 x 50 mm trapeiziodal element and the reasonable unit price, motivated the choice of Ge as material of internal reflection element for ATR measurement within the frame of this work. On the other hand, silicon is the support routinely used for the production of *arrayon* bioanalytical platforms, applied in this study for the investigation of proteins–carbohydrate interaction's. It must be pointed out that the chemico-physical properties of germanium are comparable to silicon. The latter, when used as IRE material, has the disadvantage that the spectral range below 1500 is not accessible. Therefore the dextran fingerprint region, with strong bands in the 1000-1200 cm^{-1} range, would be unavailable. Although specifying that all the spectroscopic information collected

apply to dextran based polymer observed at the water/Ge interface, the information gathered contribute to the better understanding of the mechanisms associated to the photobonding technology in general.

1.4. Scope of the thesis

The potential of ATR-IR spectroscopy has been largely explored in the last years in specific domains such as biochirality[78-83], metal surface chirality[84-86], heterogeneous catalisis[73, 87-89], photocatalysis[90]. The application of the technique to the modification of the surface by high molecular weight polymers, seemed to be work investing. Despite the widely spread use and their "biomimetic" functionality, there is a lack of molecular level insight on the behavior of dextran based polymers at interfaces, which prevents a more rational design of surface modification. The former experience of the candidate in the group of Surface Engineering at CSEM (Centre Suisse d'Electronique et Microtechnique, Neuchâtel, Switzerland) led by Dr. Hans Sigrist, and the interest in furthering photobonding technology, motivated this work. Meanwhile the success of the OptoDex® related technology led to the creation of the company *arrayon* biotechnology and CSEM strengthened his position in development of optical biosensor, interface design and imaging. Another aim of this work was to blend together highly specific competences in polymer science, surface modification and surface engineering and stress their complementarity.

1.5. References

1. Mathieu , H. J.; Gao, X.; Chevolot, Y.; Balazs, D. J., Surface Functionalization for Biomedical Applications In *Surface Chemistry in Biomedical and Environmental Science*, Springer Netherlands: 2006; pp 145-158

2. Kingsmore, S. F., Multiplexed Protein Measurement: Technologies and Applications of Protein and Antibody Arrays. *Nat. Rev. Drug Discov.* **2006,** 5, (4), 310-321.

3. MacBeath, G.; Schreiber, S. L., Printing Proteins as Microarrays for High Throughput Function Determination. *Science* **2000,** 289, 1760-1762.

4. Fodor, S. P.; Rava, R. P.; Huang, X. C.; Pease, A. C.; Holmes, C. P.; Adams, C. L., Multiplexed Biochemical Assays with Biological Chips. *Nature* **1995,** 364, (6437), 555-6.

5. Merkel, J. S.; Michaud, G. A.; Salcius, M.; Schweitzer, B.; Predki, P. F., Functional Protein Microarrays: Just How Functional Are They? *Curr. Opin. Biotech.* **2005,** 16, 447–452.

6. Ye Fang, Y.; Frutos, A. G.; Lahiri, J., Membrane Protein Microarrays. *J. Am. Chem. Soc.* **2002,** 124, (11), 2394 -2395.

7. Chan, S. M.; Ermann, J.; Su, L.; Fathman, C. G.; Utz, P. J., Protein Microarrays for Multiplex Analysis of Aignal Transduction Pathways. *Nat. Med.* **2004,** 10, (12), 1390-1396.

8. Funeriu, D. P.; Eppinger, J.; Denizot, L.; Miyake, M.; Miyake, J., Enzyme Family-Specific and Activity-Based Screening of Chemical Libraries Using Enzyme Microarrays. *Nat. Biotech.* **2005,** 23, (5), 622-627.

9. Vorderwülbecke, S.; Cleverley, S.; Weinberger, S. R.; Wiesner, A., Protein Quantification by the SELDI-TOF-MS-Based ProteinChip® System. *Nat. Meth.* **2005,** 2, (5), 393-395.

10. Kuruvilla, F. G.; Shamji, A. F.; Sternson, S. M.; Hergenrother, P. J.; Schreiber, S. L., Dissecting Glucose Signalling with Diversity-Oriented Synthesis and Small-Molecule Microarrays. *Nature* **2002,** 416, (6881), 653-657.

11. Manimala, J. C.; Roach, T. A.; Li, Z.; Gildersleeve, J. C., High-Throughput Carbohydrate Microarray Analysis of 24 Lectins. *Angew. Chem. Int. Ed.* **2006,** 45, 3607-3610.

12. Fall, B. I.; Eberlein-Konig, B.; Behrendt, H.; Niessner, R.; Ring, J.; Weller, M. G., Microarrays for the Screening of Allergen-Specific IgE in Human Serum. *Anal. Chem.* **2003,** 75, (3), 556-562.

13. Kim, S. H.; Tamrazi, A.; Carlson, K. E.; Katzenellenbogen, J. A., A Proteomic Microarray Approach for Exploring Ligand-Initiated Nuclear Hormone Receptor Pharmacology, Receptor Selectivity, and Heterodimer Functionality. *Mol. Cell Proteomics* **2005,** 4, (3), 267-277.

14. Ramachandran, N.; Hainsworth, E.; Bhullar, B.; Eisenstein, S.; Rosen, B.; Lau, A. Y.; Walter, J. C.; LaBaer, J., Self-Assembling Protein Microarrays. *Science* **2004,** 305, (5680), 86-90.

15. Vemuri, G. N.; Aristidou, A. A., Metabolic Engineering in the -Omics Era: Elucidating and Modulating Regulatory Networks. *Microbiol. Mol. Biol. Rev.* **2005,** 69, (2), 197-216.

16. Phizicky, E. M.; Grayhack, E. J., Proteome-Scale Analysis of Biochemical Activity. Crit. Rev. Biochem. Mol. Biol. **2006**, 41, (5), 315-327.

17. Hartley, P. G.; McArthur, S. L.; McLean, K. M.; Griesser, H. J., Physicochemical Properties of Polysaccharide Coatings Based on Grafted Multilayer Assemblies. Langmuir **2002**, 18, (7), 2483-2494.

18. Dai, L.; StJohn, H. A. W.; Bi, J.; Zientek, P.; Chatelier, R. C.; Griesser, H. J., Biomedical Coatings by the Covalent Immobilization of Polysaccharides onto Gas-Plasma-Activated Polymer Surfaces. Surf. Interface Anal. **2000**, 29, (1), 46-55.

19. Elam, J. H.; Nygren, H., Covalent Coupling of Polysaccharides to Silicon and Silicon Rubber Surfaces. *J. Biomed. Mater. Res.* **1984,** 18, 953-959.

20. Elender, G.; Kühner, M.; Sackmann, E., Functionalisation of Si/SiO_2 and Glass Surfaces with Ultrathin Dextran Films and Depostion of Lipid Bilayers. *Biosens. Bioelectron.* **1996,** 11, 565-577.

21. Löfas, S.; Johnsson, B.; Tegendal, K.; Rönnberg, I., Dextran Modified Gold Surfaces for Surface Plasmon Resonance Sensors: Immunoreactivity of Immobilized Antibodies and Antibody-Surface Interaction Studies. *Colloid. Surface. B* **1993,** 1, 82-89.

22. Löfas, S.; Johnsson, B., A Novel Hydrogel Matrix on Gold Surface Plasmon Resonance Sensors for Fast and Efficient Covalent Immobilization of Ligands. *J. Chem. Soc., Chem. Commun.* **1990**, 1526-1528.

23. Piehler, J.; Brecht, A.; Geckeler, K. E.; Gauglitz, G., Surface Modification for Direct Immunoprobes. *Biosens. Bioelectron.* **1996,** 11, (67), 579-590.

24. Piehler, J.; Brecht, A.; Hehl, K.; Gauglitz, G., Protein Interactions in Covalently Attached Dextran Layers. *Colloid. Surfaces B.* **1999,** 13, 325-336.

25. Ombelli, M.; Eckmann, D. M.; Composto, R. J., Biomimetic Dextran Coatings on Silicon wafers: Thin Film Properties and Wetting. In ScholarlyCommons@Penn: 2002.

26. Akkoyun, A.; Bilitewski, U., Optimisatsion of Glass Surfaces for Optical Immunosensors. *Biosens. Bioelectron.* **2002,** 17, 655-664.

27. Miksa, D.; Irish, E. R.; Chen, D.; Composto, R. J.; Eckmann, D. M., Dextran Functionalized Surfaces via Reductive Amination: Morphology, Wetting, and Adhesion. *Biomacromolecules* **2006,** 7, (2), 557-564.

28. Ombelli, M.; Eckmann, D. M.; Composto, R. J., Dextran Grafted Silicon Substrates: Preparation, Characterization and Biomedical Applications. In *Materials Inspired by Biology*, Thomas, J. L.; Kiick, K. L.; Gower, L. A., Eds. 2003; Vol. 774, pp 93-98.

29. Lofas, S.; Johnsson, B.; Edstrom, A.; Hansson, A.; Lindquist, G.; Hillgren, R. M. M.; Stigh, L., Methods for Site Controlled Coupling to Carboxymethyldextran Surfaces in Surface-Plasmon Resonance Sensors. *Biosens. Bioelectron.* **1995,** 10, (9-10), 813-822.

30. Chen, G.; Ito, Y.; Imanishi, Y.; Magnani, A.; Lamponi, S.; Barbucci, R., Photoimmobilization of Sulfated Hyaluronic Acid for Antithrombogenicity. *Bioconjugate Chem.* **1997,** 8, (5), 730-734.

31. Sugawara, T.; Matsuda, T., Photochemical Protein Fixation on Polymer Surfaces via Derivatized Phenyl Azido Group. *Langmuir* **1995,** 11, (6), 2272-2276.

32. Mizutani, M.; Arnold, S. C.; Matsuda, T., Liquid, Phenylazide-End-Capped Copolymers of Epsilon-Caprolactone and Trimethylene Carbonate: Preparation, Photocuring Characteristics, and Surface Layering. *Biomacromolecules* **2002,** 3, (4), 668-675.

33. Prucker, O.; Naumann, C. A.; Ruhe, J.; Knoll, W.; Frank, C. W., Photochemical Attachment of Polymer Films to Solid Surfaces via Monolayers of Benzophenone Derivatives. *J. Am. Chem. Soc.* **1999,** 121, (38), 8766-8770.

34. Kanoh, N.; Kumarashiro, S.; Simizu, S.; Kondoh, Y.; Hatakeyama, S.; Tashiro, H.; Osada, H., Immobilization of Natural Products on Glass Slides by Using a Photoaffinity Reaction and the Detection of Protein-Small-Molecule Interactions. *Angew. Chem. Int. Ed.* **2002,** 42, 5584-5587.

35. Kanoh, N.; Honda, K.; Simizu, S.; Muroi, M.; Osada, H., Photo-Cross-Linked Small-Molecule Affinity Matrix for Facilitating Forward and Reverse Chemical Genetics. *Angew. Chem. Int. Ed.* **2005,** 44, (23), 3559-3562.

36. Kanoh, N.; Kyo, M.; Inamori, K.; Ando, A.; Asami, A.; Nakao, A.; Osada, H., SPR Imaging of Photo-Cross-Linked Small-Molecule Arrays on Gold. *Anal. Chem.* **2006,** 78, (7), 2226-2230.

37. Ohyama, k.; Omura, K.; Yoshihiro, I., A Photo-Immobilized Allergen Microarray for Screening of Allergen-Specific IgE. *Allergology International* **2005,** 54, 627-631.

38. Hasudaa, H.; Kwonb, O. H.; Kangc, I.-K.; Ito, Y., Synthesis of Photoreactive Pullulan for Surface Modification *Biomaterials* **2005,** 25, (15), 2401-2406.

39. Ito, Y.; Yamauchi, T.; Uchikawa, M.; Ishikawa, Y., Photoimmobilized Array of Panel Cells for Assay of Antibodies. *Biomaterials* **2006,** 27, 2502-2506.

40. Nowakowska, M.; Zapotoczny, S.; Sterzel, M.; Kot, E., Novel Water-Soluble Photosensitizers from Dextrans. *Biomacromolecules* **2004,** 5, (3), 1009-1014.

41. Sundarababu, G.; Gao, H.; Sigrist, H., Photochemical Linkage of Antibodies to Silicon Chips. *Photochem. Photobiol.* **1995,** 61, (6), 540-544.

42. Sigrist, H.; Collioud, A.; Clémence, J. F.; Gao, H.; Luginbühl, R. R.; Sänger, M.; Sundarababu, G., Surface Immobilization of Biomolecules by Light. *Optical Engineering* **1995,** 34, (8), 2339-2348.

43. Caelen, I.; Gao, H.; Sigrist, H., Protein Density Gradients on Surface. *Langmuir* **2002,** 18, 2463-2467.

44. Sigrist, H.; Gao, H.; Wegmuller, B., Light-Dependent, Covalent Immobilization of Biomolecules on 'Inert' Surfaces. *Biotechnology* **1992,** 10, (9), 1026-8.

45. Gao, H.; Guinchard, S.; Crevoisier, F.; Angeloni, S.; Sigrist, H., Microarrays and Surface Engineering for Bioanalysis. *Chimia* **2003,** 57, 651-654.

46. Sigrist, H.; Gao, H., Biosensor @ CSEM. *Chimia* **1999,** 53, 81-86.

47. Rademacher, T. W.; Parekh, R. A.; Dwek, R. A., Glycobiology. *Annu. Rev. Biochem.* **1988,** 57, 785-838.

48. Varki, A.; Cummings, R.; J, E.; Freeze, H.; Hart, G.; Marth, J., *"Essential of Glycobiology"*. Cold Spring Harbor, USA: 1999.

49. Bertozzi, C. R.; Kiessling, L. L., Chemical Glycobiology. *Science* **2001,** 291, 2357-2364.

50. Yuriev, E.; Farrugia, W.; Scott, A. M.; Ramsland, P. A., Three-Dimensional Structures of Carbohydrate Determinants of Lewis System Antigens: Implications for Effective Antibody Targeting of Cancer. *Immunol. Cell. Biol.* **2005,** 83, (6), 709-717.

51. Skehel, J. J.; Wiley, D. C., Receptor Binding and Memebrane Fusion in Virus Entry: The Influenza Hemagglutinin. *Annu. Rev. Biochem.* **2000,** 69, (1), 531-569.

52. Wang, Q.; Dordick, J. S.; Linhardt, R. J., Synthesis and Application of Carbohydrate-Containing Polymers. *Chem. Mater.* **2002,** 14, (8), 3232-3244.

53. Ladmiral, V.; Melia, E.; Haddleton, D. M., Synthetic Glycopolymers: An Overview *Eur. Polym. J.* **2004,** 40, (3), 431-449

54. Léonard, D.; Chevolot, Y.; Bucher, O.; Sigrist, H.; Mathieu, H. J., ToF-SIMS and XPS Study of Photoactivatable Reagents Designed for Surface Glycoengineering Part 1. N-(m-(3-(trifluoromethyl)diazirine-3-yl)phenyl)-4-maleimido-butyramide (MAD) on Silicon, Silicon Nitride and Diamond. *Surface Interf. Anal.* **1998,** 26, (11), 783-792.

55. Léonard, D.; Chevolot, Y.; Bucher, O.; Haenni, W.; Sigrist, H.; Mathieu, H. J., ToF-SIMS and XPS Study of Photoactivatable Reagents Designed for Surface Glycoengineering Part 2. Part 2. N- [m-(3-(TriÑuoromethyl)diazirine-3-yl)phenyl] -4-(-3-thio(-1-D-galactopyrannosyl)-maleimidyl)butyramide (MAD-Gal) on Diamond. *Surface Interf. Anal.* **1998,** 26, (11), 793-799.

56. Léonard, D.; Chevolot, Y.; Bucher, O.; Haenni, W.; Sigrist, H.; Mathieu, H. J., ToF-SIMS and XPS Study ofPhotoactivatable ReagentsDesigned for Surface Glycoengineering. Part III. 5-Carboxamidopentyl-N-[m-[3-(trifluoromethyl)diazirin-3-yl]phenyl-b-Dgalactopyranosyl]-(1->4)-1-thio-b-D-gluco-pyranoside (lactose aryl di-azirine) on Diamond. *Surf. Interface Anal.* **2001,** 31, (6), 457-464.

57. Chevolot, Y.; Bucher, O.; Léonard, D.; Mathieu, J.; Sigrist, H., Synthesis and Characterization of a Photoactivatable Glycoaryldiazirine for Surface Glycoengineering. *Bioconjugate Chem.* **1999,** 10, 169-175.

58. Chevolot, Y.; Martins, J.; Milosevic, N.; Léonard, D.; Zeng, S.; Malissard, M.; Berger, E. G.; Maier, P.; Mathieu, J.; Crout, D. H. G.; Sigrist, H., Immobilisation on Polystyrene of Diazirine Derivatives of Mono-and Disaccharides: Biological Activities of Modified Surfaces. *Bioorg. Med. Chem.* **2001,** 9 (11), 2943-2953.

59. Sprenger, N.; Sigrist, H.; Gao, H., Polysaccharides for Functional Biomolecules Display on Surface. *BioTech International, Microarrays* September, 2005.

60. McArthur, S. L.; McLean, K. M.; Kingshott, P.; St John, H. A. W.; Griesser, H. J., Effect of Polysaccharide Structure on Protein Adsorption. *Colloid Surf. B* **2000,** 17, (37-48).

61. Fringeli, U. P.; Goette, J.; Reiter, G.; Siam, M.; Baurecht, D., Structural Investigations of Oriented Membrane Assemblies by FTIR-ATR Spectroscopy. In *Fourier Transform Spectroscopy*, deHaseth, J. A., Ed. 1998; pp 729-747.

62. Buffeteau, T.; Desbat, B.; Turlet, J. M., Polarization Modulation FT-IR Spectroscopy of Surfaces and Ultra-thin Films: Experimental Procedure and Quantitative Analysis *Applied Spectroscopy* **1991,** 45, (3), 380-389.

63. Taylor, A. M.; Glover, A. M., Studies in Refractive Index. Part I and II. *J. Opt. Soc. Am.* **1933,** 23, 206.

64. Taylor, A. M.; Durfee, D. A., Studies in Refractive Index. Part III. *J. Opt. Soc. Am.* **1933,** 23, 263.

65. Taylor, A. M.; King, A., Studies in Refractive Iindex. Part IV. *J. Opt. Soc. Am.* **1933,** 23, 308.

66. Fahrenfort, J., Attenuated Total Reflection. A New Principle for the Production of Useful Infrared Reflection Spectra of Organic Compounds. *Spectrochim. Acta* **1961,** 17, 698-709.

67. Harrick, N. J., Transmission Spectra without Interference-Fringes. *Applied Spectroscopy* **1977,** 31, (6), 548-549.

68. Mirabella, F. M.; Harrick, N. J., *Internal Reflection Spectroscopy: Review and Supplement*. Harrick Sci. Corp.: Ossining, NY, 1985.

69. Harrick, N. J., *Internal Reflection Spectroscopy*. Interscience Publishers: New York, 1967.

70. Baurecht, D.; Fringeli, U. P., Quantitative Modulated Excitation Fourier Transform Infrared Spectroscopy. *Rev. Sci. Instr.* **2001,** 72, (10), 3782-3792.

71. Baurecht, D.; Porth, I.; Fringeli, U. P., A New Method of Phase SensitiveDetection inModulation Spectroscopy Applied to Temperature Induced Folding and Unfolding of RNase A. *Vibrational Spectroscopy* **2002,** 30, 85-92.

72. Müller, M.; Buchet, R.; Fringeli, U. P., 2D-FTIR ATR Spectroscopy of Thermo-Induced Periodic Secondary Structural Changes of Poly-(L)-lysine. A Cross-Correlation Analysis of Phase-Resolved Temperature Modulation Spectra. *J. Phys. Chem.* **1996,** 100, (25), 10810-10825.

73. Burgi, T.; Baiker, A., In Situ Infrared Spectroscopy of Catalytic Solid-Liquid Interfaces Using Phase-Sensitive Detection: Enantioselective Hydrogenation of a Pyrone over Pd/TiO_2. *J. Phys. Chem. B* **2002,** 106, (41), 10649-10658.

74. Wirz, R.; Burgi, T.; Baiker, A., Probing Enantiospecific Interactions at Chiral Solid-Liquid Interfaces by Absolute Configuration Modulation Infrared Spectroscopy. *Langmuir* **2003,** 19, (3), 785-792.

75. Urakawa, A.; Wirz, R.; Burgi, T.; Baiker, A., ATR-IR Flow-Through Cell for Concentration Modulation Excitation Spectroscopy: Diffusion Experiments and Simulations. *J. Phys. Chem. B* **2003,** 107, (47), 13061-13068.

76. Fringeli, U. P.; Baurecht, D.; Günthard, H. H., Biophysical Infrared Modulation Spectroscopy. In *Infrared and Raman Spectroscopy of Biological Materials*, Gremlich, H. U.; Yan, B., Eds. Dekker: New York / Basel, 2000; pp 143-192.

77. Fink, J.; Kiely, C. J.; Bethell, D.; Schiffrin, D. J., Self-Organization of Nanosized Gold Particles. *Chem. Mater.* **1998,** 10, (3), 922-926.

78. Bieri, M.; Bürgi, T., L-Glutathione Chemisorption on Gold and Acid/Base Induced Structural Changes: A PM-IRRAS and Time-Resolved in Situ ATR-IR Spectroscopic Study. *Langmuir* **2005,** 21, 1354-1363.

79. Bieri, M.; T., B., Probing Enantiospecific Interactions between Proline and an L-Glutathione Self-Assembled Monolayer by Modulation Excitation ATR-IR Spectroscopy. *J. Phys. Chem. B.* **2005,** 109, 10243-10250.

80. Bieri, M.; T., B., Adsorption Kinetics, Orientation, and Self-Assembling of N-Acetyl-L-cysteine on Gold: A Combined ATR-IR, PM-IRRAS, and QCM Study. *J. Phys. Chem. B.* **2005,** 109, 22476-22485.

81. Bieri, M.; Bürgi, T., Adsorption kinetics of L-Glutathione on Gold andStructural Changes DuringSelf-Assembly: an in situ ATR-IR and QCM Study. *Phys. Chem. Chem. Phys.* **2006**, 513-520.

82. Bieri, M.; T., B., Enantiodiscrimination between an N-Acetyl-L-Cysteine SAM and Proline: An In Situ Spectroscopic and Computational Study. *Phys. Chem. Chem. Phys.* **2006,** 7, 514-523.

83. Bieri, M.; Burgi, T., D-Penicillamine Adsorption on Gold: An in Situ ATR-IR Spectroscopic and QCM Study. *Langmuir* **2006,** 22, (20), 8379-8386.

84. Bieri, M.; Gautier , C.; Bürgi, T., Probing Chiral Interfaces by Infrared SpectroscopicMethods. *Phys. Chem. Chem. Phys.* **2007,** 9, 671 - 685.

85. Gautier, C.; Burgi, T., Chiral Chiral N-Isobutyryl-Cysteine Protected Gold Nanoparticles: Preparation, Size Selection, and Optical Activity in the UV-vis and Infrared. *J. Am. Chem. Soc.* **2006,** 128, (34), 11079-11087.

86. Gautier, C.; Bürgi, T., Vibrational Circular Dichroism of N-Acetyl-L-CysteineProtected Gold Nanoparticles. *Chem. Commun.* **2005**, 5393-5395.

87. Sonderegger, O. J.; Ho, G. M.-W.; Bürgi, T.; Baiker, A., Enantioselective Hydrogenation of Aromatic Ketones over Cinchona-Modified Rhodium: A New Opportunity? *J. Catal.* **2005,** 230, (2), 499-506.

88. Burgi, T.; Wirz, R.; Baiker, A., In Situ Attenuated Total Reflection Infrared Spectroscopy: A Sensitive Tool for the Investigation of Reduction-Oxidation Processes on Heterogeneous Pd Metal Catalysts. *J. Phys. Chem. B* **2003,** 107, (28), 6774-6781.

89. Ferri, D.; Burgi, T., An in Situ Attenuated Total Reflection Infrared Study of a Chiral Catalytic Solid-Liquid Interface: Cinchonidine Adsorption on Pt. *J. Am. Chem. Soc.* **2001,** 123, (48), 12074-12084.

90. Dolamic, I.; Bürgi, T., Photoassisted Decomposition of Malonic Acid on TiO_2 Studied by in Situ Attenuated Total Reflection Infrared Spectroscopy. *J. Phys. Chem. B* **2006,** 110, 14898-14904.

Chapter 2

Attenuated Total Reflection (ATR) Infrared spectroscopy for dextran based polymer characterization

2.1. Physisorption of dextran based polymers at interfaces

From the growing demand for natural polymers for liquid/solid and gas/solid interfaces conditioning, stems the interest in polysaccharides, which are copiously available. They combine unique structural and molecular features such as high molecular weight, well-defined molecular structure, and strong intra- and intermolecular bonding[1]. In the past, biocompatibility applied to the property of degrading under the action of specific microorganisms[2, 3], and biocompatibility stood for biodegradability. Recently, the commonly accepted meaning shifted to include bioactivity, a requirement that is particularly well met by dextran: it has been also studied as medical macromolecular carrier (drugs and diagnostic agent, with eventual smart delivery)[4-6] as well as blood plasma extender and as antithrombolytic agent[7-9]. Dextrans are bacterial exopolysaccharides commercially available in a range of well-characterized molecular weights. From the structural point of view, they consist of macromolecular glucose chains predominantly linked via a linear α-1,6-glycosidic bond. They are stable in basic and mildly acidic solutions. The solubility of dextrans in water decreases with an increase in branching. The large number of hydroxyl group provides the numerous attractive possibilities for chemical modifications. Dextran

based polymers have a long history as surface coating for biosensors and more in general tailoring agent of physical and chemical properties of surfaces[10, 11]. They remain attractive because of they provide a biocompatible surface layer[12-16]. In spite of the variety of the multifunctional modifications of dextran, especially when designed for biological assays, the chemistry leading to the covalent interaction with the surface is definitely classical[11, 17-20]. In the widely referenced scenario of dextran derivatives grafting, the photobonding technology introduced by Sigrist[21] stands out for its originality. In this unique approach, dextran based polymers are combined with arildiazirine photoactivable[22] chemical groups, which operate as hook for both, the graft of the polymer on the surface, and the immobilization of the target analyte[23-25]. The latter may serve as probe for further traceable interaction[26-30]. As shown in Figure 1-1 (pag.3), aryl-trifluoromethyl-diazirines, photoactivated at 350 nm, generate highly reactive carbenes and release molecular nitrogen (N_2)[31-33]. Carbenes spontaneously undergo insertion reactions and form covalent bonds with the surface and/or bio/molecules[34]. To fulfill the purpose of investigating dextran based polymers physisiorption, starting from dextran, a homologue series has been defined (Figure 2-1). Reductive amination reaction between primary amines and periodate-oxidated dextran allows insertion of amino groups and ring opening[1, 35-37]: such chemical pathway leads from dextran (A, Figure 2-1) to aminodextran (B, Figure 2-1). The commercial aminodextran (product D1861 Molecular Probes™, Invitrogen Detection Technologies) contains 8 amines per mol, as indicated in the container's label. Further thiocarbomoylation of aminodextran leads to the dextran derivative bearing photoactiveable aryl-tryfluoromethyl-diazirine[38] (OptoDex® A, *arrayon Biotechnology,* Switzerland, www.arrayon.com). The statistics driven chemical reaction allows semi-stoichiometric substitution. Primary amines remain available for eventual additional substitution resulting in actinic dextrans displaying both,

aryldiazirine and blocking agent (primary amines acylation, OptoDex® B) or aryldiazirine and carboxyl group (-COOH, OptoDex® C) [39, 40].

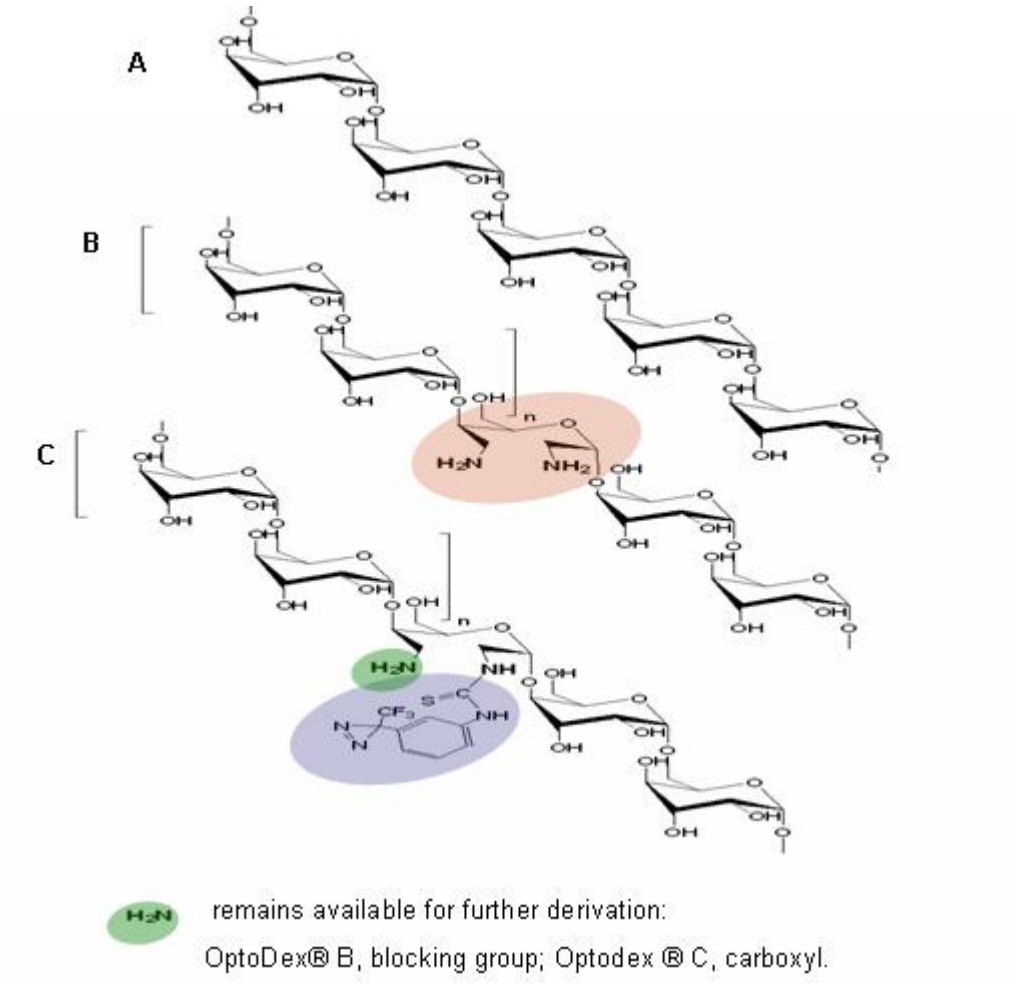

Figure 2-1. Homologue series of dextran based polymers investigated by ATR-IR spectroscopy. A, Dextran; B, aminodextran; C, OptoDex® A. The structures are simplified, they do not take in account eventual branching, but outline the expected distribution of the chemical functional groups along the glucopyranose backbone.

The OptoDex® family is actually broader[40] as well as the photolabeled derivatives (hyaluronic acid, serum albumins, mono and oligosaccharides) which accompanied the development of the photobonding technology[41-45]. Nevertheless, the above mentioned specimens represent the selection that was retained in this thesis to collect spectroscopic insight on the physico-chemical behavior at interfaces of dextran based

polymers. Summarizing the reasons supporting the significant attention that this bioengineered polymers family received, at least two point must be outlined: their hydrogel-like 3D behavior, allowing favorable conditions for bioactivity retention [46, 47] and their passivating properties[48-50]. Ideally the bioactive derivatives are covalently attached to the designated material with high loading efficiency and without loss of biological activity. The covalent immobilization of bioactive derivatives has been achieved using both chemical and photochemical methods. The chemical route applies for affinity coupling *via* streptavidin interlayer of biotinylated lectins onto OpteDex® biotin platform[34] or covalent coupling *via* EDC/NHS chemistry of antigens onto OptoDex® C platform[39] while the photochemical approach implies statistical carbene insertion. Immobilization of bioactive species via photolysis of a suitable photolabile derivative is of interesting as it is compatible with biological functions and addressability (eventual topical dispensing and mask assisted UV exposure resulting in covalent surface patterning)[38, 51]. The effectiveness of the photobonding technology is certified by the quality control procedure of the OptoDex® platform as commercialized by *arrayon Biotechnology*. From a scientific point of view, two major phenomena are of interest: the eventual spontaneous organization of the dextran based polymer onto the surface and the following fixation under UV photoactivation. The extremely low ratio of photolabile functions/ glucopyranose units indicates that the pre-organization of the polymer at the interfaces by means of adsorption plays a crucial role for the final layer quality.

2.1.1. Experimental section

2.1.1.1. Chemicals

Ethanol (EtOH, Merck p.a. was used as received). Water was purified with a Milli-Q system (≥ 18 MΩ cm). Dextran from Leukonostok, is a Fluka product; amino

dextran 40000 Dalton, and carboxymethyl dextran 70000 Dalton were Molecular Probes™ products (currently, Invitrogen Detection Technologies). OptoDex® A (amino), OptoDex® B (blocked), OptoDex® C (carboxyl) were received from *arrayon Biotechnology*, Neuchâtel, Switzerland. PBS buffer pouches (Sigma) were reconstituted in 1 L purified water yielding 10mM phosphate, buffered saline solution (0.15 M NaCl, pH 7.4). pH was verified and freshly diluted PBS 1% was prepared as required by experimental conditions. Monoclonal anti-TNFα (human tumor necrosis factor-α, a cytokine responsible for the regulation of cellular physiology) antibody (AB), 100 µg/ml in PBS was courtesy of Dr.Gerald Reiter, Institute of Physical Chemistry, University of Vienna, Austria. Sodium dodecyl sulfate (SDS, Sigma, MW 288,38), 5% v/v, was prepared by dissolving 5.0 g in 100 ml purified water and was used as anionic detergent. Eventually a blend with ethylendiamine tetracetic acid, sodium salt (EDTA, Sigma, MW 372,8) was prepared according to the following proportion: 2,16 g SDS, 0.93 g EDTA in 50 ml final volume (purified water). This leads to a final aqueous solution of SDS 150 mM and ETDA 50 mM.

2.1.1.2. Germanium plate modification

Germanium IRE pre-treatment. Germanium (Ge) internal reflection elements (IRE; 50mm X 20 mm x 1 mm, Komlas, Berlin, Germany) were used for ATR-IR experiment. IREs were first polished with a 0.25-µm-grain size diamond paste (MetaDi® II, Buehler GmbH, Germany) and afterward rinsed copiously with EtOH and water. This basic procedure assures cleaning but does not promote hydrophilic behavior. The complete disappearance of IR absorption bands at 2850 cm^{-1} and 2930 cm^{-1} associated with hydrocarbon chains indicated removal of organics. Alternatively, in order to investigate the optimization of physisorption conditions, surfaces were plasma cleaned under air flow for 5 min (PlasmaPrep 2, GaLa Instrumente GmbH, Germany). Plasma surface treatment with oxidizing species, such

as air, aimed at removing organics. At the same time this procedure leaves functional oxygen-containing groups on the surface, which increases wettability. Complete hydrophilic activation was achieved by 20 min of dipping in water to enhance formation of oxydrils (-OH groups) right before polymer functionalization[52, 53]. Wet plates were dried by nitrogen flushing. In a subsequent step, a film of dextran based polymers was cast onto the surface according to different protocols.

Ex situ Germanium IRE functionalization by a thick film of dextran based polymer. The polymers object of investigation were dextran, aminodextran, carboxymethyl dextran, OptoDex® A, OptoDex® B and OptoDex® C. 300 µl of polymer solutions 0.1 mg/ml and 1.0 mg/ml, respectively, in pure water or in PBS 1% were cast by pipetting on one whole side of the IRE. The volume used for complete surface covering depended on the surface pretreatment: 300 µl after plasma treatment (hydrophilic surface), 2 ml after cleaning without plasma (diamond polishing and ethanol, hydrophobic surface). The solution was evaporated at room temperature under hood ventilation for several hours. This casting technique does not allow any control on homogeneous polymer deposition. The evaporation phenomenon drove the film formation. A SBSR measurement was used to estimating the functionalization quality over the entire width of the plate. The sample was not irradiated and eventually protect from UV light exposure. No rinsing step was performed before the measurement.

Ex situ Germanium IRE functionalization by a thin film of dextran based polymer. Polished, plasma treated and wetting enhanced germanium IREs were dipped for 1 hour in 5 ml of dextran based polymer 0.1 mg/ml in pure water or in PBS 1%. The technique provided *physisorption mediated polymer functionalization*, on both sides of the IRE. Alternatively, the solution was temporary put in contact with one

side of the IRE by pipetting defined volumes (see above, the thick film formation). Incubation of two hours was followed by rinsing (water).

In situ Germanium IRE functionalization by a thin film of dextran based polymer. Thin film casting was carried out *in situ* using the double cell micro fluidic kit to differentiate sample and reference compartment. The same solutions as described above were used in connection with a peristaltic pump alimenting the microfluidics systems. The *in situ* set-up was used also to investigate the behavior of an antibody over the dextran modified surface.

2.1.1.3. ATR measurements

Data Acquisition. ATR-IR measurements were performed on a Bruker EQUINOX 55 FT-IR spectrometer equipped with a nitrogen-cooled narrow-band mercury cadmium telluride (MCT) detector. Spectra were recorded at a resolution of 4 cm^{-1}. The pretreated Ge IRE served as reference for absorbance spectra. In the case of OptoDex ® A, ATR spectra were registered after casting, prior and post UV light exposure, before and after mild or thorough rinsing. A wire grid polarizer was used to generate linear polarized light parallel and perpendicular to the plane of incidence. Measurements were performed using the SBSR lift accessories, which allowed to set the IRE in the beam at well established positions and to estimate the best functionalized region. An air purging system removed humidity and CO_2 from the beam path. OPUS software (Bruker) allowed the right control and utilization of the spectrometer and of the SBSR accessories (lift, polarizer). The OPUS software furthermore allowed mathematical manipulation of spectra to correct for water absorption and to identify the contribution deriving from multi-step functionalization.

2.2. Results and discussion

2.2.1. Dextran physisorption

The red spectrum in Figure 2-2 refers to a dextran thick layer. As expected, the spectrum closely resembles a dextran spectrum recorded in transmission mode. In the region between 1200-1000 cm^{-1} a complex band with several maxima at 1147, 1104, 1068, 1025 and 1007 cm^{-1} is observed. These bands have been commonly found in most carbohydrates and according to normal mode analysis, have been assigned as coupled vibrations involving C-O, C-O-C, C-C-C and C-C-O antisymmetric stretches[54]. The high frequencies at 1147 and 1104 cm^{-1} are considered to be mainly due to antisymmetric stretching modes of the glycoside bridge group. The degree of chain branching is probably very low[54]. When glucopyranose units with C1 chair conformation are present, the infrared spectra exhibit one band in the region between 925-885 cm^{-1} and another one around 855-820 cm^{-1}. In this spectral region, at least two weak bands around 900 cm^{-1} and 840 cm^{-1} are observed, which are assigned to mixed C-CH deformation vibrations[55-57]. In the region between 1500 and 1250 cm^{-1}, C-H bending modes are found while C-H stretches are observed at 2950-2850 cm^{-1}. The spectra in Figure 2-2 were recorded on a Ge IRE pre-treated by EtOH extensive washing (dipping and shaking, further rinsing by fresh EtOH) and nitrogen flushing to ensure a homogenous fast evaporation, without smearing, and full dust removal. IREs were not submitted to plasma treatment. The surface is clean but hydrophobic, as judged from the shape of water drops dispensed on it. The red spectrum depicts a thick film obtained by casting 2 ml of an aqueous (PBS buffer 1%) 1.0 mg/ml dextran solution and subsequent overnight evaporation under a ventilated hood at room temperature. The black spectrum depicts a thick film obtained with the same technique, but using a solution ten times diluted (dextran 0.1 mg/ml in PBS 1%).

Obviously, the dextran/PBS 1% ratio differs sensitively in the two cases (of a factor of 10). To estimate the buffer contribution, an ATR spectrum of PBS 1% cast on a Ge IRE is reported as black dashed profile. Comparison demonstrates that in the case of the more diluted dextran solution the buffer contribution interferes significantly with typical absorptions of the polymers.

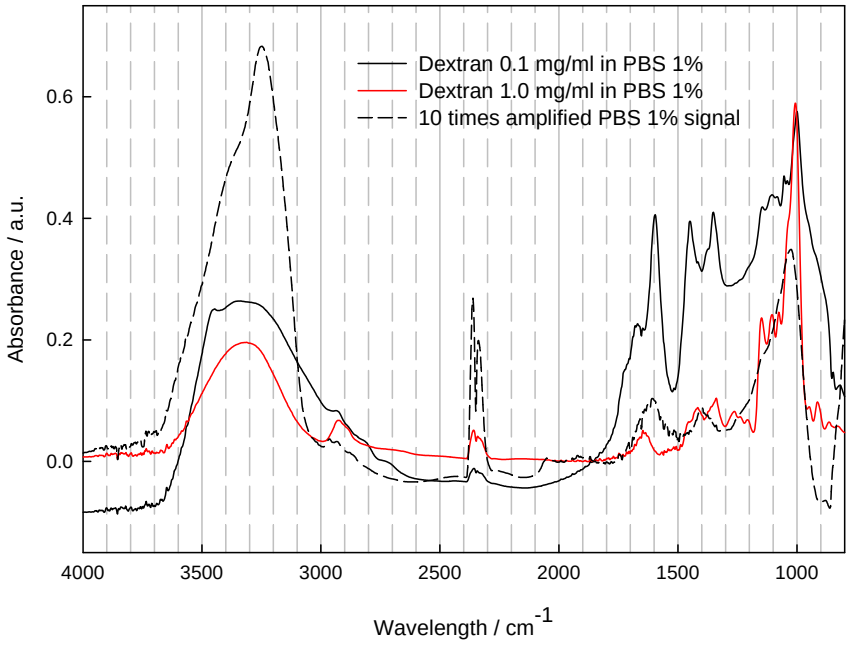

Figure 2-2. ATR spectra of dextran thick film obtained by casting PBS 1% buffered solutions on clean (*not plasma* activated) Ge IRE. The black spectrum refers to the film obtained from 0.1 mg/ml solution. The red spectrum refers to the film obtained from 1.0 mg/ml solution. The black dashed profile is an ATR spectrum of PBS 1% buffer cast and evaporated on the Ge IRE. It is shown to better identify the salts contribution to the spectrum of the dextran film (10 times amplified).

In the case of the ten times higher dextran concentration, the signals of the buffer are almost negligible. It must be noted that despite the ten fold higher concentration, the IR signals are not ten times more intense. This lack of scaling is due to two factors. The film is considerably thicker than the penetration depth of the evanescent field. Furthermore, the casting technique does not consent control over evaporation, then favoring clotting of the analyte, especially on a hydrophobic support. A strict

quantification can not be applied under these conditions. The red spectrum in Figure 2-2 serves as reference spectrum of a dextran polymer on a surface. The preparative conditions led to wide presence of water both *loosely linked to* and *embedded in* the polymer film. Water absorbs at 3600-3000 cm^{-1}. This broad band contains the symmetric and antisymmetric stretching vibrations, ν_s (HOH) and ν_{as} (HOH). The bending vibration, δ (HOH), arises at 1645 cm^{-1}. In Figure 2-3 the same "drop and evaporate" casting technique as described previously was applied on plasma pretreated Ge IREs. The contribution of PBS 1% buffer can be estimated considering the black dashed profile.

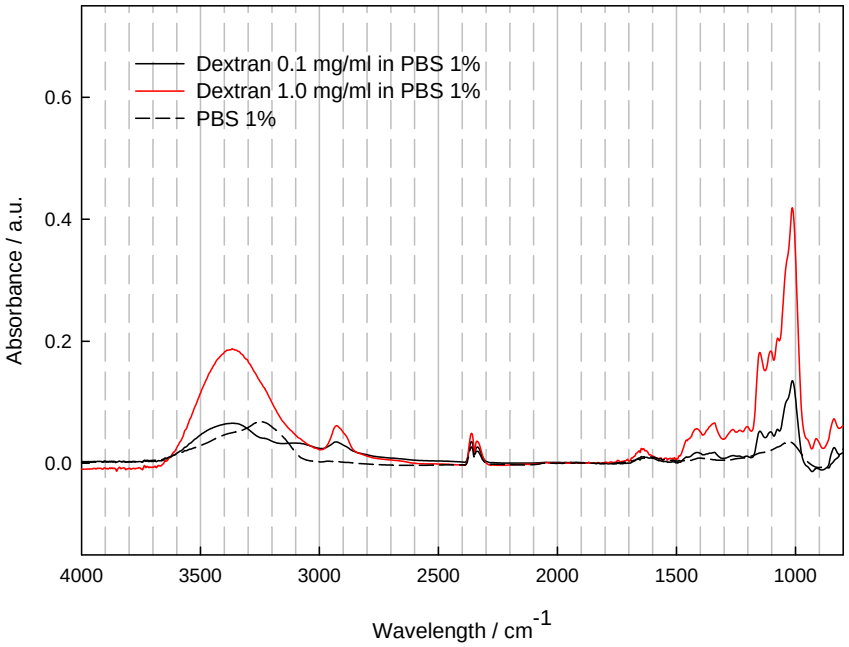

Figure 2-3. ATR spectra of a dextran thick film obtained by casting PBS 1% buffered solutions on clean and *plasma* activated Ge IRE. The black spectrum refers to the film obtained from 0.1 mg/ml solution. The red spectrum refers to the film obtained from 1.0 mg/ml solution. The black dashed profile is the ATR spectrum of PBS 1% buffer cast and evaporated on the Ge IRE.

The red spectrum refers to dextran 1.0 mg/ml in PBS 1% and the black line refers to the ten times diluted solution. The good featured profile of both spectra outstands: it

can be attributed to the plasma pretreatment. The same quantity of analyte and buffer is more homogenously spread over the plate and the evaporation leaves behind an almost ubiquitously homogenous thick film. The plasma pretreatment enhances the reproducibility of the measured spectra. Moreover, comparison with the untreated sample (Figure 2-2) reveals that the signals of the buffer are much less pronounced after plasma treatment, in particular for the lower dextran concentration. First, this indicates that buffer and dextran have a distinct way to interact with the surface; second, dextran, when blended with PBS, displays a more favorable dispersion over the plasma pretreated surface.As a consequence, a larger concentration of dextran relative to the buffer is detected near the interface which is probed by the evanescent field.

2.2.1.1. Effect of plasma pre-treatment

Pretreatment procedures play obviously a crucial role in polymer adsorption[58-60]. The effect of plasma activation as eventual enhancement for dextran physisorption was object of investigation in this work. Figure 2-4 depicts two pairs of ATR spectra referring to germanium IRE temporary put in contact with solution of dextran 0.1 mg/ml in PBS 1% after cleaning with and without plasma treatment (the dotted and solid line, respectively). The difference between the red and black spectra lies in the way dextran and surface entered in contact. In one case (red) by dipping in 10 ml of the mentioned aqueous solution for 2 hours, in the other by spotting 0.2 ml to cover one side of the IRE and incubating for the same time. After incubation, the IREs were gently rinsed in water.The conditions applied respond to the requirement of polymer physisorption on the surface[61, 62]. Two conclusions can be drawn. First, the spontaneous interaction of dextran and germanium, under this condition, is not detectable. The bands reveal the presence of PBS on the surface. Second, the plasma pretreatment favors and stabilizes the interaction between the PBS buffer and the

surface. It must be noted that casting with the same technique over not plasma pretreated IREs, did not generate any detectable interaction, neither for dextran nor for PBS buffer.

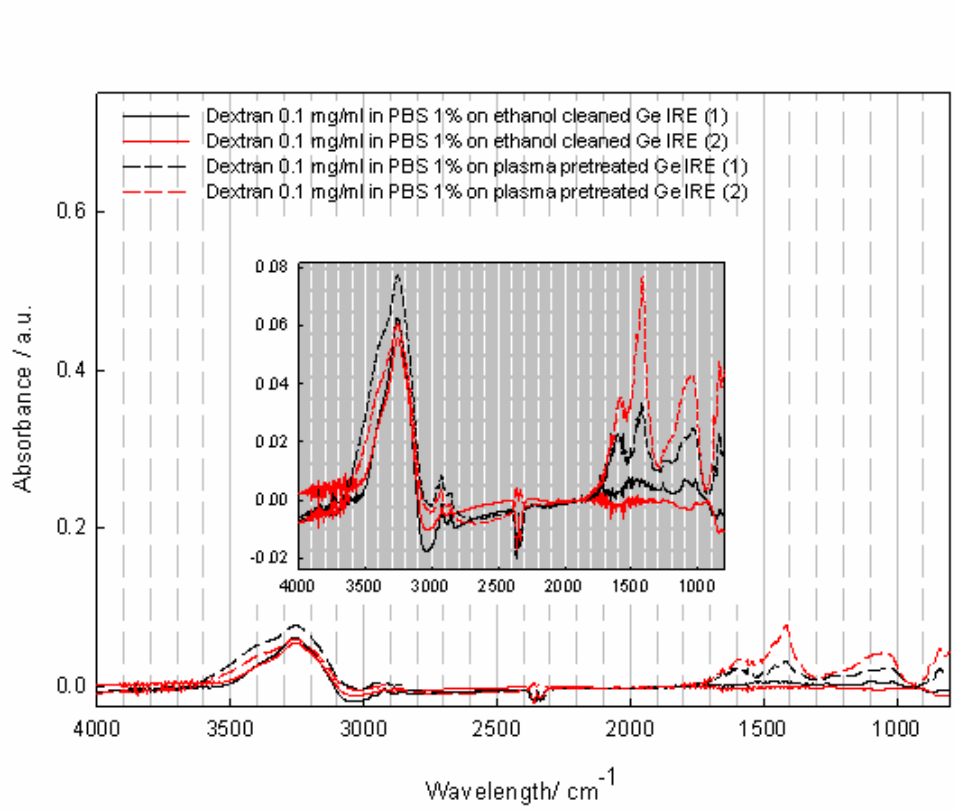

Figure 2-4. ATR spectra (*ex situ*) IREs put in contact with a dextran solutions according to different casting methods and pretreatments. The dashed spectra relate to dextran applied to plasma pretreated IRE. The solid line spectra relate to dextran applied to *not plasma* pretreated IRE. Black and red profiles discriminate the physisorption techniques. Black profiles refer to dextran liquid film spotting and 2 hours incubation before removal, technique (1). Red profiles refer to 2 hours dipping in a dextran PBS 1% buffered solution, technique (2). The scale was kept the same as in previous Figures to facilitate comparison. The gray inset shows a blow up of the spectra. Using both techniques, plasma activation enhances adsorption of PBS 1%.

The findings described above refer to *ex situ* measurements and endow the required information to optimize the design of *in situ* measurements, using a double cell holder embedded in a SBSR attachment. Plasma pretreatment allows detectable interaction with the PBS buffer also after water rinsing and favors a more homogenous casting of

dextran and PBS on the surface. This was judge in the right direction to set plasma cleaning as routine protocol step. The confirmation arrived when the role of charges was elucidated (cfr. later on in the text).

2.2.1.2. Effect of ionic strength effect

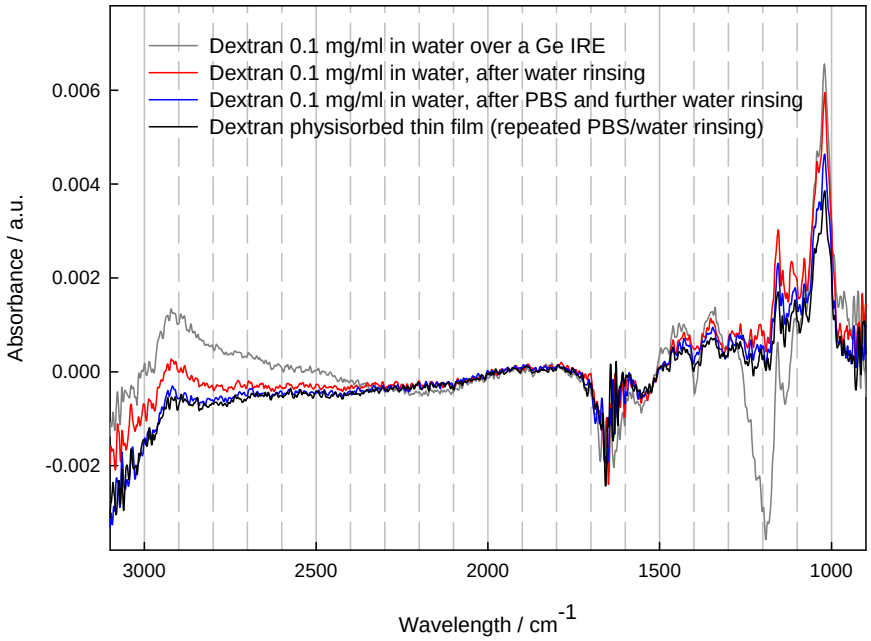

Figure 2-5. Dextran physisorption applied to plasma pretreated Ge IRE and investigated in situ by ATR spectroscopy using the SBSR attachment. The gray spectrum relates to the IRE exposed to the dextran 0.1 mg/ml aqueous solution for 30 min. The signal contains thin film (absorbed) and bulk (dissolved) contribution. The red spectrum relates to the same functionalized IRE when flooded with water after the exposure to the dextran solution. This spectrum contains only the contribution belonging to the thin film and stays stable. Further rinsing is performed to test the stability of the physisorbed polymer layer: one cycle of PBS and water resulted in the blue spectrum and after three repeated cycles of PBS and water the black spectrum was registered. A tiny removal is observed but the dextran, when applied in pure water, can be stated to adsorb on to the surface.

A first *in situ* series of experiments using dextran 0.1 mg/ml in aqueous solution helped to evaluate the ionic strength effect linked to the presence of the PBS buffer. The Ge IRE when flooded with dextran 0.1 mg/ml in PBS 1% does not result in significant dextran signals, meaning that no detectable spontaneous interaction

between dextran and surface occurs under the applied conditions (data not shown). Figure 2-5 shows a set of spectra recorded while flowing dextran 0.1 mg/ml in water (i.e. in the absence of PBS). The gray spectrum was recorded after 30 min. The signal appears and stays constant. It is the sum of dissolved (bulk) and adsorbed dextran. The following water rinsing step allowed to get rid of the bulk dextran signal, and to verify the presence of signal due to adsorbed dextran. The dextran signal diminishes but still stays even after two supplementary cycles of PBS and water rinsing. The final signal is stable enough to claim the presence of physisorbed dextran. This finding clearly shows that the PBS buffer competes with dextran and largely prevents physisorption of the latter.

2.2.1.3. Effect of concentration

After the exploration of the salt effect (presence/absence), the influence of dextran concentration on adsorption was investigated. From Figure 2-6, it appears that the remaining adsorbed dextran, after washing, is almost the same even after 10 or 50 fold increase of concentration. Therefore the surface is saturated already at solution concentration of 0.1 mg/ml.

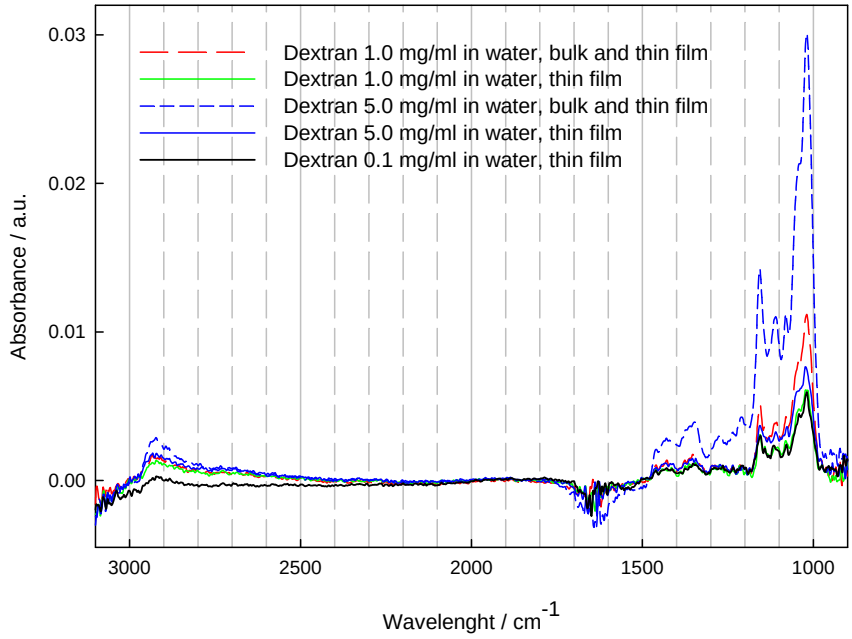

Figure 2-6. Influence of the solution concentrations of dextran on physisorption investigated by *in situ* ATR. When the dextran solution is flown over the surface, the ATR spectra are composed of bulk and thin film contributions. The isolated thin film contribution can be appreciated only when water is flown through, afterwards. The black spectrum related to dextran 0.1 mg/ml in water (thin film) is the same as the one reported in Figure 2-5

2.2.1.4. Competitive antibody-dextran adsorption onto the surface

Passivation properties of dextran are well known for dextran covalently linked to the surface[13, 48, 50]. It was therefore judged worthy to explore a competitive antibody/dextran physisorption toward a germanium IRE (internal reflecting element).

For this test a solution of monoclonal anti-TNFα (human tumor necrosis factor-α, a cytokine responsible for the regulation of cellular physiology) antibody (AB), 100 µg/ml in PBS was used[63].

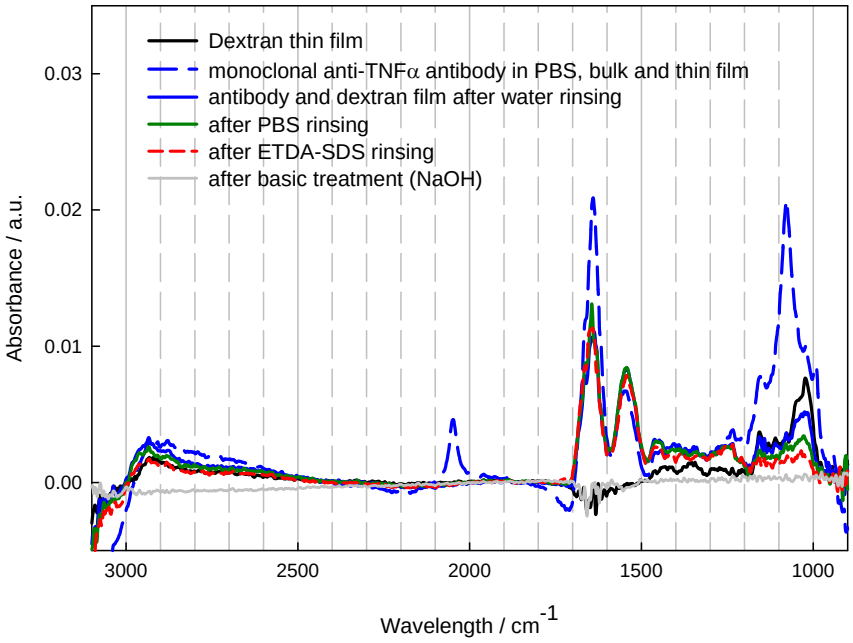

Figure 2-7. *In situ* ATR spectra of the competitive antibody-dextran adsorption on to Ge IRE (SBSR technique applied). After performing *in situ* dextran physisorption (black spectrum) the antibody was flown through the sample chamber of the microfluidics system of the SBSR attachment (blue dashed spectrum). After water washing contributions coming from both dextran and antibody were registered (plane blue spectrum). PBS rinsing and water (green spectrum, registered while water was flowing), ETDA-SDS and water (red dashed spectrum, registered while water was flowing), and NaOH treatment (gray spectrum, registered while water was flowing afterwards) were performed.

The solution was pumped into the sample compartment previously functionalized by absorbed dextran (in water, black spectrum in Figure 2-7) for 30 min. The blue dashed line depicts the characteristic IR absorption bands of an antibody (bulk and eventual thin film contribution). To estimate the adsorption, both compartments were rinsed with water. The resulting spectrum (solid blue line) assessed adsorption of anti-TNFα AB and the decrease of dextran related signal due to desorption. Further and

harsher rinsing technique using ETDA 50 mM (ethylenediaminetetraacetic acid disodium salt dehydrate, chelating agent) in combination with SDS 150 mM (sodium dodecyl sulfate) determined almost no removal of the AB and important desorption of dextran (red spectrum). The experiment guides to the conclusion that the antibody has a higher affinity for the surface and the competitive adsorption of antibody and dextran under these condition results in preferred direct interaction of the antibody with the Ge IRE. Such an experiment was designed to sustain, within the experimental grasp of this work, that dextran needs to be covalently linked to the surface to unfold the effectiveness of its passivation properties. The photobonding technology responds to this demand[38, 48, 49]. Furthermore, the described experiment emphasizes the importance of a deeper understanding of the physisorption phenomenon.

2.2.2. Amino Detran physisorption

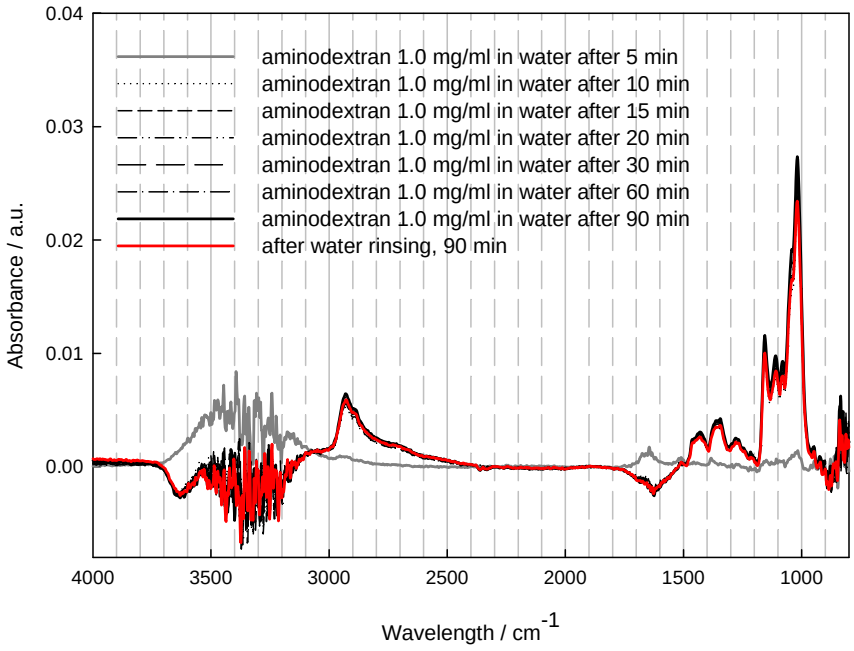

Figure 2-8. In-situ ATR (SBSR) spectra of physisorption of aminodextran. Plasma activated GE IRE was exposed to 1.0 mg/ml solution in pure water over 90 min and rinsed with for 30 min. A characteristic negative band is observed at 3630 cm^{-1}.

The amino dextran investigated is the same as the one used as starting material for the OptoDex® family synthesis. It is an Invitrogen product (former Molecular Probes, batch 6501-1), characterized by a glucose α-1,6- glucosidic linkage with molecular weight of 40.000 Dalton. Each polymeric unit contains 8 amino groups in total, more precisely 4 pairs of 2 primary amines coupled in the same unit per 55 glucose units. These numbers derive from a rough calculation if considering the dextran/ single glucose unit molecular weight ratio (cfr. Figure 2-1).

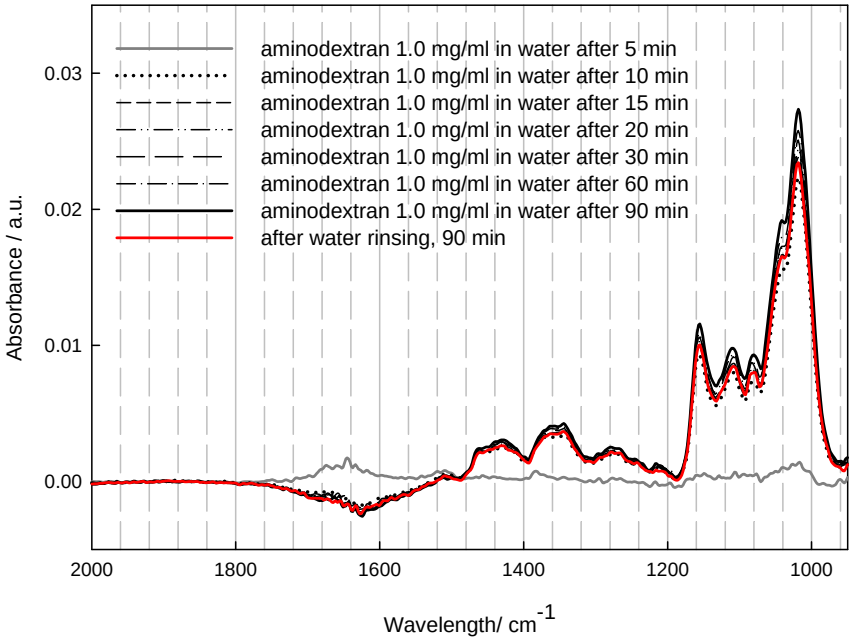

Figure 2-9. Blow up of Figure 2-8 in the aminodextran finger print region. OH water bending δ (OH) region at 1650 cm^{-1} is also included.

Figure 2-8 shows ATR-IR (SBSR) spectra of *in situ* physisorption of aminodextran recorded while flowing aminodextran solution over the IRE. Plasma activated Ge IRE was exposed to 1.0 mg/ml solution in pure water over 90 min and rinsed with water for 30 min. Overlapping of spectra suggested fast physisorption kinetics (cfr. Figure 2-14). A blow-up of the same spectra is given in Figure 2-9. The same in situ

functionalization and SBSR measurements were carried out using aminodextran 0.1 mg/ml in water on plasma activated Ge IRE as reported in Figure 2-10 and Figure 2-11 (blow-up).

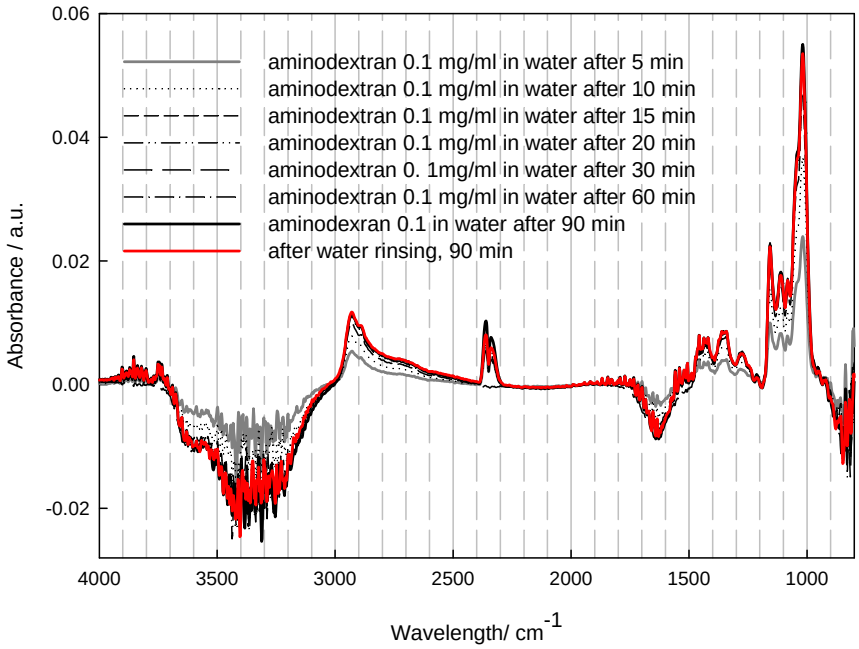

Figure 2-10. In situ ATR (SBSR) spectra of physisorption of aminodextran. Plasma activated Ge IRE was exposed to 0.1 mg/ml solution in pure water over 90 min and rinsed with water for 30 min. A characteristic negative band is observed at 3630 cm^{-1}.

Upon adsorption of aminodextran, water is removed from the volume probed by the evanescent field. This can be deduced from the increasing signal at 1157 cm^{-1} while decreasing absorption is registered at 1650 cm^{-1} associated with the water bending vibration, δ(OH). The same is observed for the water stretching in the region 3200-3600 cm^{-1} (cfr. Figure 2-8 and Figure 2-10). A very characteristic negative band is observed at 3630 cm^{-1} upon adsorption of aminodextran. This band can be ascribed to the O-H stretching vibration of Ge−OH groups on the surface[59]. These groups are generated by the plasma treatment and subsequent immersion in water[64]. The appearance of this negative band can be ascribed to the deprotonation of the Ge−OH

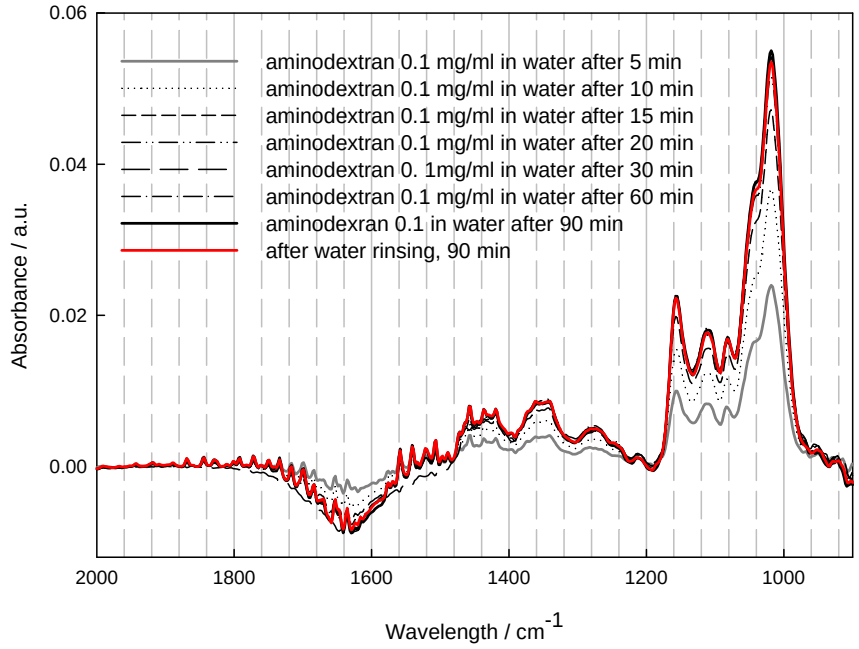

Figure 2-11. Blow up of Figure 2-10 in the aminodextran fingerprint region. OH water bending region at 1650 cm^{-1} is also included, δ (OH).

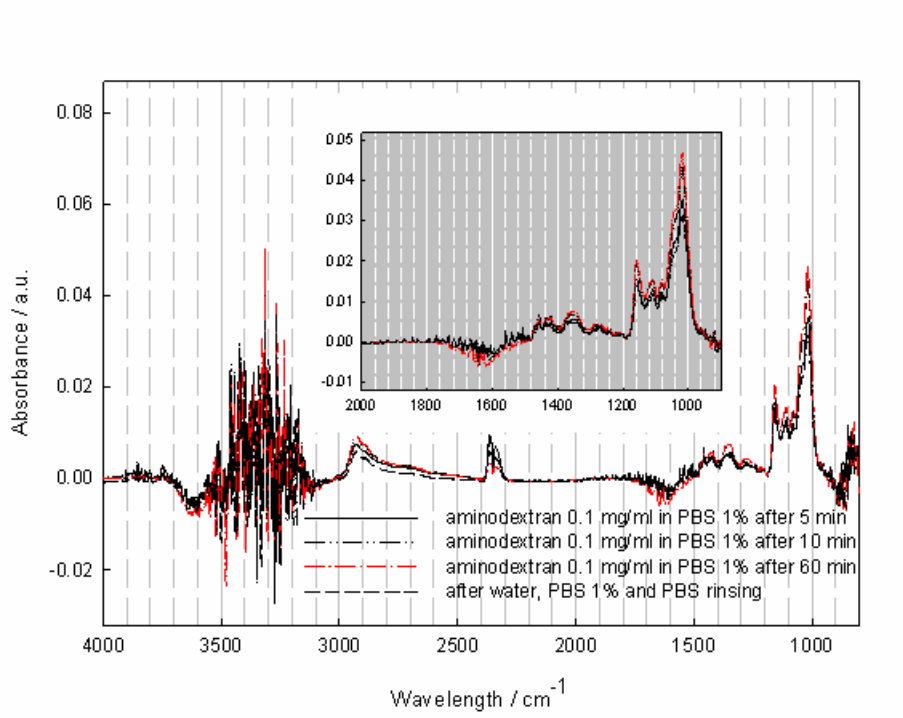

Figure 2-12 *In situ* ATR (SBSR) spectra of physisorption of aminodextran. *Plasma* activated Ge IRE was exposed to 0.1 mg/ml solution in PBS 1% over 90 min and rinsed with water for 30 min. A blow-up in the aminodextran fingerprint region is included (gray backplane graphic). A characteristic negative band is observed at 3630 cm^{-1}.

or to a strong red-shift, due to intermolecular interaction, leading to a superposition with the water band. In any case this observation may be the key for the understanding of the positive effect of plasma activation on physisorption and for the understanding of the mechanism of physisorption in general.It is worthy to note that without plasma cleaning this band at 3630 cm^{-1} is not observed (see Figure 2-13, later on). Similarly, it is known that in the case of typical alkyl silanes SAMs (self-assembled-monolayers) formation on Si/SiO_2 the number of direct Si-O-Si bond with the surface is relatively low[59, 60, 65].It supports the model of a pre-organization before the direct surface interaction[66] and stresses the role of the hydroxyl layer in the mechanism of bonding between polymer and surface. Furthermore, in some model the surface-polymer coupling is estimated to exclusively depend to the surface hydroxy groups[65, 67].

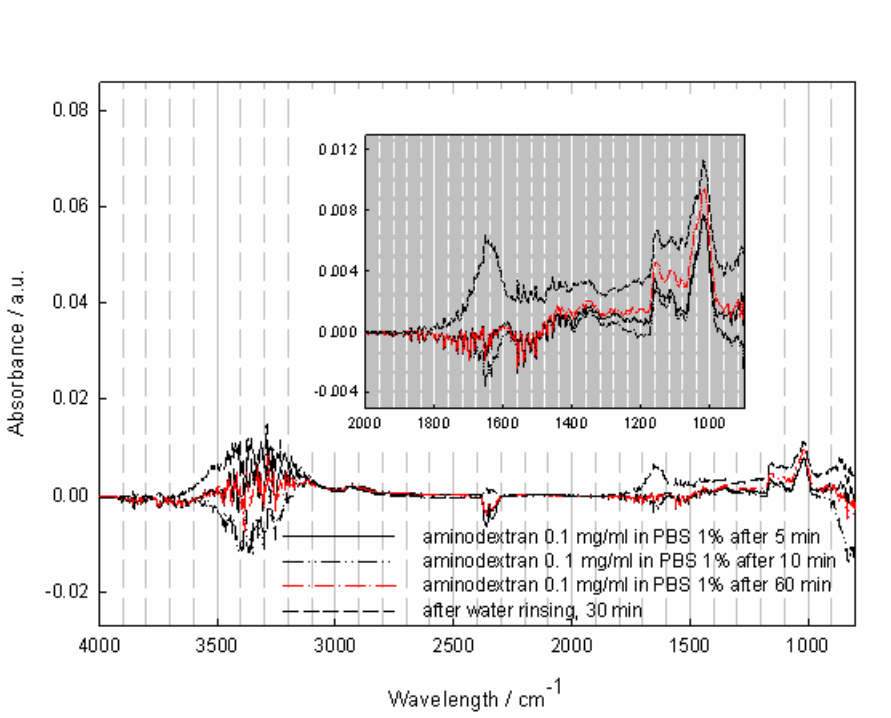

Figure 2-13. *In situ* ATR (SBSR) spectra of physisorption of aminodextran. Not plasma activated Ge IRE was exposed to 0.1 mg/ ml solution in PBS 1% over 90 min and rinsed with water for 30 min. A blow-up in the aminodextran fingerprint region is included (gray backplane graphic). The characteristic negative band at 3630 cm^{-1} is not observed.

The band at 3630 cm^{-1} was not observed for dextran, which suggests an interaction between the O-H groups of the surface and the amino groups of aminodextran acting as anchor to the surface. Interestingly, this anchor is close to the photolinker group in the OptoDex®, fact which could promote the photobonding to the surface. Aminodextran is mostly used for bioassays format and the use of buffer is often recommended. This consideration inspired the investigation of the physisorption behavior in presence of PBS 1% buffer. Figure 2-12 depicts ATR spectra and blow-up of aminodextran 0.1 mg/ml in PBS 1% physisorption on plasma activated Ge IRE. Clearly aminodextran does absorb under these conditions, in contrast to dextran. Because the ionic strength changes significantly (and furthermore in this case the polymer is positively charged) it seemed worthy to carry out a series of measurements using PBS 1% buffered solution over *not plasma* pretreated Ge IRE, as reported in Figure 2-13**.** From this experiment it can be concluded that some physisorption occurs but not as much as with plasma pretreatment. Additionally, it can be noted that there is no sign of PBS, indicating that, PBS does not adsorb under these conditions.

2.2.2.1. Kinetics of the adsorption process

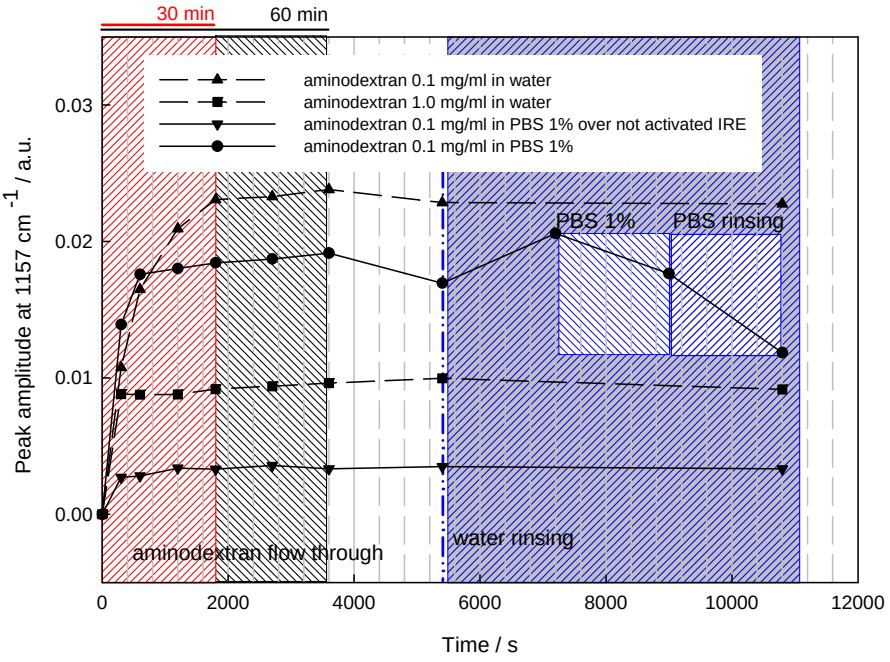

Figure 2-14. Physisorption kinetics of aminodextran under different conditions: solutions differed for concentration (0.1 mg/ml and 1.0 mg/ml) and ionic strength (pure water and PBS 1% buffer). The same conditions were applied (90 min aminodextran flow through and 1 hour water rinsing) except for the aminodextran solution 0.1 mg/ml in PBS 1%. In this case the presence of the buffer in the solution containing the polymer justified the use of progressive ionic strength solution for rinsing to test the stability of the adsorbed thin film. Ge IREs were plasma cleaned and activated. In one case (top down triangle) the Ge IRE was plasma cleaned, but used 24 hours after the activation and stored in water.

The spectra reported so far can be considered for the investigation of the kinetics of physisorption of aminodextran. The influence of the three following factors was considered: concentration (1.0 mg/ml and 0.1 mg/ml), ionic strength (water and PBS 1%) and surface pretreatment (basic polishing and ethanol rinsing or plasma activation). The absorption peak at 1157 cm-1 was selected in order to follow the kinetics of adsorption due to the strength of this band and due to the fact that at this wavenumber Ge (Ge oxide) does not interfere. To get rid of any baseline drift during the longterm experiments, the peak amplitude was calculated as difference of the

absorbance value at 1157 cm^{-1} and the value at 1182 cm^{-1} where no absorbance bands are observed.

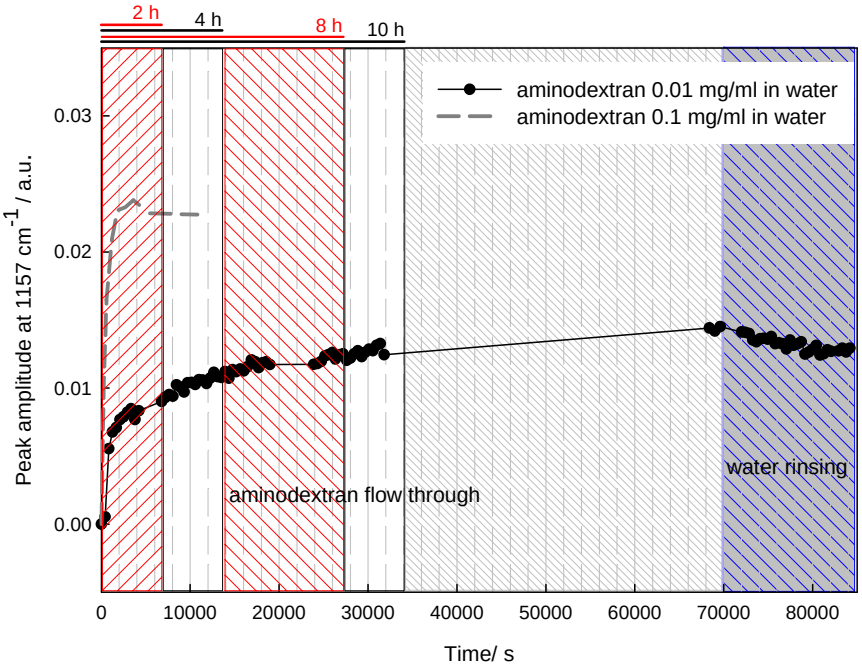

Figure 2-15. Physisorption kinetics behavior of aminodextran solution 0.01 mg/ml and 0.1 mg/ml in pure water. Because of the ten times diluted concentration, the solution was allowed to flow over the surface for more than 10 hours and the rinsing step by water last 3 hours. The dashed gray line refers to the behavior of aminodextran solution 0.1 mg/ml in water.

For a solution concentration of 0.1 mg/ml in water it takes about 1880 s to saturate the surface, whereas in the presence if PBS 1% this takes only 600 s. This effect may be due to the compression of the diffuse electrical double layer in the latter case[68, 69]. At high aminodextran coverage the surface is positively charged, which leads to coulomb repulsion between surface and dissolved aminodextran. This reduces the adsorption rate. Due to the increased ionic strength the repulsion is less effective and adsorption is faster[70]. Data reported in Figure 2-14 lead to the following conclusion: (1) the absence of plasma pretreatment tremendously affects the physisorption capacity; (2) the lower concentration establishes a slower but more effective adsorption on plasma

pretreated surfaces; (3) the presence of salts slightly reduces the final physisorption amount. In the case of aminodextran 0.1 mg/ml in PBS 1% a rinsing step varying the ionic strength was judged opportune to amplify the eventual effect of the buffer on the polymer surface interaction. Finally, it can be claimed that PBS at such concentration renders the adsorption faster but also promotes desorption. These data will be further discussed later on, as basis for the film thickness determination. The observation that the lowest concentration at the lowest ionic strength seems to provide the best physisorbtion performance, inspired the investigation of the polymer behavior at even ten fold lower concentration, namely 0.01 mg/ml. Figure 2-15 shows that at this concentration the adsorption becomes very slow after some time. A main conclusion emerging from these experiments is that charge plays a crucial role. The charge of the polymer itself at a certain pH, the charge as buffer contribution (ionic strength), and the charge on the activated surface. In this perspective, the plasma activated Ge IRE can be regarded as a negatively charged partner in the surface/polymer interaction during the physisorbtion. This was the reason for moving towards the investigation of a negatively charged dextran based polymer.

2.2.3. Carboxymethyl dextran physisorption

Carboxymethyl dextran is an Invitrogen product (former Molecular Probes), characterized by a glucose α-1,6- glucosidic linkage with molecular weight of 70.000 Dalton. Each polymeric unit contains 71 carboxyls in total, namely 8 carboxylic groups per 11 glucose units.

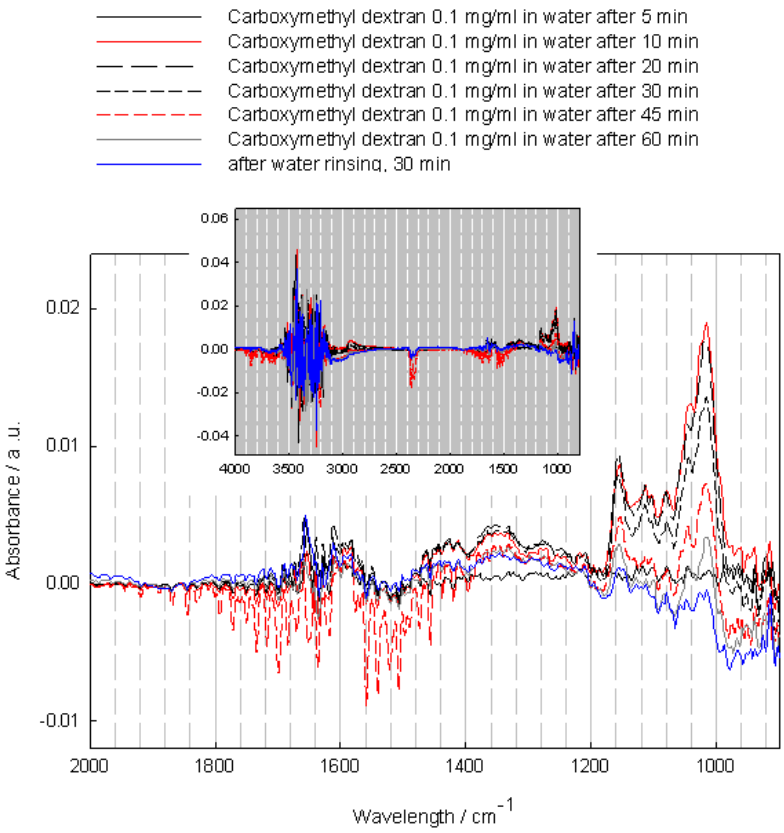

Figure 2-16. *In situ* ATR (SBSR) spectra of physisorption of carboxymethyl dextran in the 2000-900 cm^{-1} wavelength range (dextran fingerprint region). *Plasma activated* Ge IRE was exposed to 0.1 mg/ml solution in pure water over 60 min and rinsed with water for 30 min. The original spectra in the 4000-800 cm^{-1} wavelength range are depicted in the gray backplane graphic.

These numbers derive from a rough calculation considering the dextran/single glucose unit molecular weight ratioAt pH comprised between 5.5 and 7.4 (as determined using deionized water or PBS 1% buffer as solvent, respectively) carboxymethyl dextran is

negatively charged. From the experiments described above, 0.1 mg/ml could be assessed as the best concentration for the purpose of this work.

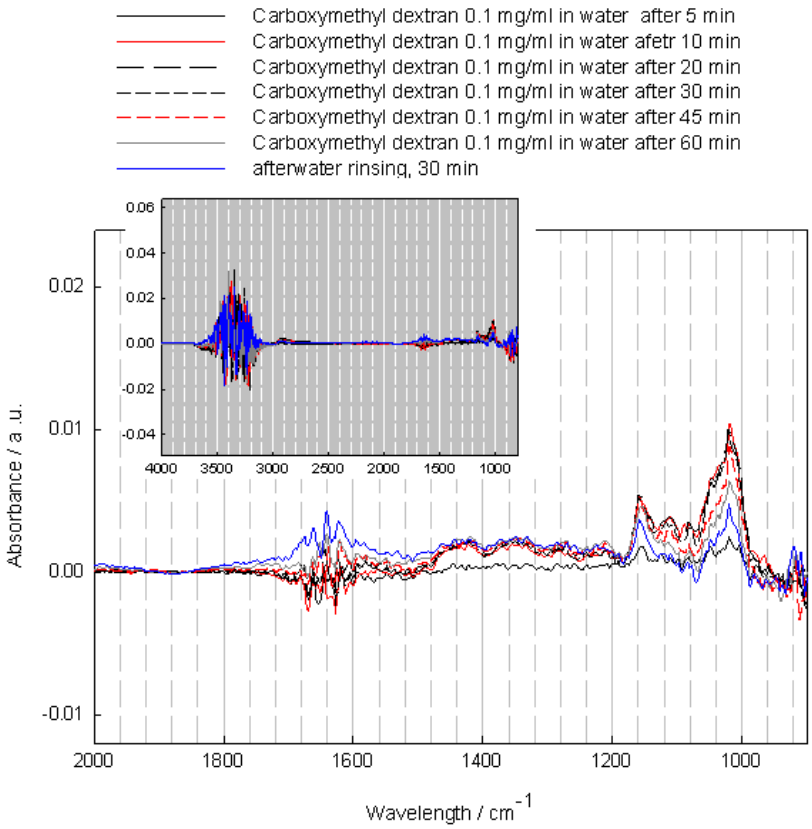

Figure 2-17. *In situ* ATR (SBSR) spectra of in situ physisorption of carboxymethil dextran in the 2000-900 cm^{-1} wavelength range (dextran fingerprint region). *Not plasma* activated Ge IRE was exposed to 0.1 mg/ml solution in pure water over 60 min and rinsed with water for 30 min. The spectra in the 4000-800 cm^{-1} wavelength range are depicted in the gray backplane graphic.

In Figure 2-16 the ATR spectra depicting the physisorption of carboxymethyl dextran over plasma activated Ge IRE are reported. A further experiment was carried out using carboxymethyl dextran 0.1 mg/ml in PBS 1% over plasma pretreated surface. Figure 2-17 depicts spectra referring to the same solution over not activated Ge IRE. The observation of the kinetic behavior facilitated the comparison and the conclusions harvest.

2.2.3.1. Kinetics of the adsorption process

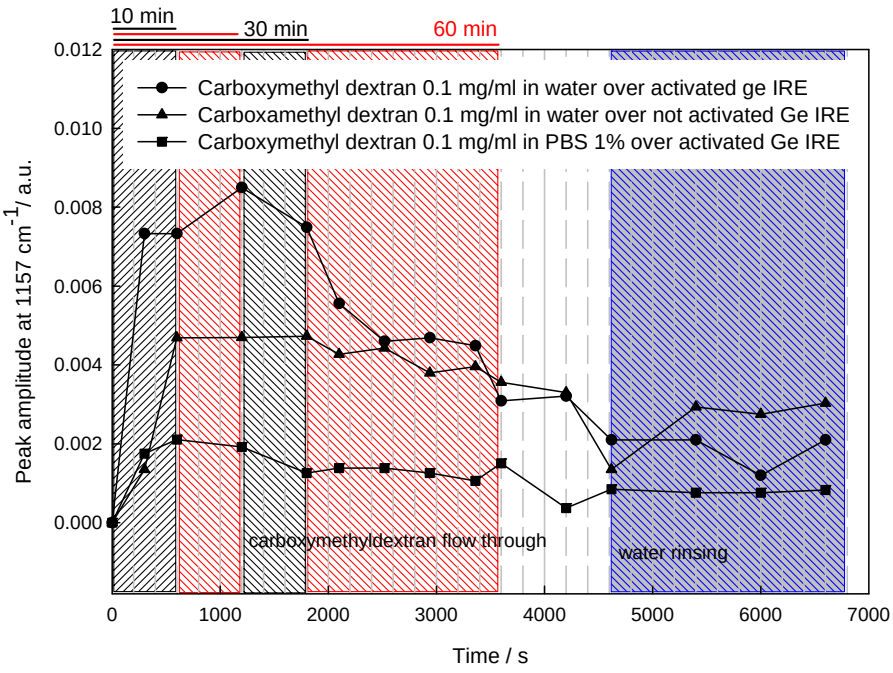

Figure 2-18. Comparison of physisorption kinetics behavior of carboxymethyl dextran 0.1 mg/ml solutions differing for ionic strength (pure water and PBS 1% buffer) and surface activation. The same conditions were applied (75 min carboxymethyl dextran flow through and 45 min water rinsing). In one case (top up triangle) the Ge IRE was plasma cleaned and kept in pure water for 24 hours.

Figure 2-18 allows comparison of kinetics of carboxymethyl dextran adsorption from water and PBS 1% on activated and not activated Ge IRE. According to this data, it can be evidenced that plasma induced physisorption enhancement is lost in the case of a negatively charged dextran based polymer. The following conclusion can be drawn. The carboxy sample adsorbs weaker than the amino dextran. Moreover, after a short-term interaction the polymer starts desorbing.

2.2.4. OptoDex ® dextran based polymers physisorption.

2.2.4.1. OptoDex ® C physisorption

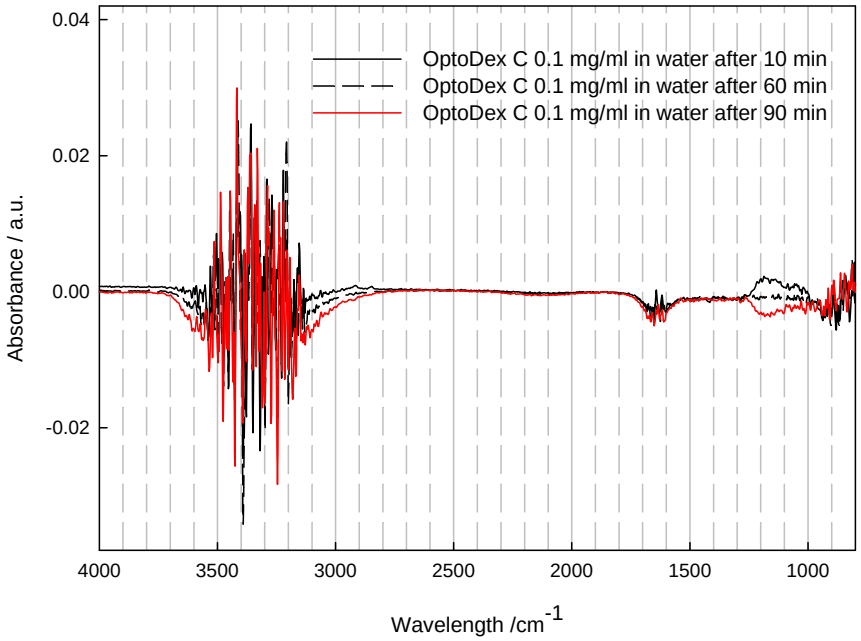

Figure 2-19. *In situ* ATR (SBSR) spectra of physisorption of OptoDex® C. *Plasma activated* Ge IRE was exposed to 0.1 mg/ml solution in pure water over 90 min.

Figure 2-19 reports the *in situ* investigation via ATR spectroscopy of OptoDex® C physisorption on plasma activated Ge IRE. A solution of OptoDex® C 0.1 mg/ml in water was put in contact with the plasma pretreated IRE for 90 min. Within this period no significant interaction was observed.

2.2.4.2. OptoDex ® B physisorption

OptoDex® B is an actinic dextran based polymer *a priori* not charged in the considered pH range (5.5 up to 7.4). In Figure 2-20 physisorption of such a polymer from 0.1 mg/ml in water on plasma activated Ge IRE is shown as investigated by ATR

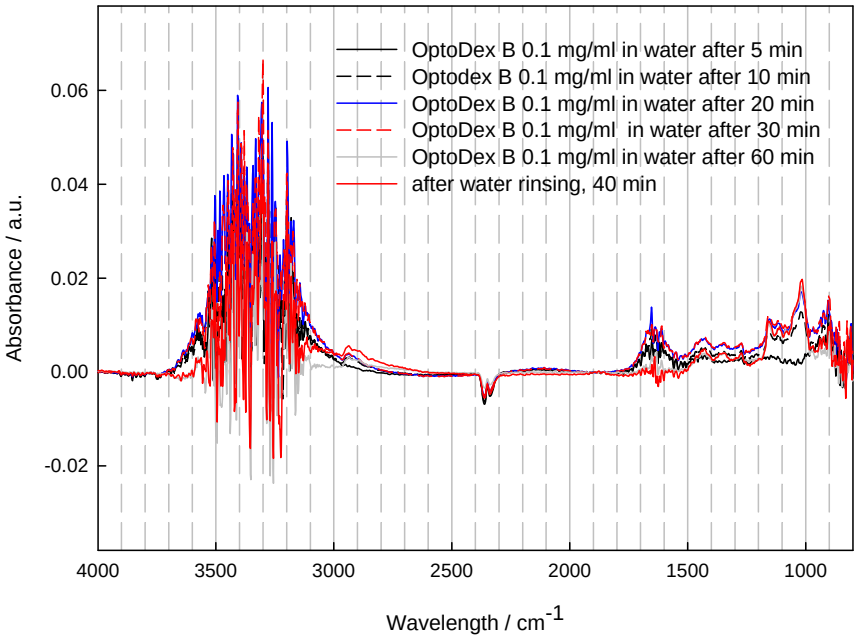

Figure 2-20. *In situ* ATR (SBSR) spectra of physisorption of OptoDex® B. Plasma activated Ge IRE was exposed to 0.1 mg/ml OptoDex® B in pure water over 60 min and rinsed with water for 40 min.

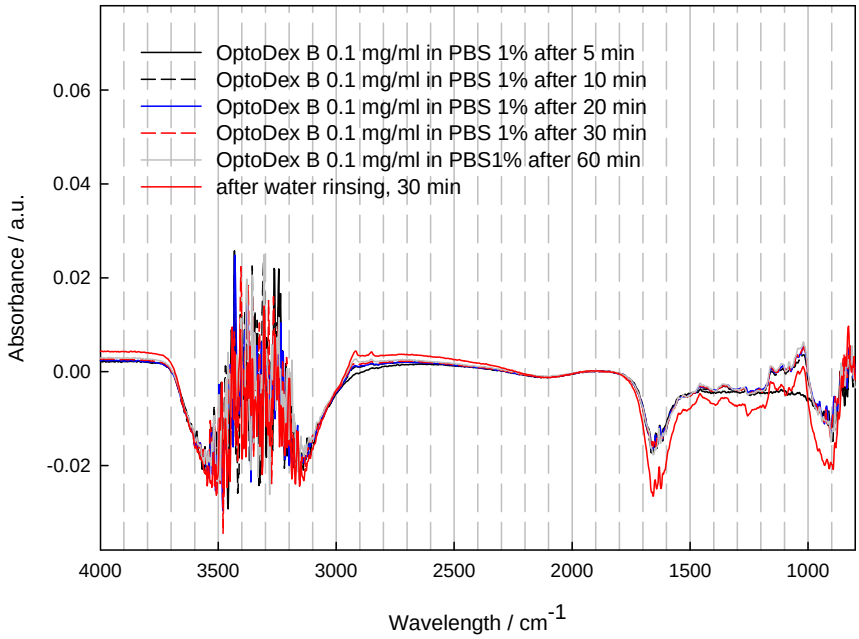

Figure 2-21. *In situ* ATR (SBSR) spectra of physisorption of OptoDex™ B. Plasma activated Ge IRE was exposed to 0.1 mg/ml OptoDex® B in PBS 1% over 60 min and rinsed with water for 40 min.

spectroscopy. Again the influence of ionic strength was probed using PBS 1% buffer as solvent. Figure 2-21 shows the physisorption of OptoDex® B 0.1 mg/ml in PBS 1% over plasma activated Ge IRE. Also in this case the increased ionic strength inhibits the polymer/surface interaction. This consideration is supported by Figure 2-22 where the kinetics behavior under the different conditions (adsorption from water or PBS 1%) is outlined.

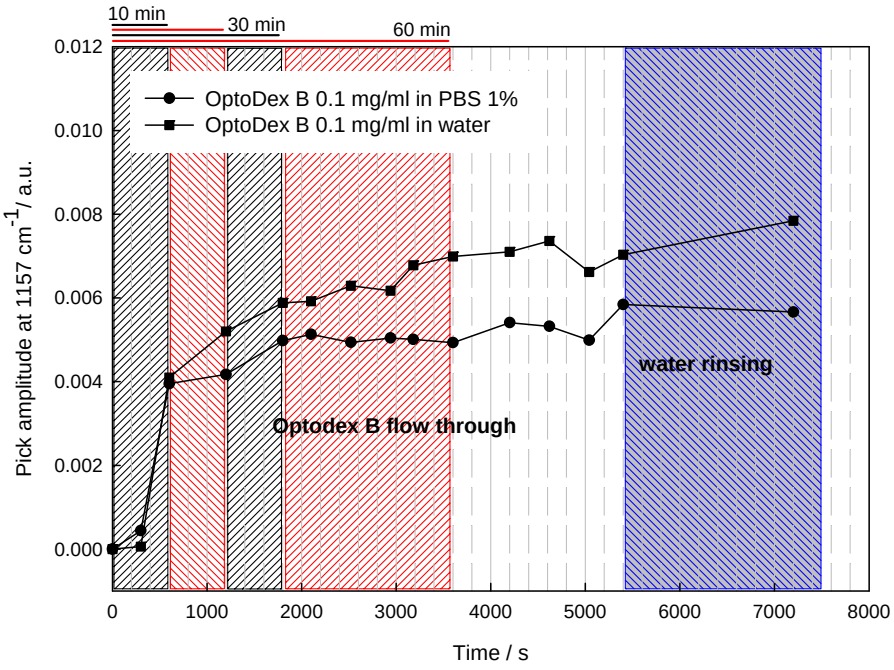

Figure 2-22. Physisorption kinetics behavior comparison of OptoDex® B 0.1 mg/ml solutions differing for ionic strength (pure water and PBS 1% buffer) on plasma activated Ge IRE. The same conditions were applied (90 min OptoDex B flow through and 30 min water rinsing).

2.2.4.3. OptoDex ® A physisorption

OptoDex® A is an actinic dextran based polymer a priori positively charged in the considered pH range (5.5 up to 7.4).

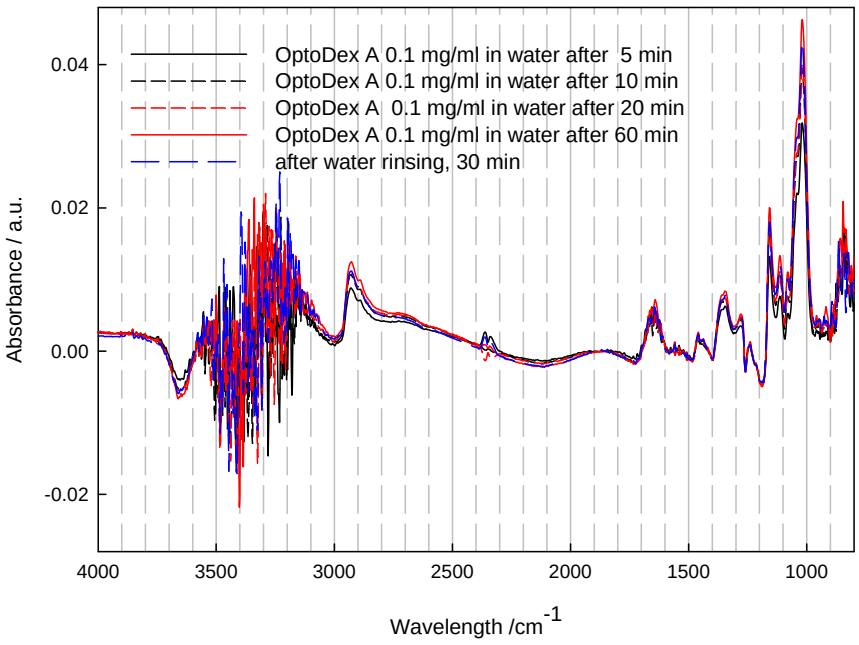

Figure 2-23. *In situ* ATR (SBSR) spectra of physisorption of OptoDex® A. Plasma activated Ge IRE was exposed to 0.1 mg/ml OptoDex® A in pure water for 60 min and rinsed with water for 30 min. Kinetic behavior is further explored in Figure 2-25.

In Figure 2-23 and Figure 2-24 ATR spectra are shown that were recorded during physisorption of this polymer 0.1 mg/ml in water and PBS 1%, respectively, on plasma activated Ge IRE. The increased ionic strength inhibits the polymer/surface interaction which is also supported by Figure 2-25 which depicts the kinetics of the adsorption process. A negative band at 3650 cm^{-1} appeared following the physisorption kinetics. It is observed only for OptoDex® A (not for B and C). This spectroscopic behavior is consistent with a specific interaction of the amino groups with the superficial $Ge-O-H$, which can be regarded as protonated germanium

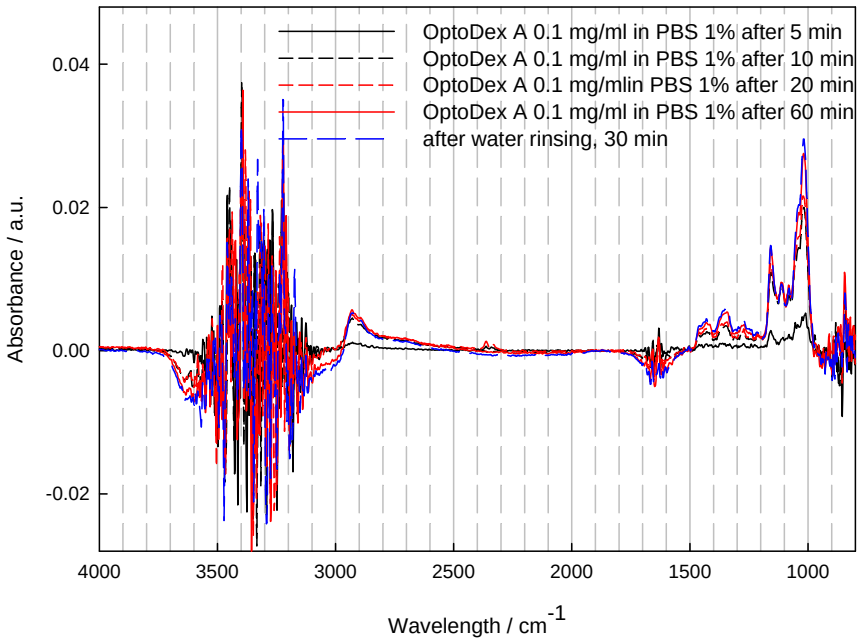

Figure 2-24. *In situ* ATR (SBSR) spectra of physisorption of OptoDex® A. Plasma activated Ge IRE was exposed to 0.1 mg/ml OptoDex® A in PBS 1% over 60 min and rinsed with water for 30 min. Kinetic behavior is further explored in Figure 2-25.

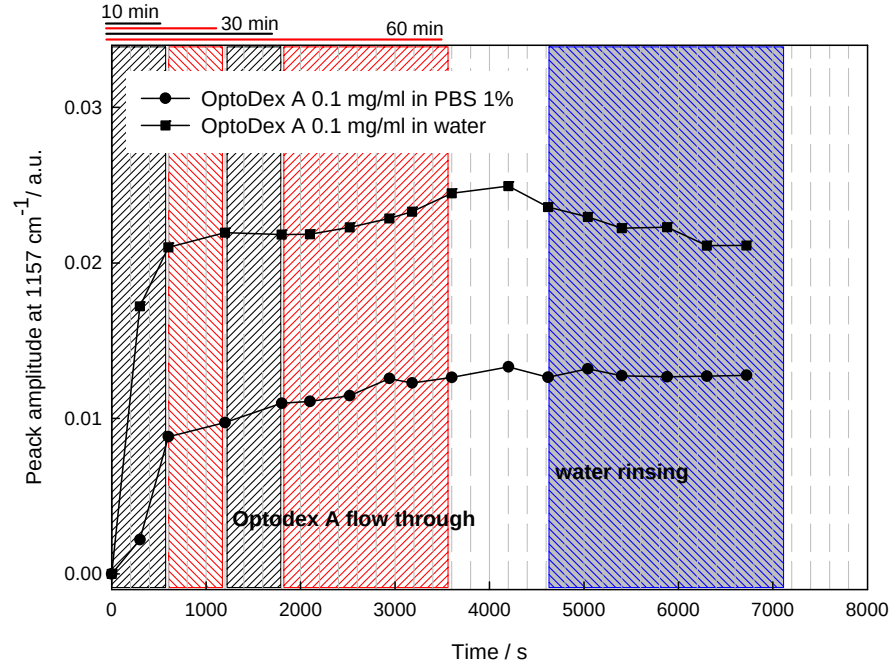

.

Figure 2-25. Comparison of physisorption kinetics behavior of OptoDex® A 0.1 mg/ml solutions differing for ionic strength (pure water and PBS 1% buffer) on plasma activated Ge IRE. The same conditions were applied as for OptoDex® B (75 min OptoDex® A flow through and 40 min water rinsing)

monoxide[68]. The charge separation at interface can be visually described as $Ge-O^{-}.....^{+}NH_3-dextran$. This observation represents a strong insight toward the understanding of the role of both, the charge and the plasma hydrophilic pretreatment.

2.2.5. Dextran based polymers covalent immobilization by photobonding

An ambitious goal of this work was to obtain spectroscopic evidence of the carbene generation. An on purpose tailored set-up for *in situ* UV exposure was designed and realized (Figure 2-26). The limitation, which turned out hard to overcome, was that the highest performance of the spectroscopic observation was achieved for the water/Germanium interface. These conditions led to spectra quality amenable for quantitative estimation even of monolayer adsorption. Unfortunately, the UV exposure does not suit to such conditions because water competitively interferes with the surface in the photobonding process.

Figure 2-26. PMIRRAS set up on porpose modified for *in situ* UV exposure. The left hand picture shows the spectrometer external layout (top view) with the optical bundles fixed on the holder, inside the measurement chamber. On the right hand is depicted a blow up of the metallic surface (20x12 mm) installed for simultaneous PM-IRRAS measurement and UV irradiation.

Nevertheless, spectroscopic measurements were carried out using another surface-sensitive IR spectroscopic method, notably Polarization Modulation Infrared Reflection Absorption Infrared Spectroscopy (PM-IRRAS). This technique, based on external reflection at metallic surfaces (namely Al/aluminium oxide) was considered more suitable for the analyisis of solid-gas interfaces. UV esposure can be performed in nitrogen atmosphere and in humid atmosphere in order to study the effect of water.

Such conditions were considered appropriate, to follow the kinetics of the formation of the highly reactive carbene intermediates and the carbene insertion reactions. The major interest lied in observing the interface during the irradiation, with the possibility to spot instable intermediates. It must be outlined that the ratio aryldiazirine/polymer unit is highly unfavourable to point out diazirine related changes: the eventual signal linked to the aryldiazirine breaking is damped by the dextran spectral fingerprint. Due to these difficulties, this branch of investigation was left out. ATR spectroscopy was used to provide indirect but unquestionable proof of the photobonding process, by comparing absorbance signals intensity before and after UV exposure and thorough rinsing. OptoDex® derived Ge IRE, presenting interface modified by thin or, alternatively, thick film as described in 2.1.1.2 where further dried by nitrogen flushing (2 minutes) and submitted to UV light exposure.

UV photo-exposure. Four minutes of high-power UV exposure at 365 nm at the power intensity of 11 mW/cm^2 were previously demonstrated to be necessary for light driven carbenes generation from an OptoDex® matrix[38]. The light source for the set of measurements using ATR-IR was a coupled optical bundle connected to high power ultraviolet lamp (Xenon Arc lamp, Oriel, USA). The light intensity from the bundle outlet was measured with a UV light intensimeter equipped with the 350 nm filter (Suss MicroOptics, Switzerland). Distance from the surface and time were adjusted to supply the required calculated irradiance. According to the optimized set-up, a Ge IRE was illuminated for 6 min setting the optical fibers outlet 15 mm away from the functionalized edge. Repeated exposures under the same conditions were performed all along the IRE length. Exposure was carried out eventually for an exceeding time without generating significant change in the photobonded polymer. After irradiation the sample was rinsed with water. The rinsing process was considered gentle when consisting of a few seconds of water flushing. The extensive

rinsing of the surface consisted of repetitive cycles followed by water dipping for 90 min.

2.2.5.1. ATR spectra and discussion

By *in situ* ATR measurements (see. Figure 2-19) it was demonstrated that OptoDex® C does not physisorb onto Ge IRE under the applied conditions.

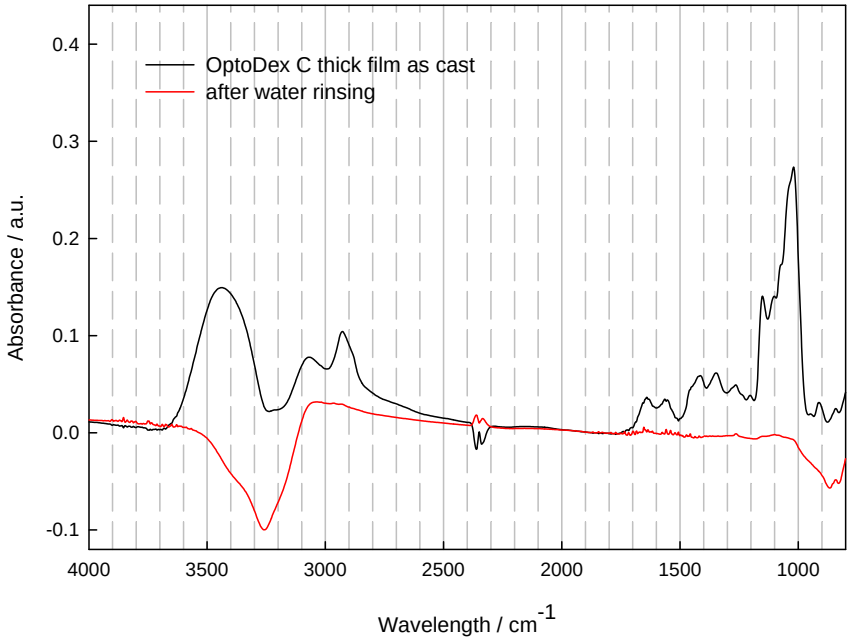

Figure 2-27. ATR spectra of OptoDex® C thick film obtained by casting 0.1 mg/ml solution in pure water on *plasma* activated Ge IRE (black spectra). The film was rinsed with water, without previous UV light exposure (red spectra).

Ex situ measurements were performed to have further evidence: a thick film was prepared on the surface. The prolonged contact and drying did not improve the quality of the interaction between the polymer and the surface. This conclusion can be drawn from Figure 2-27 which reveals no signal of OptoDex® C after water rinsing. In contrast, Figure 2-28 clearly shows that the UV exposure leads to the immobilization of the polymer on the surface even after copious rinsing. This series of spectra gives proof

of the photobonding effect: the polymer, which does not interact at all with the surface spontaneously, results immobilized onto Ge IRE as a consequence of the photoexposure. The figure furthermore shows that water rinsing and dipping lead to removal of a considerable amount of the polymer. In fact, the intensity of the band at 1157cm-1 drops to about 25% of the intensity after water rinsing and dipping.

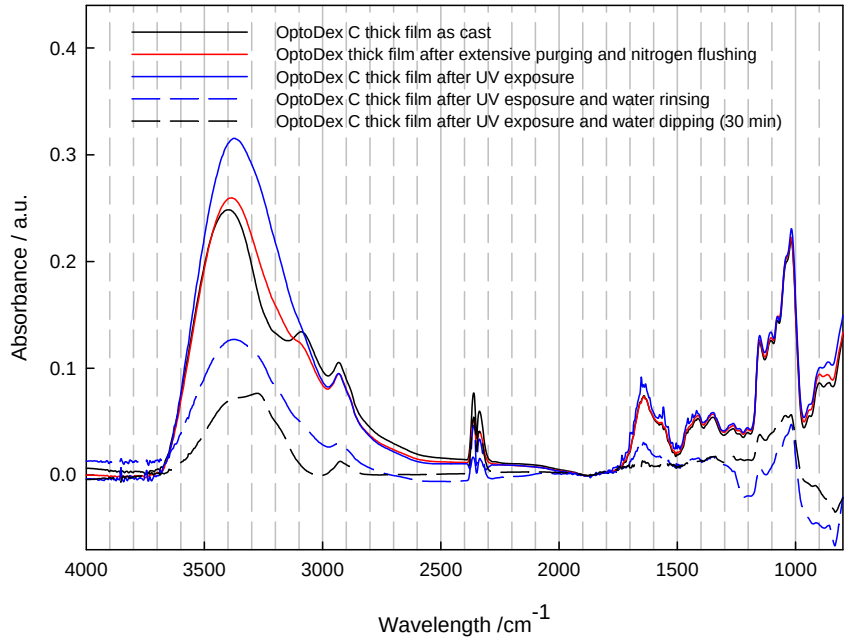

Figure 2-28. ATR spectra of OptoDex® C thick film obtained by casting 0.1 mg/ml solution in pure water on *plasma* activated Ge IRE (black spectra). Such a film was kept 1 hour under purging and further dried by nitrogen flushing (red spectrum). After UV exposure (blue solid line), quick rinsing by water was performed (blue dashed line). Finally the functionalized IRE was dipped in water for 30 min (black dashed line).

It can be deduced that after photoexposure the polymer molecules within the thick film (multilayers) are not completely interlinked. This finding indicates that photobonding to the surface is preferred over photobonding between polymer molecules. The same ex situ functionalization by thick film generation was performed using OptoDex® B 0.1 mg/ml in water. As can be seen from Figure 2-29 the UV exposure generates the expected carben hooks to fix the polymer onto the surface.

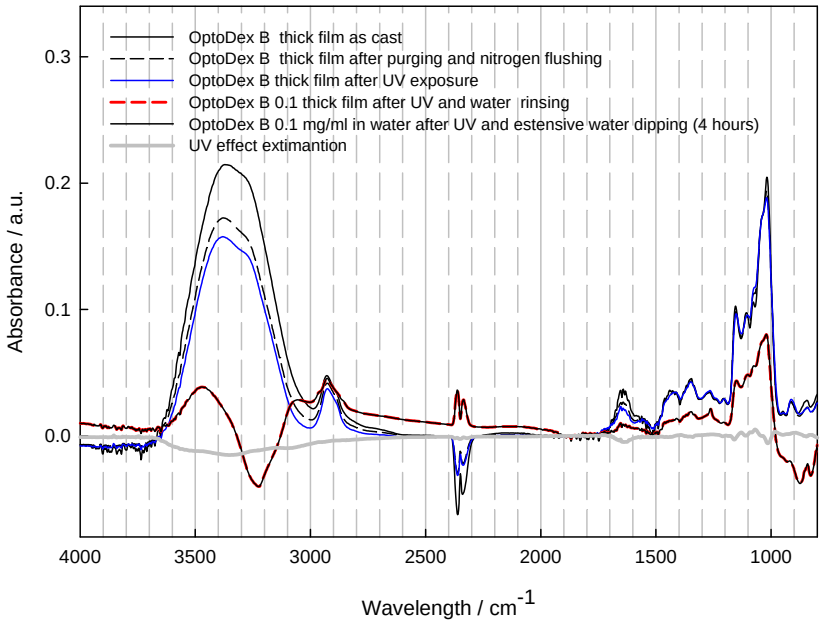

Figure 2-29. ATR spectra of OptoDex ®B thick film: the film was obtained by casting 0.1 mg/ml solution in pure water on plasma activated Ge IRE (black line).Then it was extensively purged (1 hour and further dried by nitrogen flushing, black dashed line). After UV exposure (blue plain line), quick rinsing by water was performed (red dashed line). Finally the functionalized IRE was dipped in water for 4 hours (black plain line, weaker). The gray spectrum is the difference between the registered spectrum before and after UV exposure.

The effectiveness of such a procedure will be evaluated quantitatively later in this work. OptoDex® A was claimed the best physisorber specimen according to the previously shown data. For this reason *ex situ* functionalization was performed using the thick film generation technique (Figure 2-30) and the dipping technique (physisorption mediated photobonding, see Figure 2-31 and Figure 2-32). In Figure 2-31, Figure 2-30 and in Figure 2-32 is reported also an estimation of the effect of the UV exposure is reported. In Figure 2-32 the coating homogeneity before and after UV exposure, is evaluated too. After water evaporation the functionalized IRE was exposed to UV light and rinsed. The effect of UV exposure on the IR spectra is highlighted by reporting the differences between the spectra recorded before and after UV exposure. Spectra were registered at two different positions (200 and 800 lift steps

in the SBSR attachments) to estimate the coating homogeneity.It can be concluded that the dipping technique leads to uniform surface functionalization.

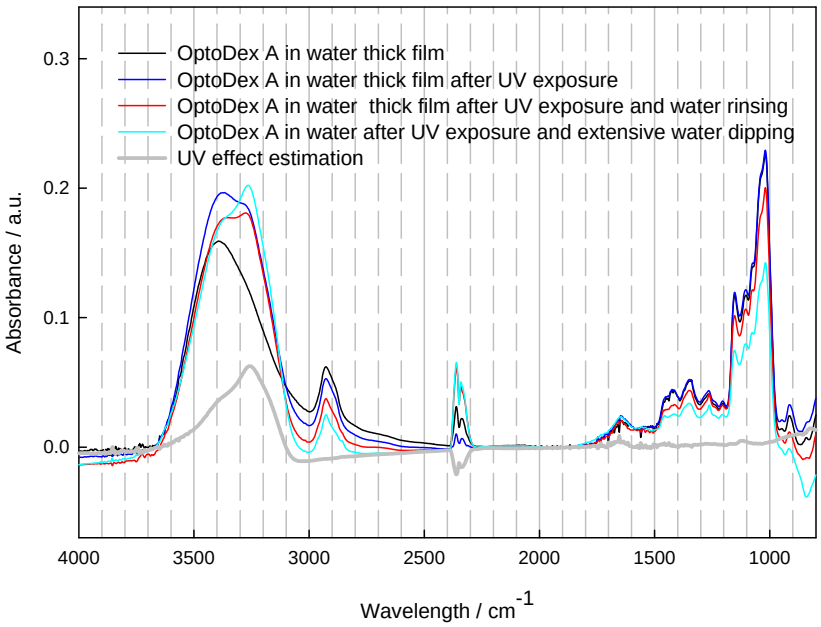

Figure 2-30. ATR spectra of OptoDex® A thick film. The film was obtained by casting 0.1 mg/ml solution in pure water on *plasma* activated Ge IRE (black line). The spectrum was registered after extensive purging (1 hour) and further drying by nitrogen flushing. After UV exposure (blue line), quick rinsing by water was performed (red line). Finally the functionalized IRE was dipped in water for 4 hours (cyan profile). The gray spectrum is obtained by subtraction of the spectra registered before and after UV exposure.

The SBSR lift permitted an estimation of the UV light effect in the two different regions. In Figure 2-31, the subtraction of the spectra recorded after UV exposure and the spectra recorded before is shown.The gray and black lines mainly show a difference in the water content (3500-3000 cm^{-1}) and slight changes in the dextran fingerprint region. It can be stated that the UV exposure does not change significantly the spectrum of the polymer first adsorbed and later immobilized on the surface.

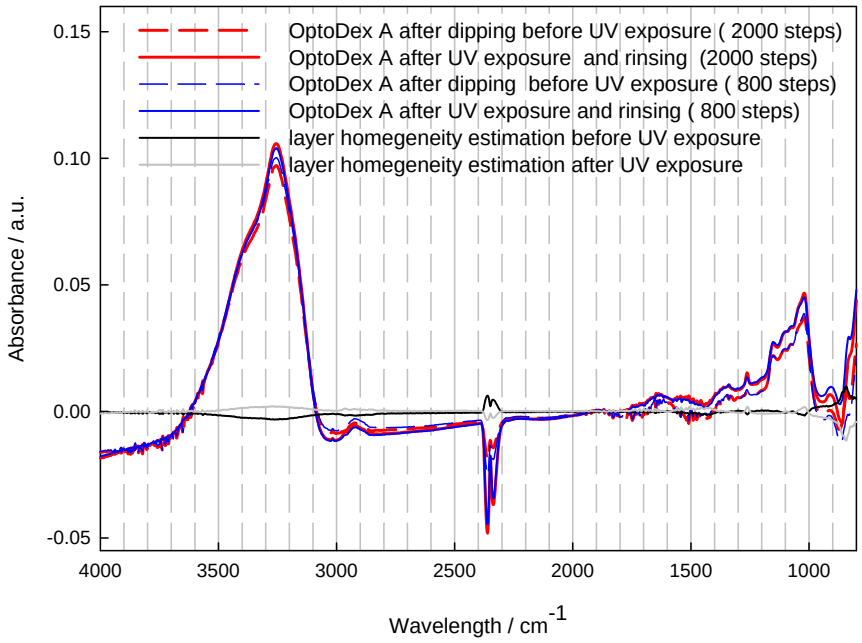

Figure 2-31. OptoDex® A physisorption mediated photobonding applied to Ge IRE *ex situ* and investigated by ATR spectroscopy. The dashed spectra relate to dextran applied to plasma pretreated IRE by dipping a Ge IRE in a solution of OptoDex A 0.1 mg/ml in water solution for 1 hour and then drying the surface by nitrogen flushing. The solid line spectra relate to such a film exposed to UV light and submitted to water rinsing. This procedure was ubiquitously applied to the whole IRE and the spectroscopic investigation was performed at two different positions of the IRE centered at 2000 and at 800 SBSR lift steps. The spectrum registered at 2000 steps minus the one registered at 800 steps allows one to estimate the homogeneity of functionalization, before (black spectrum) and after UV exposure (gray spectrum).

Furthermore, the quantity of product in contact with surface remains almost constant. Finally, it can be concluded that the whole procedure, investigated step by step, results in a homogeneous modification over the entire surface of the IRE.

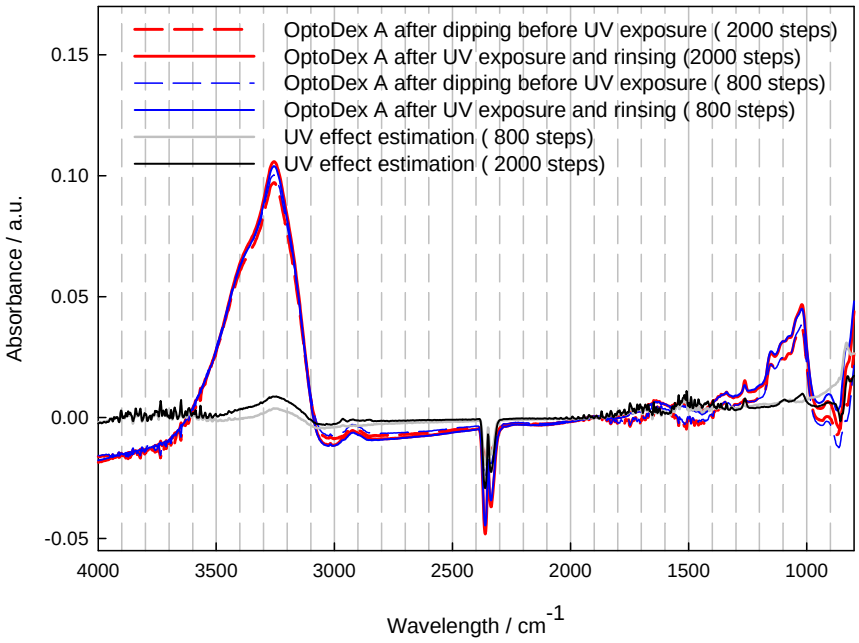

Figure 2-32. OptoDex A physisorption mediated photobonding conditions applied to Ge IRE *ex situ* and investigated by ATR spectroscopy. The same spectra as in Figure 2-31 are depicted: in this case subtraction of spectrum registered at 2000 steps minus the one registered at 800 steps before (black spectrum) and after UV exposure (gray lined spectrum) allows one to estimate the effect of photobonding.

2.2.6. Orientation measurements

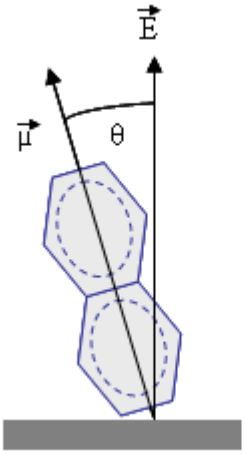

Figure 2-33. Schematic representation of the orientation between the electric field $\vec{E}$ and the transition moment $\vec{\mu}$ of a molecule on a surface.

The extent of infrared absorption of a specific chemical group or a molecule depends on the orientation between the transition moment of the associated vibration and the electric field. The mutual relation is described by the following equation (see. also Figure 2-33):

$$I \propto (\vec{\mu} \bullet \vec{E})^2 = |\vec{\mu}|^2 |\vec{E}| \cos^2(\theta) \qquad \textbf{2-1}$$

Obviously, to determine the magnitude of a signal of an oriented sample one must consider the relative orientation, given by the angle θ, of the two vectors, the electric field vector $\vec{E}$ and the transition moment vector $\vec{\mu}$. The orientation of a molecule can therefore be deduced by measuring the absorption of parallel and perpendicular polarized incident light. To avoid the use of tedious physical units and molecular constants, the so-called dichroic ratio $R = \int A_{\parallel}(\tilde{\nu})\,\mathrm{d}\tilde{\nu} / \int A_{\perp}(\tilde{\nu})\,\mathrm{d}\tilde{\nu}$ is introduced. $\int A_{\parallel}(\tilde{\nu})\,\mathrm{d}\tilde{\nu}$ and $\int A_{\perp}(\tilde{\nu})\,\mathrm{d}\tilde{\nu}$ denote the integrated absorbance of measured spectra for parallel and perpendicular incident light.

Absorbance peaks ($A_{\parallel}$ and $A_{\perp}$) may be used for analysis by introducing the relative electric field components $E_x(\tilde{\nu})$, $E_y(\tilde{\nu})$ and $E_z(\tilde{\nu})$ at a distinct wavenumber as obtained according to Harrick's approximation of Fresnel's equations (thin film in contact with a bulk rarer medium).

$$R = \frac{\int A_{\parallel}(\tilde{\nu})\,\mathrm{d}\tilde{\nu}}{\int A_{\perp}(\tilde{\nu})\,\mathrm{d}\tilde{\nu}} = \frac{A_{\parallel}}{A_{\perp}} = \frac{d_{e,\parallel}}{d_{e,\perp}} = \frac{E_x^2\, m_x^2 + E_z^2\, m_z^2 + 2E_x E_z\, m_x m_y}{E_y^2\, m_y^2}. \qquad \textbf{2-2}$$

Here the $m_{x,y,z}$ denote the component of the transition moment $\vec{\mu}$. Assuming uniaxial arrangement a further simplification can be introduced and the dichroic ratio expression becomes

$$R = \frac{E_x^2}{E_y^2} + 2\frac{E_z^2}{E_y^2}\frac{\overline{\langle \cos^2\theta \rangle}}{1 - \overline{\langle \cos^2\theta \rangle}}. \qquad \textbf{2-3}$$

$\overline{\langle \cos^2\theta \rangle}$ indicates the average over the mean squares of the cosines of the angles between the transition moments of a given vibration and the z-axis of the laboratory coordinate system, which is defined by the internal reflection element.

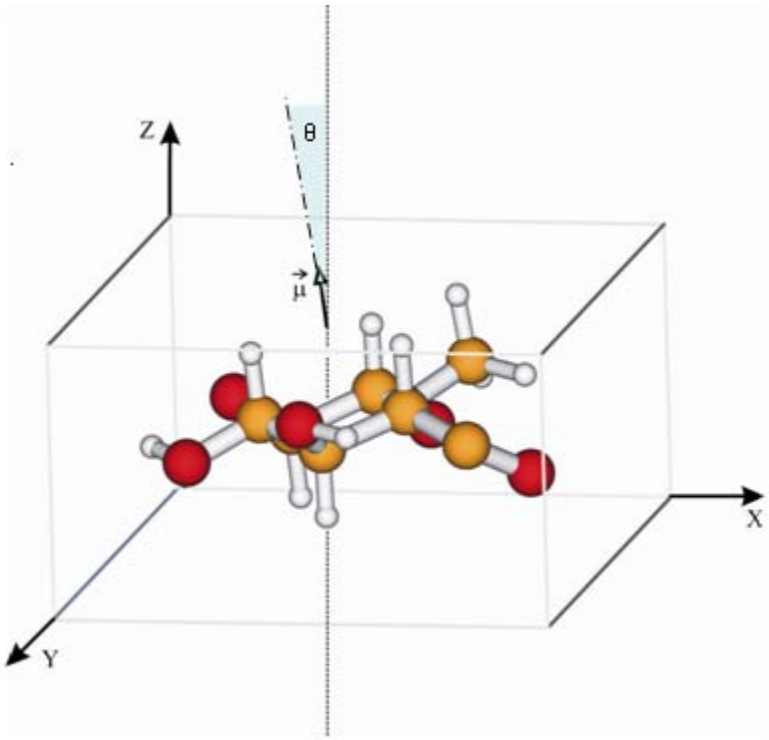

Figure 2-34. Schematic representation of a glucopyranose ring whose position and orientation are observed in regard to the laboratory coordinates system. $\vec{\mu}$ depicts the averaged transition moment of the symmetric stretching vibrations of the CH groups in the ring. Note that C atoms are represented by gold medium sized spheres and H atoms by white small spheres. θ is the angle between $\vec{\mu}$ and the z-axis.

The *xy*-plane denotes the surface of the IRE and the x-axis points along the direction of light propagation.The *z*-axis is perpendicular to the IRE surface. In Figure 2-34 such system is applied to a glucopyranose molecule as monomer of a dextran based polymer, and in particular the vibration generating the considered transition moment $\vec{\mu}$ was the symmetric C-H vibration. Obviously, the dichroic ratio R is experimentally directly accessible, while the relative electric filed components Ex, Ey and Ez must be calculated by means of Fresnel's equations. Solving Eq. 2-3 for the mean square cosine results in

$$\overline{\langle \cos^2 \theta \rangle} = \frac{E_x^2 - RE_y^2}{E_x^2 - RE_y^2 - 2E_z^2} \qquad \textbf{2-4}$$

For the sake of completeness, it must be mentioned that a rigorous calculation necessitates the support of a model probability density function which can provide information on the flexibility of a molecular segment. Three special cases of molecular orientation deserve to be outlined here: the isotropic arrangement of dipole moments, resulting in $\overline{\langle \cos^2\theta \rangle}_{iso} = 1/3$; the perfect alignment of the transition dipole moments parallel to the surface of the IRE (xy-plane), resulting in $\overline{\langle \cos^2\theta \rangle}_{xy} = 0$ and perfect alignment of transition moments along the normal to the IRE (*z*-axis) resulting in $\overline{\langle \cos^2\theta \rangle}_{z} = 1$. Introducing these values in Eq. 2-1, the corresponding dichroic ratios are

$$R_{iso} = \frac{E_x^2 + E_z^2}{E_y^2},\ R_{xy} = \frac{E_x^2}{E_y^2},\ R_z = \infty \qquad \textbf{2-5}$$

Contrary to transmission spectroscopy, R_{iso} differs from unity and has to be calculated in each case depending on the optical constants of the sample. A situation considered common for large molecules is the existence of several populations of equal functional groups, featuring different orientation ordering. Strictly speaking, each group is characterized by its own mean square cosine. The corresponding vibration band will therefore composed of overlapped absorptions.

Considering the dextran based polymer and the hundreds of CH groups of the glucupyranose rings chain networked on the surface, it appears reasonable that only mean absorbences are accessible, resulting in mean dichroic ratio. The following values of relevant parameters have been used for the calculation.

$n_1 = 4.00 \pm 0.00$ *Ge refractive index*

$n_2 = 1.45 \pm 0.05$ *thin film refractive index*

$n_3 = 1.44 \pm 0.05$ $H_2O_{(2850\,cm^{-1})}$ *refractive index*

$\cos\theta_i = \frac{\sqrt{2}}{2}, \quad \theta_i = 45°$

Note that the anomalous dispersion of water at 2850 cm^{-1} has been taken into account ($n_3 = 1.33$ is valid outside of strong water absorption). The components of the relative electric fields strength in the rarer medium resulted in

$$E_x = 1.400 \pm 0.002,\ E_y = 1.511 \pm 0.008,\ E_z = 1.527 \pm 0.162 \qquad \textbf{2-6}$$

The corresponding axial effective thickness for an isotropic thin layer was calculated to be

$$\langle d_{e,x} \rangle_{iso} = 2.51 \pm 0.11\,\text{nm},\quad \langle d_{e,y} \rangle_{iso} = 2.93 \pm 0.13\,\text{nm},\quad \langle d_{e,z} \rangle_{iso} = 3.00 \pm 0.68\,\text{nm} \qquad \textbf{2-7}$$

Thus one obtains for an isotropic thin layer a dichroic ratio of

$$R_{iso} = (\langle d_{e,x} \rangle_{iso} + \langle d_{e,z} \rangle_{iso}) \big/ \langle d_{e,y} \rangle_{iso} = 1.88 \pm 0.22 \qquad \textbf{2-8}$$

while for perfect alignment of the transition moments parallel to the IRE surface (*xy*-plane) the dichroic ratio would result in

$$R_{xy} = 0.858 \pm 0.009 \qquad \textbf{2-9}$$

Orientation information can also be deduced through the dichroic difference spectra (D^*) defined as the weighted difference spectrum between the absorbance spectra measured with parallel and perpendicular polarized light

$$D^* = A_{\parallel}(\tilde{\nu}) - R_{iso}\, A_{\perp}(\tilde{\nu}) \qquad \textbf{2-10}$$

Consequently, the dichroic difference spectrum as defined above results in a flat line if the sample is isotropic or if the respective mean transition moment assumes the so-called magic angle of $\langle\bar{\theta}\rangle = 54.74^{\circ}$ (uniaxial orientation) with the axis normal to the IRE. A positive D^* band indicates predominant alignment of the transition moments of a given vibration in the direction of the *z*-axis, while a negative D^* band is significant for predominant alignment of the transition moments parallel to the surface of the IRE (*xy*-plane).

Error Analysis. The uncertainties indicated in this section and later on this work are all based on a straightforward error propagation calculation. Analytical expression for partial derivatives has been evaluated by means of the symbolic Mathematical Toolbox of MATLAB, whereas the final numeric calculation of the overall uncertainties has been performed using MATLAB program. The uncertainties correspond to 95% limit of confidence.

2.2.6.1. Orientation analysis

Dichroic difference spectra D^*, as resulting from Eq. 2-10 were applied as well as the experimentally derived dichroic ratio, R_{exp}, to assess the orientation of aminodextran, OptoDex® A and OptoDex® B phisysorbed thin films. Attention was paid to the bands related to the ν_s(CH) stretching vibration at 2850 cm^{-1}. The angle between the transition moment of ν_s(CH) and the *z*-axis, was calculated. The stretching vibration related to the C-H bond was selected for the analysis, because in an ideal case the transition moment is perpendicular to the ring. By inspecting Figure 2-35 and Figure 2-36 (aminodextran and OptoDex ® A, respectively) one can realize that the magnitude of the signal related to the same vibration does not differ

significantly when absorbing parallel or perpendicular polarized light. If considering the dichroic difference spectrum, a nearly horizontal line typical for isotropic orientation is observed. The same was observed for OptoDex® B (data not shown). The calculations of the experimentally derived dichroic ratio, R_{exp}, for the three polymers are reported in Table 2-1. The calculations were performed using a program developed by Fringeli and coworkers[69-71].

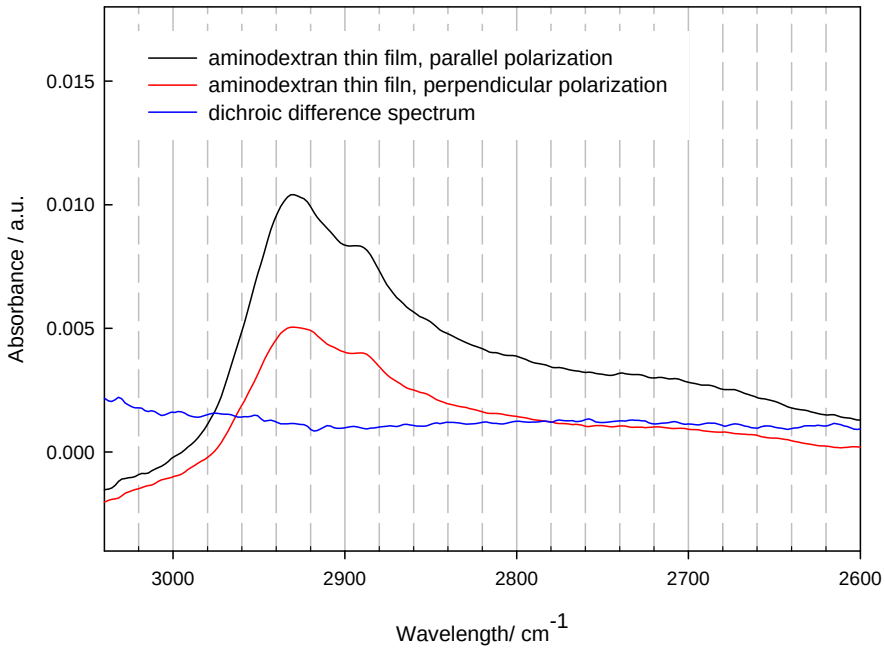

Figure 2-35. Blow-up of ATR-IR spectra in the region of the symmetric stretching vibration, ν_s(C-H) of aminodextran. The black and red lines refer to parallel and perpendicular polarized incident light, respectively. The functionalization and the following rinsing were observed *in-situ* (physisorbed thin film). The blue line, featuring an almost flat profile, represents the calculated dichroic difference spectrum, *D**.

The spread sheet reporting all the data for such calculations is depicted in Table 2-2 at page 82. The small deviation of the values calculated on the basis of experimental data from the theoretical value of $R_{iso} = 1.88 \pm 0.22$, allows the conclusion that the glucopyranose molecules within the dextran polymers assume a quasi-perfect isotropic distribution onto the surface. Weak signals in the dichroic difference D^* are

observed in other spectral regions (see Figure 2-37). As in Figure 2-35 and in Figure 2-36, the blue line relates to D^*, in this case in the 4000-800 cm^{-1} wavelength range. For two spectral regions the observations are different.A flat line in the 3000-2600 cm^{-1} spot is consistent whit an isotropic orientation, when focused on the ν_s(C-H). A negative adsorption result for D^* in the 1500-1000 cm^{-1} range. It must be outlined that a negative value for D^* can be attributed to a predominant parallel alignment of the transition moments with respect to the surface of the IRE. It is not difficult to imagine a quasi-isotropic orientation, and a local situation, minoritary but still detectable, of glucose units laying parallel to the surface.

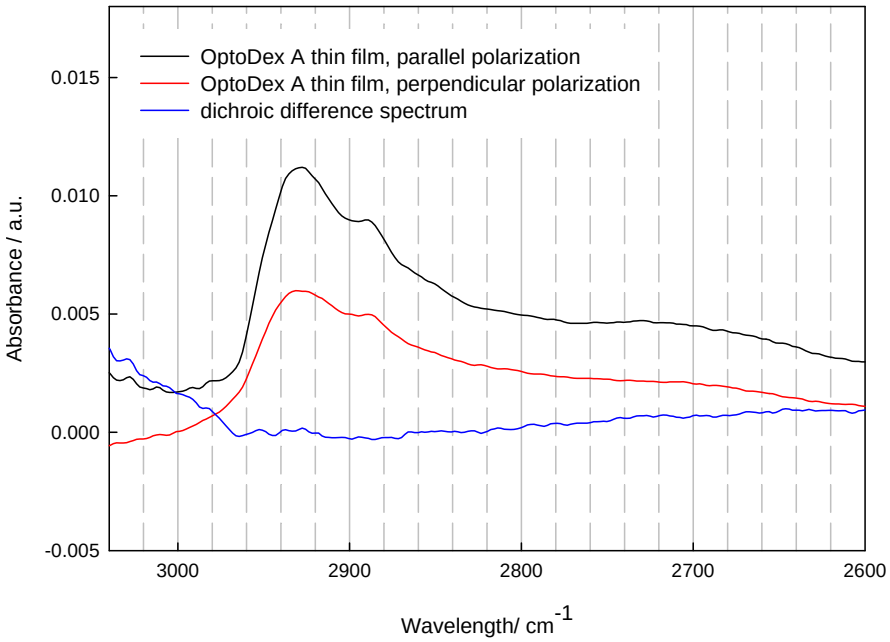

Figure 2-36. Blow-up of ATR-IR spectra in the region of the symmetric stretching vibration, ν_s(C-H) of OptoDex® A thin film. The black and red lines refer to parallel and perpendicular polarized incident light, respectively. The functionalization and the following rinsing were observed *in-situ* (physisorbed thin film). The blue line, featuring an almost flat profile, represents the calculated dichroic difference spectrum, *D**.

Both configurations apply for a branched, not rigid polymer, displaying interactions at the water/ germanium interface. Moreover, it must be noted that the optical constant

of water are not the same in the two spectral region. As consequence, R_{iso} does not have the same value. The results presented justifies the assumption of an isotropic film for the calculation of surface concentration, as outlined below.

2.2.7. Determination of volume concentration and surface concentration

The quantities volume concentration, c , and the surface concentration, Γ , are related to each other via the thickness of the sample *d* and the Lambert-Beer law by

$$c = \frac{\Gamma}{d} = \frac{A_{\perp}}{N\, v\, d_{e,\perp} \int \varepsilon(\tilde{\nu})\, \mathrm{d}\tilde{\nu}} \qquad \textbf{2-11}$$

Dextran based polymer	$a_{\perp}$ [i]	$a_{\parallel}$ [ii]	$R_{exp} = \frac{a_{\parallel}}{a_{\perp}}$
0.1 mg/ml in water, after 60 min physisorption and 30 min water rinsing			
Amino dextran *Molecular Probes*	*0.64 ± 0.05*	*0.35 ± 0.03*	*1.83 ± 0.21*
OptoDex™ A *arrayon biotechnology®*	*0.67 ± 0.05*	*0.36 ± 0.03*	*1.85 ± 0.21*
OptoDex™ B *arrayon Biotechnology®*	*0.17 ± 0.01*	*0.09 ± 0.007*	*1.83 ± 0.18*

[i] $a_{\parallel} = \int A_{\parallel}(\tilde{\nu})\, \mathrm{d}\tilde{\nu}$, integration performed using OPUS software.

[ii] $a_{\perp} = \int A_{\perp}(\tilde{\nu})\, \mathrm{d}\tilde{\nu}$, integration performed using OPUS software.

Table 2-1. For each investigated dextran based polymer, enabling film physisorbtion on the Ge IRE, the experimental dichroic ratio, R_{exp}, was calculated. (*i*) and (*ii*) are the integrated adsorption bands related to ν_s(C-H) for perpendicular and parallel polarized incident light, respectively. OPUS software was applied for integration, and the selected method maintained for entire data processing. The ratio of parallel over perpendicular integrated absorption, furnish the R_{exp} values , as reported in the right column

Unvarying Input parameters	*symbol*	*magnitude*	*uncertainty*
Angle of incidence (°)	Θ	*45.00*	*1.50*
Refractive index of Ge IRE	n_1	*4.00*	*0.00*
Refractive index of Thin film	n_2	*1.45*	*0.05*
Refractive index of aqueous environment at 2850 cm-1	n_3	*1.41*	*0.05*
Unvarying Output values	*symbol*	*magnitude*	*uncertainty*
Dichroic ratio for isotropic distribution of $\vec{\mu}$	R_{iso}	*1.88*	*0.22*
Dichroic ratio for alignment of $\vec{\mu}$ *parallel to the surface*	R_{xy}	*0.86*	*0.01*
Magic Angle (°)	$\overline{\langle\theta\rangle}$	*54.7*	
Polymer depending input parameters	*symbol*	*magnitude*	*uncertainty*
aminodextran (Molecular Probes)			
Integrated absorbance of ν_s(CH) *for parallel polarized light*	$a_{\parallel}^{i}$	*0.64*	*0.05*
Integrated absorb. of ν_s(CH) *for perpendicular polarized light*	$a_{\perp}^{ii}$	*0.35*	*0.03*
OptoDex ™A (arrayon biotechnology®)			
Integrated absorbance of ν_s(CH) *for parallel polarized light*	$a_{\parallel}^{i}$	*0.67*	*0.05*
Integrated absorb. of ν_s(CH) *for perpendicular polarized light*	$a_{\perp}^{ii}$	*0.36*	*0.03*
OptoDex ™B (arrayon biotechnology®)			
Integrated absorbance of ν_s(CH) *for parallel polarized light*	$a_{\parallel}^{i}$	*0.17*	*0.01*
Integrated absorb. of ν_s(CH) *for perpendicular polarized light*	$a_{\perp}^{ii}$	*0.09*	*0.007*
Measurement depending output values	*symbol*	*magnitude*	*uncertainty*
aminodextran (Molecular Probes)			
Experimentally obtained dichroic ratio	R_{exp}	*1.83*	*0.21*
Angle (°) between $\vec{\mu}$ *and the z-axis*	θ_k	*55.4*	*4.1*
OptoDex ™A (arrayon biotechnology®)			
Experimentally obtained dichroic ratio	R_{exp}	*1.85*	*0.21*
Angle (°) between $\vec{\mu}$ *and the z-axis*	θ_k	*55.1*	*4.0*
OptoDex ™B (arrayon biotechnology®)			
Experimentally obtained dichroic ratio	R_{exp}	*1.83*	*0.18*
Angle (°) between $\vec{\mu}$ *and the z-axis*	θ_k	*55.4*	*3.8*

[i] $a_{\parallel} = \int A_{\parallel}(\tilde{\nu})\,d\tilde{\nu}$, integration performed using OPUS software.

[ii] $a_{\perp} = \int A_{\perp}(\tilde{\nu})\,d\tilde{\nu}$, integration performed using OPUS software.

Table 2-2. Dextran based polymers orientation evaluation spread sheet.

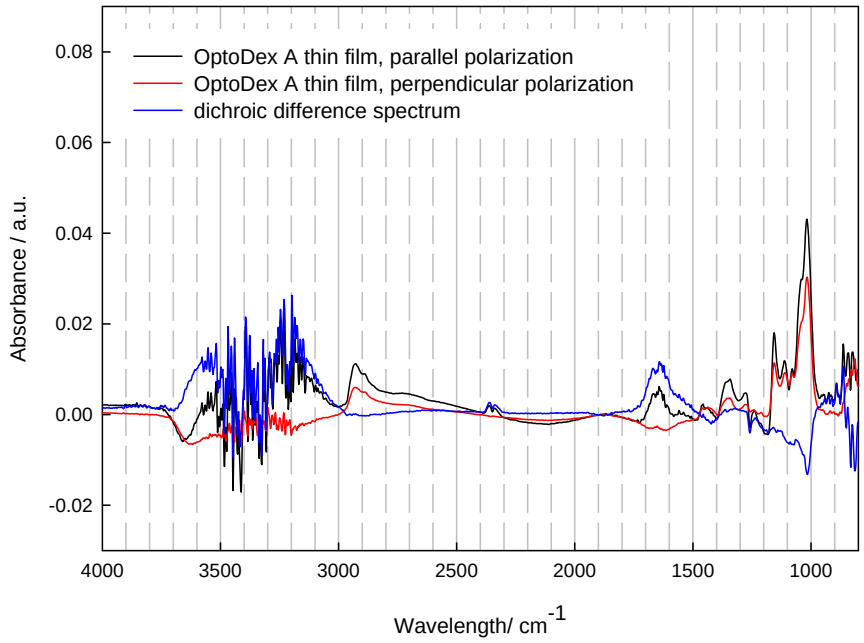

Figure 2-37. ATR-IR spectra of OptoDex® A physisorbed thin film. The blue line represents the calculated dicroic difference spectrum, D^*. Note the flat outline in the 3000 - 2500 cm^{-1} region and the negative profile in the 1200-1000 cm^{-1} wavelength range.

In Eq. 2-11, $A_\perp$ denotes the integrated absorbance of a given absorption band measured with perpendicular polarized light; N and v are the mean number of active internal reflections and the number of equal functional groups per molecule. The effective thickness of an arbitrary oriented sample per internal reflection is denoted by $d_{e,\perp}$ whereas $d_{e,\perp}^{iso}$ is the effective thickness for an isotropic sample, $\int \varepsilon(\tilde{\nu})\, \mathrm{d}\tilde{\nu}$ denotes the integrated molar absorption coefficient of this band. According to Eq. 2-11, the surface density, Γ, may be conceived as the projection on the surface of the molecules in the volume defined by the unit area and the height d. Consequently, d is the sample thickness. For systems consistent with the isotropic model, the equation relating volume concentration c, [mol cm^{-3}], and the surface concentration Γ, [mol cm^{-2}], via the sample thickness d can be simplified to

$$c = \frac{\Gamma}{d} = \frac{A_{\perp}}{N\, d_{e,\perp}\, \varepsilon} \qquad \textbf{2-12}$$

Under the thin film approximation, it follows

$$d_e = \frac{n_{21}}{\cos\theta_i} d\ E_{o2}^{r\,2} \qquad \textbf{2-13}$$

and then

$$\frac{d_e}{d} = \frac{n_{21}}{\cos\theta_i}\ E_{o2}^{r\,2} \qquad \textbf{2-14}$$

where $E_{o2}^{r\,2}$ can be calculated using the Fresnel's equations. In contrast to the parallel electric field component, the derivation of the perpendicular component is straightforward

$$E_{\perp} = \frac{2\ \cos\theta_i}{\sqrt{1 - n_{31}^2}} = 1.485 \qquad \textbf{2-15}$$

For the calculation of the surface concentration Γ the following parameters were used:

$n_1 = 4.0$ *Ge refractive index*

$n_2 = 1.45$ *thin film refractive index*

$n_3 = 1.224$ $H_2O_{(1020\,cm^{-1})}$ *refractive index*

$\varepsilon_{(1157\,\mathrm{cm}^{-1})} =$ $178.831\,\mathrm{cm}^2\ \mathrm{mol}^{-1}$

$N = 42.5$ *number of IRE active reflections*

$\cos\theta_i = \frac{\sqrt{2}}{2}, \quad \theta_i = 45°$

According to these mathematical operations and deriving from Eq. 2-11 and Eq 2-13 $\frac{d_e}{d}$, it follows

$$\Gamma = c \cdot d = \frac{d}{d_e} \cdot \frac{A_\perp}{N\varepsilon} = \frac{\cos\theta_i}{n_{21}} \cdot \frac{1}{E_\perp^2} \cdot \frac{A_\perp}{N\varepsilon} =$$

$$= \frac{\sqrt{2}/2}{0{,}3625} \cdot \frac{1}{2{,}205} \cdot \frac{A_\perp}{42{,}5 \cdot 178.831\,\mathrm{cm^2\,mol^{-1}}} = A_\perp \cdot 11{,}66 \cdot 10^{-8}\ \mathrm{mol\,cm^{-2}} \qquad \textbf{2-16}$$

$$\Gamma = c \cdot d = A_\perp \cdot 11{,}66 \cdot 10^{-8}\ \mathrm{mol\,cm^{-2}}$$

Therefore, thin film thickness is proportional to absorbance according to the subsequent equation

$$d = \frac{\Gamma}{c} = \frac{A_\perp \cdot 11{,}66 \cdot 10^{-8}\ \mathrm{mol\,cm^{-2}}}{c} \qquad \textbf{2-17}$$

The missing data to calculate the film thickness *d*, is at that point the volume concentration *c [mol cm^{-3}]*, which can be deduced from the polymer density. Glucose density is *1,54 g cm^{-3}* and its molecular weight is MW= *180.16 g mol^{-1}*. Then

$$c = \frac{density}{MW} = \frac{1{,}54\ \mathrm{g\,cm^{-3}}}{180{,}16\ \mathrm{g\,mol^{-1}}} = 0{,}0085\ \mathrm{mol\,cm^{-3}} \qquad \textbf{2-18}$$

The volume of 1 glucopyranose unit is then (considering Avogadro's Number and $1\,\mathrm{cm^3} = 10^{24}\,\mathrm{Å^3}$)

$$V_{(1\,unit)} = 194\ \mathrm{Å^3} \qquad \textbf{2-19}$$

All required data are in conclusion available:

$$d = \frac{\Gamma}{c} = \frac{A_\perp \cdot 11{,}66 \cdot 10^{-8}\ \mathrm{mol\,cm^{-2}}}{0.0085\ \mathrm{mol\,cm^{-3}}} = A_\perp \cdot 13.71 \cdot 10^{-6}\ \mathrm{cm} \qquad \textbf{2-20}$$

Under the set experimental conditions, $13.71 \cdot 10^{-6}\,\mathrm{cm}$ is the factor that relates the absorbance $A_{\perp}$ to the film thickness. This paragraph furnishes the theoretical base for the elaboration of experimental data as reported in paragraph 2.4 (Determination of polymer film thickness *at interface*, p. 90), Table 2-4 and Table 2-5.

2.3. Charge driven Physisorbtion

The density of charged groups within the molecules yields the total charge per volume. It is given in m^{-3}. For each dextran based polymer dissolved in water in concentration up to 0.1 mg/ml, the charge density was calculated according to Eq. 2-21, applying the parameters given.

$$\frac{polymer\ concentration\ (g/ml)}{polymer\ MW\ (g/mol)} \cdot N \cdot \frac{N°of\ charges}{mol} \cdot F = charge\ \ carrier\ density$$

$$F = \frac{ml}{10^{-6} \cdot m^3},$$

$$N = Avogadro\ Number = 6,023 \cdot 10^{23}$$

2-21

$$\frac{N°\ of\ charges}{mol}, specific\ \ of\ \ polymer, cfr.\ \ Table\ 2-1$$

$$MW = 70.000\ \ dalton\ \ for\ carboxymethyl\ dextran$$
$$MW = 40.000\ \ dalton\ \ for\ aminodextran, and\ OptoDex\ ®$$

A pH 7 was measured for Millipore purified water and it was found to decreases with time down to 5.5, due to the uptake of atmospheric CO_2 in water. At such conditions, simple dextran can be assumed to be uncharged. The same holds for the backbone of the dextran derived polymers: it stays uncharged. In contrast the pH variation in such a range, determines amines protonation (positively charged) and carboxyls deprotonation (negatively charged). Taking the specific function per mole (cfr. Table 2-3) which is reported in the product specifications, the charge carrier density was quantified as parameter for the establishment of a trend. The chemical modification which leads from aminodextran to OptoDex ® affects marginally the total molecular weight. For this reason, the molecular weight of OptoDex ® A, B and C is assumed to be the same as for aminodextran (i.e. 40000 daltons).

Dextran based polymer (0.1 mg/ml in water)	*Specific function per mole of polymer*	*Charge carrier density, m^{-3} (pH= 7.0 ÷ 5.0)*
Amino dextran *Molecular Probes*	*8 amines/mol*	***12.20 · 10 ^{22}*** *protonated amines, NH^{3+}*
OptoDex™ A *arrayon Biotechnology®*	*4 amines/mol* *4 aryldiazirines/mol*	***6.10 · 10 ^{22}*** *protonated amines, NH^{3+}*
OptoDex™ B *arrayon Biotechnology®*	*4 protected amines/mol* *4 aryldiazirines/mol*	--
OptoDex™ C *arrayon Biotechnology®*	*4 carboxyls/mol* *4 aryldiazirines/mol*	***6.10 · 10 ^{22}*** *deprotonated carboxyl, COO^-*
Carboxymethyl dextran *Molecular Probes*	*71 carboxyls/mol*	***61.09 · 10 ^{22}*** *deprotonated carboxyls, COO^-*

Table 2-3. Calculated charge carrier density as calculated from Eq. 2-21. The specific chemical function per mole of polymer is reported as depicted in the datasheet of the respective product.

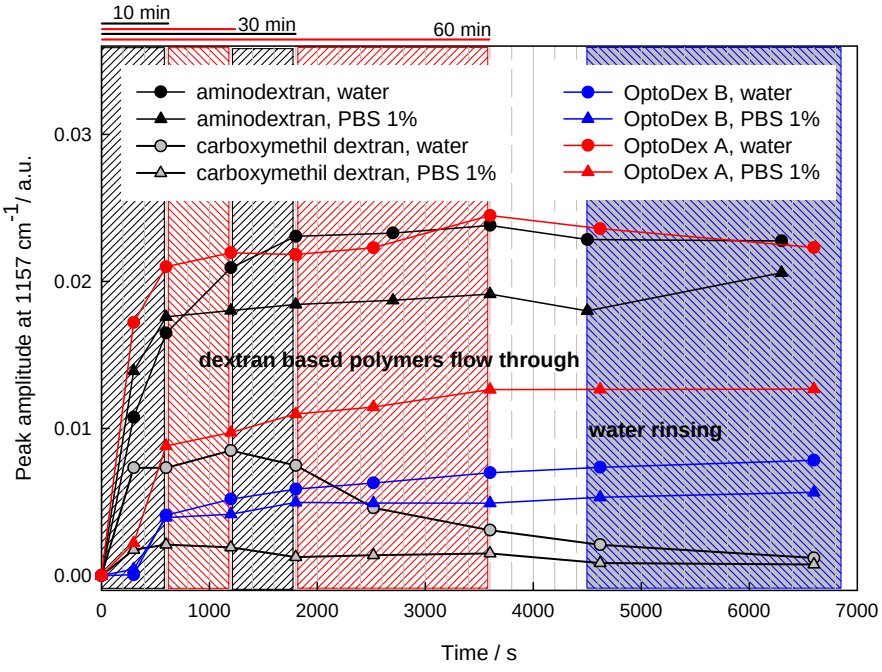

Figure 2-38. Comparison of physisorption kinetics behavior of aminodextran (black plot), carboxymethyl dextran (grey plot), OptoDex® B (blue plot) and OptoDex® A (red plot), 0.1 mg/ml aqueous solutions differing for ionic strength, namely pure water (circle scattered plots), and PBS 1% buffer, (triangle scattered plots) on plasma activated Ge IRE. The same conditions were applied on polymer surface exposure and rinsing time.

From Table 2-3 it can be evinced that the aminodextran in solution is positively charged when flowing in contact with the Ge IRE, and its *a priori* charge density is twice that of the OptoDex® A homologue. OptoDex® B is uncharged, OptoDex® C has the same charge as OptoDex® A, but negative and carboxymethyl dextran is ten times more charged than OptoDex® C. A dextran based polymer with the same charge density as aminodextran but opposite in sign, was not commercially available. To correlate the charge density with the physisorption behavior. the kinetics observations are summarized in Figure 2-38. It should be noted that the errors of the peak amplitude values are on the order of a few % for values around 0.01. Errors between different experiments due to optics alignment are estimated to be on the order of 19%. Aminodextran and OptoDex® A solutions, at the same concentration in pure water (0.1 mg/ml), show similar behavior. A slight difference lays in the kinetics at short time. In water, the peak amplitude at 1157 cm^{-1} of OptoDex® A rises faster than for aminodextran, and after 10 min the physisorption is at 95% of completion. In the case of higher ionic strength, aminodextran results more effective than OptoDex® A (cfr. triangles up scatter plot, black and red respectively). Ionic strength is one of the parameters, together with time, to control the thickness of the layer. Adsorption kinetics of aminodextran and OptoDex® A kinetics behavior is reprensed by the lines in the upper part of the graphic. OptoDex® B, as an uncharged polymer, physisorbs on the Ge IRE without much reacting to the ionic strength change (see circle and triangle up scatter blue plots). As already outlined previously, carboxymethyl dextran (highly negative charge carrier) does not physisorb (actually desorbs after a short time of surface interaction). The explored layout is consistent with a germanium IRE, plasma treated, slightly negative, which preferably interacts with analytes offering positive charges.

2.4. Determination of polymer film thickness *at* interface

The straightforward application of Eq. 2-20 allowed the compilation of Table 2-4 and Table 2-5. The first one refers to ATR monitored *in situ* physisorption, leading to thin film adlayers of aminodextran, OptoDex® A and OptoDex® B, in both, water and PBS 1%. Under such experimental conditions the film at the interface fully stays within the evanescent field. The outstanding interest in this method stays in the possibility of measuring film thickness at interfaces, actually in presence of water. In aqueous media dextran based polymers are expected to unfold their properties of hydrogel-like materials. Furthermore they are typically asked to act in such environments for bioassay formats. The calculated thickness range swipes from 19 Å to 5 Å. For sure, the interest in the absolute value stands, but significance of these values increases if considering the size of the glucopyranose unit. In Eq.2-19 it was estimated that the volume of a dextran monomer is $194\ \mathring{A}^3$. According to the assumed isotropic orientation, we can reasonably consider that one glucopyranose ring measures in one dimension:

$$\sqrt[3]{194\mathring{A}^3} \cong 5.8\ \mathring{A} \qquad \textbf{2-22}$$

Under this vision, the calculated thicknesses correspond to a monolayer of glycopyranose for OptoDex® B in water, two and three layers in the cases of OptoDex® A in PBS 1% and water, respectively, 4 and 5 layers in the cases of aminodextran in PBS 1% and water, respectively. The thin film layer left over by OptoDex® B in PBS 1% results in an incomplete monolayer. The same calculations were applied to the cases of OptoDex® A, B and C thick film casting (*ex situ*). The considered experimental data (peack values) and the derived film thickness are reported in Table 2-5**.** In this case only films cast from pure water were taken into

account. The pertinent interest of this set of values is in the elucidation of the film thickness before and after UV exposure: in this way the effectiveness of the photobonding process was inquired (see 2.4). It must be noted that the calculation of the film thickness applied here assumes that the film thickness is much smaller than the penetration depth of the evanescent field, which is not necessary correct for the cast films.

Dextran based polymer	***Peak amplitude***[i]	***Thin film thickness***[ii]
(0.1 mg/ml) *in situ physisorption*		
Amino dextran *(water)* *Molecular Probes*	$1.44 \cdot 10^{-2}$	*19.19 Å*
Amino dextran *(PBS 1%)* *Molecular Probes*	$1.01 \cdot 10^{-2}$	*13.85 Å*
OptoDex™ A *(water)* *arrayon Biotechnology®*	$1.16 \cdot 10^{-2}$	*15.90 Å*
OptoDex™ A *(PBS 1%)* *arrayon Biotechnology®*	$7.20 \cdot 10^{-3}$	*9.871 Å*
OptoDex™ B *(water)* *arrayon Biotechnology®*	$3.66 \cdot 10^{-3}$	*5.018 Å*
OptoDex™ B *(PBS 1%)* *arrayon Biotechnology®*	$2.73 \cdot 10^{-3}$	*3.715 Å*

[i] $(A_{\perp,1157\,cm^{-1}}) - (A_{\perp,1182\,cm^{-1}})$

[ii] Cfr. Eq. 2-20

Table 2-4. Thin film thicknesses as calculated inserting data of relative peak amplitude at 1157 cm^{-1} in Eq. 2-20.

This means that the calculated values represent lower limits. The thick film casting technique leads to dextran based polymer layers at least 5 times thicker. One fact is

remarkable: *via* "non physisorption mediated» casting technique, thicker layers are displayed by the polymers with a better surface adsorption performance (see Table 2-5).

2.5. OptoDex® family's photobonding effectiveness

The number of actinic arildiazirine groups in the OptoDex® structure is high enough to act as surface/probe hook, but is too low to be directly identified by spectroscopic observation. The polymer (MW 40000 daltons)/ isotiocianato-aryl-trifluoro-diazirine (MW 243, 4 units in average per mole of polymer) ratio, roughly equals to 165. This means that the carbene generating groups are buried in the dextran signal.

OptoDex™	***before UV (a)*** *cast and evaporated*		***after UV (b)*** *and mild rinsing*		***after UV (c)*** *and thorough rinsing*	
0.1mg/ml (water) ex situ casting	*Peak amplitude*[i]	*Film thickness*[ii]	*Peak amplitude*[i]	*Film thickness*[ii]	*Peak amplitude*[i]	*Film thickness*[ii]
A, *thick film*	$7.99 \cdot 10^{-2}$	*109.5 Å*	$6.64 \cdot 10^{-2}$	*91.0 Å*	$47.5 \cdot 10^{-2}$	*65.1 Å*
B, *thick film*	$5.08 \cdot 10^{-2}$	*69.6 Å*	$2.59 \cdot 10^{-2}$	*35.5 Å*	$23.5 \cdot 10^{-2}$	*32.2 Å*
C, *thick film*	$5.50 \cdot 10^{-2}$	*75.4 Å*	$22.6 \cdot 10^{-2}$	*31.0 Å*	$18.2 \cdot 10^{-2}$	*24.9 Å*

[i] $(A_{\perp,1157\ cm^{-1}}) - (A_{\perp,1182\ cm^{-1}})$

[ii] Cfr. Eq.2-17

Table 2-5. Thin film thicknesses as calculated inserting data of relative peak amplitude at 1157 cm-1 in Eq. 2-20, applied to the thick film casting (ex situ functionalization). Peak amplitude referring to three cases are reported: cast and evaporated aqueous solution, mild water rinsing after UV exposure and subsequent thorough water rinsing to ascertain the efficiency of the carbene insertion and polymer grafting onto the surface.

Nevertheless, one of the major goals of this thesis work was to quantify via ATR-IR spectrometry the effectiveness of the photobonding process, demonstrated

alternatively *via* radioactive and fluorescence labeling[26, 28, 30, 38]. Firstly, it must be noted that the photobonding procedure implies UV exposure of dried polymer film. Even if the physisorption can be performed *in situ*, complete water removal determines demounting of the microfluidics system. In fact, the characterization of subsequent steps is compatible only with an *ex-situ* functionalization and spectroscopic observation. Therefore, for physisorbtion mediated photobonding effectiveness estimation, the thin film was adsorbed via dipping (*ex situ*, Table 2-7). Table 2-6 concerns the effectiveness of photobonding processes mediated by actinic polymer thick film deposition. The film thickness of the cast polymer varies from 75 to 105 Å (cfr. Table 2-5). It can be due to the lack of control of water content. But the effectiveness calculation, as ratio, get rid of of such uncertainty.

OptoDex™	***Photobonding effectiveness***[i]
0.1 mg/ml (water) ex situ casting	*(c/a) x 100*
A, *thick film*	*59,4 %*
B, *thick film*	*46.2 %*
C, *thick film*	*33.0 %*

[i] Cfr. Table 2-5 for *(a)* and *(c)* values.

Table 2-6. Photobonding effectiveness in the case of OptoDex® A, B and C thick film casting. *(a)* as reported in Table 2-5, represents the peak amplitude of the thick film as cast and evaporated. *(c)*, reports the final peak amplitude after UV exposure and extensive rinsing. The ratio *(c/a)* indicates the percentage of the polymer grafted onto the surface. Surface functionalization was performed *ex-situ.*

OptoDex™ A	***before UV (a)*** *after dipping*		***after UV (b)*** *and thorough rinsing*		***Photobonding effectiveness***
0.1 mg/ml (water) ex situ physisorption	*Pick amplitude*[i]	*Film thickness*[ii]	*Pick amplitude*[i]	*Film thickness*[ii]	*(b/a) x 100*
***A**, thin film*	$9.49 \cdot 10^{-3}$	*13.01 Å*	$9.43 \cdot 10^{-3}$	*12.92 Å*	*99.37%*

[i] $(A_{\perp,1157\ \mathrm{cm}^{-1}}) - (A_{\perp,1182\ \mathrm{cm}^{-1}})$

[ii] Cfr. Eq.2-17

Table 2-7. Photobonding effectiveness in the case of OptoDex® A thin film casting. *(a)* represents the peak amplitude of the thin film adsorbed by dipping. *(b)*, reports the final peak amplitude after UV exposure and extensive rinsing. The ratio *(b/a)* indicates the percentage of the polymer grafted onto the surface. Surface functionalization was performed ex-situ.

Clearly the photobonding effectiveness correlates with the physisorption effectiveness. It could be that the anchoring site for physisorption is close to the arildiazine group. The arildiazine is automatically close to the surface, which may explain the higher efficiency. The observed trend is: OptoDex® A results more effective than B and C. OptoDex® C does not allow physisorption (see again Figure 2-38). The most interesting result is shown in Table 2-7. The physorprtion mediated UV activation of OptoDex® A leads to a quasi total immobilization of the arildiazirine derivative of the aminodextran, on to the Ge IRE.The carbene generation allows lossless immobilization of a dextran based polymer displaying a multilayers (3-4 layers, cfr. 19.19 *Å in* Table 2-4), isotropic configuration on to the surface.

2.6. References

1. Heinze, T.; Liebert, T.; Heublein, B.; Hornig, S., Functional polymers based on dextran. In *Polysaccharides Ii*, 2006; Vol. 205, pp 199-291.

2. Confer, D. R.; Logan, B. E., Molecular Weight Distribution of Hydrolysis Products during Biodegradation of Model Macromolecules in Suspended and Biofilm Cultures II: Dextran and Dextrin. *Wat. Res.* **1997,** 31, (9), 2127-2145.

3. Chandra, R.; Rustgi, R., Biodegradable polymers. *Progress in Polymer Science* **1998,** 23, (7), 1273-1335.

4. Dhaneshwar, S. S.; Kandpal, M.; Gairola, N.; Kadam, S. S., Dextran: A promising macromolecular drug carrier. *Indian J Pharm Sci* **2006,** 68, (6), 705-714.

5. De Geest, B. G.; Dejugnat, C.; Verhoeven, E.; Sukhorukov, G. B.; Jonas, A. M.; Plain, J.; Demeester, J.; De Smedt, S. C., Layer-by-layer coating of degradable microgels for pulsed drug delivery. *Journal of Controlled Release* **2006,** 116, (2), 159-169.

6. Piehler, J.; Brecht, A.; Hehl, K.; Gauglitz, G., Protein interactions in covalently attached dextran layers. *Colloid. Surfaces B.* **1999,** 13, 325-336.

7. Thoren, L., The dextrans--clinical data. *Devel. Biol. Stand.* **1981,** 48, 157-67.

8. De Belder, A. N., Dextran. In *Industrial gums: Polysaccharides and their derivatives (3rd ed.)*, Whistler, R. L.; BeMiller, J. N., Eds. Academic Press: New York, 1992; pp 399-423.

9. De Belder, A. N., Dextran. In *Amersham Bioscience*, 2003; Vol. Article no 18-1166-12.

10. Löfas, S.; Johnsson, B., A Novel Hydrogel Matrix on Gold Surface Plasmon Resonance Sensors for Fast and Efficient Covalent Immobilization of Ligands. *J. Chem. Soc., Chem. Commun.* **1990**, 1526-1528.

11. Löfas, S.; Johnsson, B.; Tegendal, K.; Rönnberg, I., Dextran modified gold surfaces for surface plasmon resonance sensors:immunoreactivity of immobilized antibodies and antibody-surface interaction studies. *Colloid. Surface. B* **1993,** 1, 82-89.

12. Löfas, S.; Malmqvist, M.; Rönnnberg, I.; Stenberg, E.; Liedberg, B.; Lundström, I., Bioanalysis with surface plasmon resonance. *Sensors and Actuators B* **1991,** 5, 79-84.

13. Löfas, S., Dextran modified self-assembled monolayer surfaces for use in biointeraction analysis with surface plasmon resonance. *Pure & Appl. Chem.* **1995,** 67, 829-834.

14. Brecht, A.; Gauglitz, G., Optical probes and transducers. *Biosens. Bioelectron.* **1995,** 10, (9-10), 923-936.

15. Xu, F.; Persson, B.; Lofas, S.; Knoll, W., Surface plasmon optical studies of carboxymethyl dextran brushes versus networks. *Langmuir* **2006,** 22, (7), 3352-3357.

16. Miksa, D.; Irish, E. R.; Chen, D.; Composto, R. J.; Eckmann, D. M. In *Biomimetic surfaces via dextran immobilization : grafting density and surface properties*, 2004; ScholarlyCommons@Penn: 2004.

17. Dai, L.; StJohn, H. A. W.; Bi, J.; Zientek, P.; Chatelier, R. C.; Griesser, H. J., Biomedical coatings by the covalent immobilization of polysaccharides onto gas-plasma-activated polymer surfaces. *Surf. Inter. Anal.* **2000,** 29, (1), 46-55.

18. Elender, G.; Kühner, M.; Sackmann, E., Functionalisation of Si/SiO_2 and glass surfaces with ultrathin dextran films and depostion of lipid bilayers. *Biosens. Bioelectron.* **1996,** 11, 565-577.

19. Piehler, J.; Brecht, A.; Geckeler, K. E.; Gauglitz, G., Surface modification for direct immunoprebes. *Biosens. Bioelectron.* **1996,** 11, (67), 579-590.

20. Ombelli, M.; Eckmann, D. M.; Composto, R. J., Dextran grafted silicon substrates: Preparation, characterization and biomedical applications. In *Materials Inspired by Biology*, Thomas, J. L.; Kiick, K. L.; Gower, L. A., Eds. 2003; Vol. 774, pp 93-98.

21. Sigrist, H.; Gao, H., Biosensor @ CSEM. *Chimia* **1999,** 53, 81-86.

22. Dolder, M.; Michel, H.; Sigrist, H., 3-(Trifluoromethyl)-3-(m-isothiocyanophenyl)diazirine: synthesis and chemical characterization of a heterobifunctional carbene-generating crosslinking reagent. *J. Protein Chem.* **1990,** 9, (4), 407-15.

23. Sigrist, H.; Collioud, A.; Clémence, J. F.; Gao, H.; Luginbühl, R. R.; Sänger, M.; Sundarababu, G., Surface immobilization of biomolecules by light. *Optical Engineering* **1995,** 34, (8), 2339-2348.

24. Sigrist, H.; Gao, H.; Wegmuller, B., Light-dependent, covalent immobilization of biomolecules on 'inert' surfaces. *Biotechnology* **1992,** 10, (9), 1026-8.

25. Collioud, A.; Clemence, J. F.; Sanger, M.; Sigrist, H., Oriented and covalent immobilzation of target moleculed to solid supports: synthesis and application of a light-activatable and thiol-reactive cross-linking reagent. *Bioconjugate Chem.* **1993,** 4, (6), 528-36.

26. Gao, H.; Kislig, E.; Oranth, N.; Sigrist, H., Photolinker-polymer-mediated immobilization of monoclonal antibodies, $F(ab')_2$ and F(ab') fragments. *Biotechnol. Applied. Biochem.* **1994,** 20, 251-263.

27. Gao, H.; Sänger, M.; Luginbühl, R.; Sigrist, H., Immunosensing with photo-immobilized immunoreagents on planar optical wave guides. *Biosens. Bioelectron.* **1995,** 10, 317-328.

28. Gao, H.; Sigrist, H., kinetic analysis of immunocomplexation with photoimmobilized $F(ab')_2$ on planr optical waveguides. *Journal of Materials Science: Materials in Medicine* **1996,** 7, 13-16.

29. Heyse, S.; Vogel, H.; Sänger, M.; Sigrist, H., Covalent attachment of functionalized lipid bylayers to planar waveguides for measuring protein binding to biomimetic membranes. *Protein Science* **1995,** 4, 2532-2544.

30. Sundarababu, G.; Gao, H.; Sigrist, H., Photochemical linkage of antibodies to silicon chips. *Photochem. Photobiol.* **1995,** 61, (6), 540-544.

31. Liu, M. T. H., Chapter 7-9. In *Chemistry of Diazirines*, Liu, M. T. H. E., Ed. CRC Press, Boca Raton, FL.: 1987; p 160.

32. Blencowe, A.; Hayes, W., Development and application of diazirines in biological and synthetic macromolecular systems. *Soft Matter* **2005,** 1, (3), 178-205.

33. Moss, R. A., Diazirine: Carbene Precursors Par Excellence. *Acc.Chem.Res.* **2006,** 39, 267-272.

34. Angeloni, S.; Ridet, J. L.; Kusy, N.; Gao, H.; Crevoisier, F.; Guinchard, S.; Kochhar, S.; Sigrist, H.; Sprenger, N., Glycoprofiling with Micro-Arrays of Glycoconjugates and Lectins. *Glycobiology* **2005,** 15, (1), 31-41.

35. Azzam, T.; Raskin, A.; Makovitzki, A.; Brem, H.; Vierling, P.; Lineal, M.; Domb, A. J., Cationic Polysaccharides for Gene Delivery. *Macromolecules* **2002,** 35, (27), 9947-9953.

36. Miksa, D.; Irish, E. R.; Chen, D.; Composto, R. J.; Eckmann, D. M., Dextran Functionalized Surfaces via Reductive Amination: Morphology, Wetting, and Adhesion. *Biomacromolecules* **2006,** 7, (2), 557-564.

37. Hughes, G.; Nevell, T. P., The Mechanism of the Oxidation of Glucose by Periodate. *Trans. Faraday Soc.* **1948,** 44, . 941-948.

38. Caelen, I.; Gao, H.; Sigrist, H., Protein Density Gradients on Surface. *Langmuir* **2002,** 18, 2463-2467.

39. Gao, H.; Guinchard, S.; Crevoisier, F.; Angeloni, S.; Sigrist, H., Microarrays and Surface Engineering for Bioanalysis. *Chimia* **2003,** 57, 651-654.

40. Sprenger, N.; Sigrist, H.; Gao, H., Polysaccharides for functional biomolecules display on surface. *BioTech International, Microarrays* September, 2005.

41. Chevolot, Y.; Bucher, O.; Léonard, D.; Mathieu, J.; Sigrist, H., Synthesis and Characterization of a Photoactivatable Glycoaryldiazirine for Surface Glycoengineering. *Bioconjugate Chem.* **1999,** 10, 169-175.

42. Chevolot, Y.; Martins, J.; Milosevic, N.; Léonard, D.; Zeng, S.; Malissard, M.; Berger, E. G.; Maier, P.; Mathieu, J.; Crout, D. H. G.; Sigrist, H., Immobilisation on Polystyrene of Diazirine Derivatives of Mono-and Disaccharides : Biological Activities of Modified Surfaces. *Bioorg. med. chem.* **2001,** 9 (11), 2943-2953.

43. Léonard, D.; Chevolot, Y.; Bucher, O.; Sigrist, H.; Mathieu, H. J., ToF-SIMS and XPS study of photoactivatable reagents designed for surface glycoengineering Part 1. N-(m-(3-(trifluoromethyl)diazirine-3-yl)phenyl)-4-maleimido-butyramide (MAD) on silicon, silicon nitride and diamond. *Surface Interf. Analys.* **1998,** 26, (11), 783-792.

44. Léonard, D.; Chevolot, Y.; Bucher, O.; Haenni, W.; Sigrist, H.; Mathieu, H. J., ToF-SIMS and XPS study of photoactivatable reagents designed for surface glycoengineering Part 2. Part 2. N-[m-(3-(TriÑuoromethyl)diazirine-3-yl)phenyl] -4-(-3-thio(-1-D-galactopyrannosyl)-maleimidyl) butyramide (MAD-Gal) on Diamond. *Surf. Interf. Anal.* **1998,** 26, (11), 793-799.

45. Léonard, D.; Chevolot, Y.; Bucher, O.; Haenni, W.; Sigrist, H.; Mathieu, H. J., ToF-SIMS and XPS study of photoactivatable reagents designed for surface glycoengineering. Part III. 5-

Carboxamidopentyl-N-[m-[3-(trifluoromethyl)diazirin-3-yl]phenyl-b-Dgalactopyranosyl]-(1->4)-1-thio-b-D-glucopyranoside (lactose aryl diazirine) on diamond. *Surf. Interf. Anal.* **2001,** 31, (6), 457-464.

46. Yoshimura, I.; Miyahara, Y.; Kasagi, N.; Yamane, H.; Ojida, A.; Hamachi, I., Molecular Recognition in a Supramolecular Hydrogel to Afford a Semi-Wet Sensor Chip. *J. Am. Chem. Soc.* **2004,** 126, (39), 12204-12205.

47. Nowakowska, M.; Zapotoczny, S.; Sterzel, M.; Kot, E., Novel Water-Soluble Photosensitizers from Dextrans. *Biomacromolecules* **2004,** 5, (3), 1009-1014.

48. Wiki, M.; Gao, H.; Juvet, M.; Kunz, R. E., Compact integrated optical sensor system. *Biosens. Bioelectron.* **2001,** 16, 37-45.

49. Linder, V.; Verpoorte, E.; Thormann, W.; de Rooij, N. F.; Sigrist, H., Surface Biopassivation of Replicated Poly(dimethylsiloxane) Microfluidic Channels and Application to Heterogeneous Immunoreaction with On-Chip Fluorescence Detection. *Anal. Chem.* **2001,** 73, (17), 4181-4189.

50. Martwiset, S.; Koh, A. E.; Chen, W., Nonfouling characteristics of dextran-containing surfaces. *Langmuir* **2006,** 22, (19), 8192-8196.

51. Dankbar, D., M. ; Gauglitz, G., A study on photolinkers used for biomolecule attachment to polymer surfaces. *Anal. Bioanal. Chem.* **2006,** V386, (7), 1967-1974.

52. Suni, T.; Henttinen, K.; Suni, I.; Makinen, J., Effects of Plasma Activation on Hydrophilic Bonding of Si and SiO[sub 2]. *Journal of The Electrochemical Society* **2002,** 149, (6), G348-G351.

53. Amirfeiz, P.; Bengtsson, S.; Bergh, M.; Zanghellini, E.; Borjesson, L., Formation of Silicon Structures by Plasma-Activated Wafer Bonding. *Journal of The Electrochemical Society* **2000,** 147, (7), 2693-2698.

54. Cakić, M.; Cvetković, D.; Stojanoski, K.; Premović, P.; Ristova, M., Structural Study of Dextran, Hydrogenated Dextran and Their Iron (III) Complexes. Part I. Infrared and ESR Spectra. *Spectroscopy Letters* **1995,** 28, 167-176.

55. Panov, V., *Konformacii Sacharov*. Nauka i teknika: Minsk, 1975.

56. Sivchik, V. V.; Zhbankov, R. G.; Astreiko, M. V., Theoretical Investigation of the Vibrational Spectrum of Dextran. *Acta Polym.* **1979,** 30, 689-693.

57. Cael, J. J.; Gardner, K. H.; Koening, J. L.; Blackwell, J., Infrared and Raman Spectroscopy of Carbohydrates. Paper V. Normal Coordinated Analysis of Cellulose I *J. Chem. Phys.* **1975,** 62, (3), 1145-1153.

58. Angst, D. L.; Simmons, G. W., Moisture absorption characteristics of organosiloxane self-assembled monolayers. *Langmuir* **1991,** 7, (10), 2236-2242.

59. Tripp, C. P.; Hair, M. L., An Infrared Study of the Reaction of Octadecyltrichlorosilane with Silica. *Langmuir* **1992,** 8, (4), 1120-1126.

60. Tripp, C. P.; Hair, M. L., Direct Observation of the Surface Bonds between Self-Assembled Monolayers of Octadecyltrichlorosilane and Silica Surfaces: A Low-Frequency IR Study at the Solid/Liquid Interface. *Langmuir* **1995,** 11, (4), 1215-1219.

61. Ullman, A., Formation and Structure of Self-Assembled Monolayers. *Chem. Rev.* **1996,** 96, 1533-1554.

62. Bartic, C.; Borghs, G., Organic thin-film transistors as transducers for (bio) analytical applications. *Anal. Bioanal. Chem.* **2006,** 384, (2), 354-365.

63. Reiter, G.; Hassler, N.; Weber, V.; Falkenhagen, D.; Fringeli, U. P., In situ FTIR ATR spectroscopy study of the interaction of immobilized human tumor necrosis factor-a with a monoclonal antibody in aqueous environment. *Biochim Biophys Acta* **2004,** 1699, 253-261.

64. Zhuravlev, L. T., Concentration of hydroxyl groups on the surface of amorphous silicas. *Langmuir* **1987,** 3, (3), 316-318.

65. Silberzan, P.; Leger, L.; Ausserre, D.; Benattar, J. J., Silanation of silica surfaces. A new method of constructing pure or mixed monolayers. *Langmuir* **1991,** 7, (8), 1647-1651.

66. Bautista, R.; Hartmann, N.; Hasselbrink, E., Two-Dimensional Aggregation of Species with Weak and Strong Bonding Interactions: Modeling the Growth of Self-Assembled Alkylsiloxane Monolayers. *Langmuir* **2003,** 19, (17), 6590-6593.

67. Rye, R. R.; Nelson, G. C.; Dugger, M. T., Mechanistic Aspects of Alkylchlorosilane Coupling Reactions. *Langmuir* **1997,** 13, (11), 2965-2972.

68. Yamaguchi, Y.; RichardsJr, A.; Schaefer III, H. F., The $GeOH^{+}$-$HGeO^{+}$ system: A detailed quantum mechanical study. *J. Chem. Phys.* **1995,** 103, (18), 7975-7982.

69. Fringeli, U. P.; Goette, J.; Reiter, G.; Siam, M.; Baurecht, D., Structural investigations of oriented membrane assemblies by FTIR-ATR spectroscopy. In *Fourier Transform Spectroscopy*, deHaseth, J. A., Ed. 1998; pp 729-747.

70. Reiter, G.; Siam, M.; Falkenhagen, D.; Gollnerictsch, W.; Baurecht, D.; Fringeli, U. P., Interaction of a Bacterial Endotoxin with Different Surfaces Investigated by in Situ Fourier Transform Infrared Attenuated Total Reflection Spectroscopy. *Langmuir* **2002,** 18.

71. Schwarzott, M.; Engelhardt, H.; Klühspies, T.; Baurecht, D.; Naumann, D.; Fringeli, U. P., In Situ FTIR ATR Spectroscopy of the Preparation of an Oriented Monomolecular Film of Porin Omp32 on an Internal Reflecting Element by Dialysis. *Langmuir* **2003,** 19, 7451-7459.

Chapter 3

Gold nanoparticles immobilization on surface

3.1. Monolayer protected metal nanoparticles

The potential application in various fields such as bio-sensing1, [2], catalysis[3], electronics[4] and nanotechnology[5, 6] intensified the interest in nanostructed materials using metal or semiconductor nanoparticles as building blocks iinserted in a bio-active matrix[6]. Water soluble gold thiol monolayer protected nanoparticles (MPNs) with subnanometer-sized metal cores[7, 8], combine the unique electronic, photonic and catalytic features of the metal nub with a wide portfolio of synthetic methods enabling fine shape and size tuning[9-16].

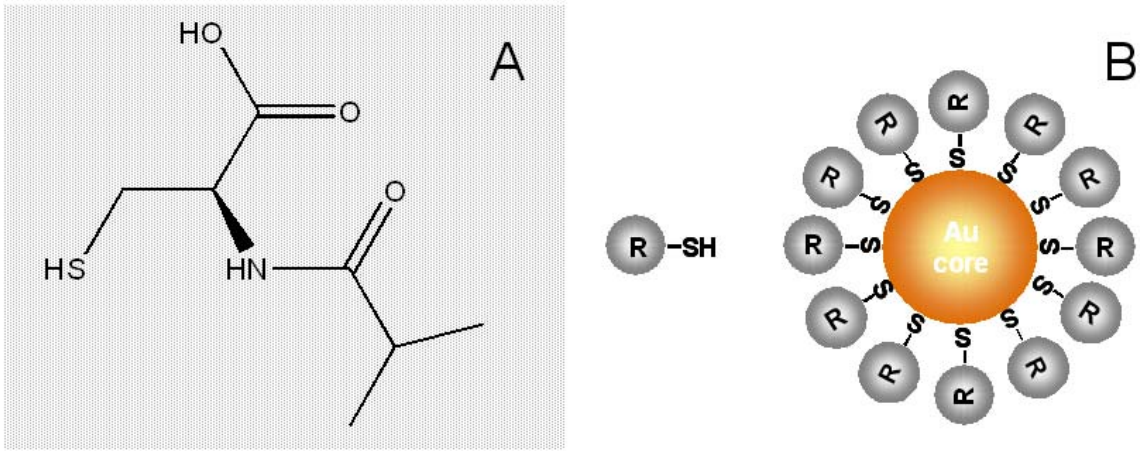

Figure 3-1. Structure of N-isobutyryl-L-cysteine (A) and schematic representation of a monolayer protected nanoparticle (B). Specifically a gold particle protected by a thiolate ligand (R-SH) is shown.

MPNs constituted of gold cores, chemically modified with N-isobutyryl-L-cysteine (capping agent, Figure 3.1), resulting in nanoparticles of 2 nm in size, with narrow size distribution, were prepared following a previously reported process[17]. Their chiroptical properties in the UV-vis and infrared were explored tracing the chemical behavior of the N-isobutyryl-L-cysteine shell. The characterization by vibrational circular dichroism helped to determine the conformation of the thiol adsorbed on the gold nanoparticles[18, 19]. The well known philicity of amino acid side-chains for photogenerated carbenes[20-22] provided preference for such material to study the surface grafting of gold nanoparticles *via* the photobonding technology.

3.2. Surface decoration using nanoparticles immobilization

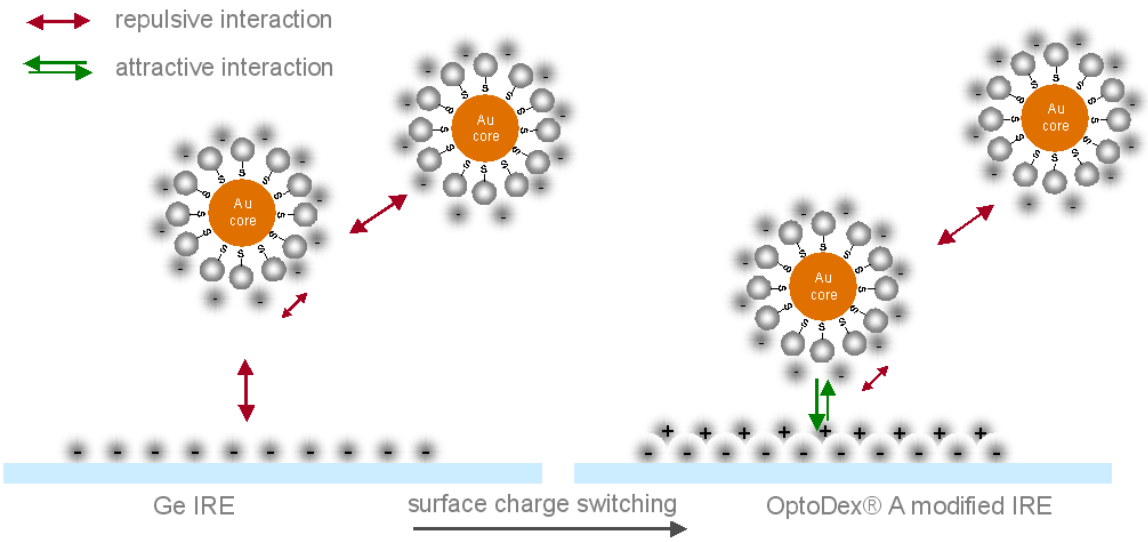

Figure 3-2. Exemplification of Au MPNs behavior towards the plain Ge IRE (plasma pretreated, on the left side) and the OptoDex® A modified IRE (right side). Repulsive interaction is expected between Au MPNs in solution, although water and PBS buffer provide counter ions. Repulsive interactions define the configuration of shell around the gold core. OptoDex® A modification of the IRE switches the MPNs-surface interaction from repulsive to attractive.

Hybrid functional materials embedding three dimensional (3-D) nanoparticles (NPs) scaffoldings or two dimensional (2-D) NPs networks have been demonstrated to display suitable features for applications in ultrasensitive (bio)-sensing[23], nanoelectronics[24], design of highly efficient catalysts[25], ultrafast quantum computing[26] and high density data storage devices[27]. A photo affinity mediated technique leading to the surface immobilization of nano-objects such as semiconductor or metal particles and nanorods, carbon nanotubes and nanowires is highly desirable. Photobonding suits this vision and OptoDex® A was selected as photolinker polymer. This approach responds to a novel bottom-up manufacturing technique for nanoparticles covalent decoration of surfaces. The choice was motivated by considering OptoDex® A as a surface charge switcher. In general, the interaction of hydrophilic capped nanoparticles with a surface is strongly influenced by charge[28]. The small size of the N-isobutyryl-L cysteine protected nanoparticles results in an elevated surface/bulk ratio. In aqueous medium, at mild pH (comprised between 5.0 and 7.0), the carboxylic acid groups are considerably deprotonated therefore inducing negative charge density. The phenomenon implies repulsive interactions both within and between particles (see Figure 3-2). The MPNs form a stable dispersion in aqueous solution and are repelled by negatively charged surfaces. Repulsion between the adsorbed ligands leads to a rigid shell. This furthermore hinders surface interaction due to the reduced flexibility of the particle. Note that the number of adsorbed ligands per surface gold atom and therefore the surface charge is much larger for a curved convex surface than for a flat one. Stated this model, the negatively charged Germanium surface, as when in contact with aqueous medium, necessitated to be converted into a (weakly) positively charged interface. OptoDex® A, displaying amino groups, was retained to fulfill this task. The same model is conceivable for MPNs nanopatterning, but implies some considerations relating to the mutual approach mechanism of the two entities, nanoparticle and

surface. Energetically, the proximity of the MPNs in solution and the surface, up to the contact, is unfavorable and the two potential partners risk never entering in a distance range suitable for establishing of a positive (detectable) interaction. Under these constraints, photobonding technology was thought apt for as unique tool of immobilization. Carben insertion gently (without injuring the external shell structure) but firmly (providing a MPN shell-dextran chemical bond), anchors the nanoparticles to the surface which they would spontaneously not even approach. Enabling the formation of self assembling monolayers (SAMs) stays as an alternative method[29]. Actinic patterns could be designed by local dispensing of the photolinker, or of the MPNs, or of both, while respecting the compatible conditions for all components. The design of local dispensing tools is not the aim of this work and depends on specific applications. Controlled volume drops casting by pipetting was used and fits this study of proof of concept. It deserves to be pointed out that preparation of SAMs requires interface conditions optimization to encourage spontaneous, unconstrained and stable interactions[5, 29]. Tailoring the photolinker polymer (grafting of functional group derivatives by using existing or novel OptoDex® family compounds) or adjusting the medium conditions (ionic strength, pH) are both combinable strategies to design MNPs patterns driven by auto-organization prior to use the photobonding technology as a fixing glue.

3.2.1. Experimental section

3.2.1.1. Chemicals

Ethanol (EtOH, Merck p.a. was used as received). Water was purified with a Milli-Q system (≥ 18 MΩ cm). Amino dextran 40000 Dalton was a Molecular Probes™ product (currently, Invitrogen Detection Technologies). OptoDex® A (amino), OptoDex® B (blocked), were received from *arrayon Biotechnology*,

Neuchâtel, Switzerland. PBS buffer pouches (Sigma) were reconstituted in 1 L purified water yielding 10mM phosphate buffered saline solution (0.15 M NaCl, pH 7.4). pH was verified and freshly dilution to PBS 1% prepared as required by experimental conditions. Gold N-isobutyryl-L-cysteine monolayer protected nanoparticles (MPNs) were courtesy of Cyrille Gautier, University of Neuchâtel. These particles have a mean particle size smaller than 2 nm. The smallest characterized particles have a core size of 10-12, 15 and 18 gold atoms and around ten N-isobutyryl-L-cysteine ligands absorbing to the metal *via* the thiol tether[17]. The synthesis yields to a blend of MPNs with a core diameter comprised between 1 and 2 nm and the surface immobilization was preformed using as-prepared samples (not monodispersed). Eight compounds could be separated according to increasing particle size and charge by PAGE (Polyacrylamide Gel Electrophoresis)[30].

3.2.1.2. Germanium plate modification

Germanium IRE pre-treatment. Germanium (Ge) internal reflection elements (IRE; 50mm X 20 mm x 1 mm, Komlas, Berlin, Germany) were used for ATR-IR experiment. The IREs were first polished with a 0,25-μm-grain size diamond paste (MetaDi® II, Buehler GmbH, Germany) and afterward rinsed copiously with EtOH and water before the surface was plasma cleaned under a flow of air for 5 min (PlasmaPrep 2, GaLa Instrumente GmbH, Germany). Plasma surface treatment with oxidizing species such as air aimed to remove organics, leaving functional oxygen-containing groups on the surface. These groups greatly enhance wetting. Complete hydrophilic activation was achieved by 20 min of dipping in water to enhance formation of oxydrils (-OH groups) right before polymer functionalization. Wet plates were dried by nitrogen flushing. In a subsequent step, a film of OptoDex® A was cast

onto the surface according to two different protocols applying alternatively for mono or multilayer photolinker polymer functionalization, respectively.

Germanium IRE functionalization by a thick film of OptoDex® A (ex situ). 300 µl of OptoDex A 0.1 mg/ml in pure water were cast by pipetting on one entire side of the plate. When using the SBSR technique, half quantity of polymer aqueous solution at the same concentration was used to cover the pre-treated IRE upper side (sample zone, roughly half area). The solution was evaporated at room temperature under enhanced hood ventilation for several hours. The basic casting technique does not allow any control on homogeneous polymer deposition. The evaporation phenomenon determines the film formation. A SBSR measurement, setting the lift steps at different positions, namely 800 and 2000 steps, provides a rough estimation of the homogeneity of the surface functionalization. No rinsing step is performed before the UV exposure and the sample is protected from exceeding UV light exposure.

Germanium IRE functionalization by OptoDex® A thin film casting (ex situ and in situ). Polished, plasma treated and wettability enhanced germanium IREs were dipped for 1 hour in 5 ml of OptoDex® A 0.1 mg/ml in pure water. The technique provides both sides physisorption-mediated polymer casting. A mild but extensive water rinsing assures the oligolayers scaffold remaining in contact with the germanium surface (Table 2-4). In this case, the thickness of the intermediate photolinker film (~ 16 *Å*) is in the same order of magnitude than the nanoparticle size (2 nm). Thin film casting was provided eventually *in situ* using the double cell micro fluidic holder to differentiate sample and reference compartment. More controlled but similar result in terms of OptoDex® monolayer surface arrangement were achieved by *ex situ* and/or *in situ* functionalization procedures. The actinic activity is preserved, avoiding UV exposure.

3.2.1.3. Gold nanoparticle immobilization technique

N-isobutyryl-cysteine MPNs, with a mean particle size smaller than 2 nm and highly soluble in water were freshly prepared and characterized (Gautier, C. *at al.* 2006). MNPs were transferred from the aqueous medium to the photolinker thick (or thin) layer by pipetting. The brownish solution 0.5 mg/ml was reconstituted in pure water without any salt or other agents which would crystallize as the solvent evaporates. The dispensed volume was depending on the size of the area to be covered: according to the measurement set-up the whole IRE was coated when measuring in standard mode, whereas only half when measuring in SBSR mode. It should be noted that the OptoDex® A derived IRE shows a slightly decreased wettability than the bare surface right after plasma treatment. Neverthless, OptoDex® A assures a hydrophilic interface. Basically two protocols were applied. The first one, conventionally named *layer coating*, is based on casting photolinker polymer and MNPs in a stepwise order before UV light exposure. This method was applied to both, OptoDex® thick and thin film pre-coated IREs. The second method, for sake of brevity named *co-coating*, consist of casting on the plate a blend of photolinker polymer and MNPs aqueous solution with concentration of the same order of magnitude. The aim was to establish a simultaneous presence of the two components on the surface, before UV exposure. Evaporation regulates the distribution of the dextran based polymer and gold nanoparticles on the surface. Theoretically the two methods would trigger the gold nanoparticle to differently organize on the surface. Under *layer coating* conditions, nanoparticles approach the surface *via* a smooth and porous layer woven of dextran chains stretched out randomly, bearing a low positive charge density. In the *co-coating* method the dextran adsorption on the surface takes place in presence of charged (negatively, high charge density) nanoparticles. Possibly the dextran interacts with the nanoparticles already in solutions.

Layer coating. 400 µl of 0.5 mg/ml aqueous solution of N-isobutyl-cysteine gold nanoparticles were dropped by pipetting on an IRE previously functionalized with a thick film of OptoDex® A (*arrayon* biotechnology, Switzerland). One should note that for the OptoDex® layer casting only 300 µl of aqueous solution were used. Dextran crystals dissolve in water drops containing nanoparticles, however not allowing the establishment of the same boundary wetting behavior as on the plain IRE right after plasma pre-treatment. The IRE was placed under a hood providing continuous air aspiration to facilitate evaporation. The air aspiration system was slowed down at the beginning to prevent the disturbance of the liquid. The element was kept under these conditions for at least five hours and then flushed with nitrogen to replace outer bound water. Nanoparticles were left behind as evaporation occurred. No rinsing action was carried out to assure the maximal amount of the cast blend of polymer and nanoparticles on the surface when the UV exposure took place. Such a functionalized IRE underwent photo exposure under controlled conditions as described below.

Co-coating. 150 µl of a brown transparent N-isobutyryl-cysteine gold nanoparticles aqueous solution 0.4 mg/ml were mixed with 150 µl of clear OptoDex® A (*arrayon* biotechnology, Switzerland) solution 0.2 mg/ml. The final blend concentration was 0.2 mg/ml in N-isobutyryl-cysteine gold nanoparticles and 0.1 mg/ml in OptoDex A. It was left 10 minutes under slow stirring and then one additional hour, protected by aluminum foil to avoid UV activation, to ascertain that no aggregation occurs with consequent precipitation. 300 µl of the actinic dextran-gold MPNs blend were dispensed by pipetting on an IRE previously pre-treated (*cf. Germanium* IRE pre-treatment above). Evaporation was conducted under the same conditions as described above and the same sequence of actions also was carried out till the UV photo-exposure (see below).

UV photo-exposure. 4 min of light exposure at 365 nm at an irradiance of 11 mW/cm^2 were previously demonstrated to be necessary for light driven carbenes generation from an OptoDex® A matrix. The light source for the series of measurements using ATR-IR was a high power ultraviolet lamp (Xenon Arc lamp, Oriel, USA) coupled to an optical fibers bundle. The light intensity after the bundle was measured with an UV light intensimeter equipped with a 350 nm filter (Suss MicroOptics, Switzerland). Distance from the surface and time were adjusted to achieve the required exposure. According to the optimized set-up, a Ge IRE was illuminated for 6 min setting the optical fibers outlet 15 mm away from the functionalized surface. Repeated exposures under the same conditions were performed all along the IRE length. Exposure was carried out eventually for an exceeding time to ensure sufficient photobonding. After irradiation the samples were rinsed with water. The mild rinsing process consisted of a few seconds water flushing. The extensive washing consisted of repetitive renewed water flooding of the surface followed by water dipping for 90 min. The extensive washing did not cause complete removal of the cast nanoparticles if the photobonding was effective.

ATR measurements were performed as described in chapter 2.1.1.3.

3.3. Results and discussion

3.3.1. MPNs immobilization via OptoDex A thick film (*layer coating*)

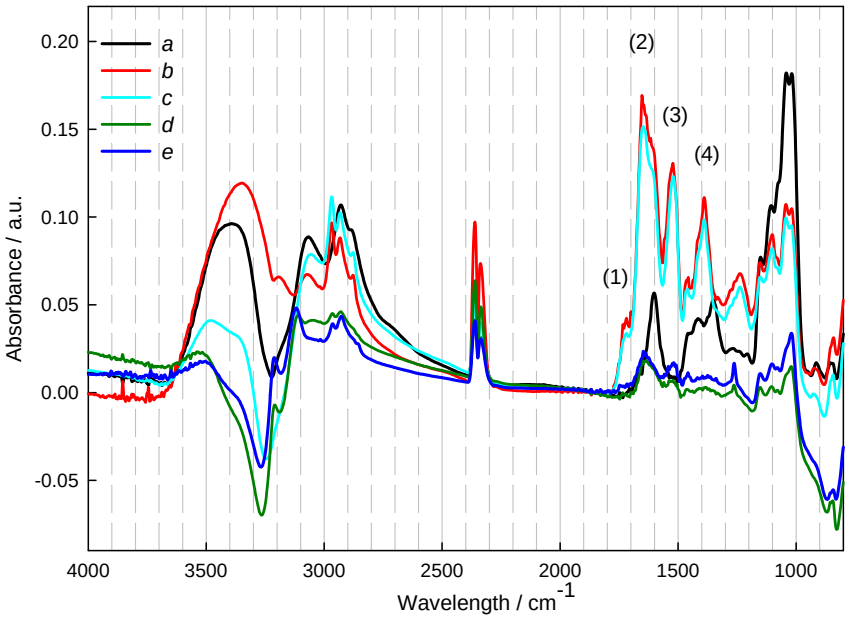

Figure 3-3. ATR spectra corresponding to OptoDex® A thick film prior (a, dark line), post N-isobutyl-cysteine Au nanoparticles layer casting (b, red line), after illumination (c, cyan line) and then submitted to mild (d, green line) and thorough water rinsing (e, blue line). (1) to (4) refers to typical.bands for N-isobutyryl-cisteine Au nanoparticles. Spectra were registered using parallel polarized light. The lift position was set at 800 steps.

The entire procedure leading to the immobilization of N-isobutyryl-cysteine MPNs according to the *layer coating* technique can be resumed in five steps as follows:

a) OptoDex ® A thick film casting;

b) N-isobutyryl-cysteine Au nanoparticles thick film casting;

c) UV light exposure;

d) mild water rinsing;

e) extensive water rinsing.

This sequence of actions, resulting in a continuous surface modification, was monitored by ATR measurements as reported in Figure 3-3**.** The region between 950 cm^{-1} and 1100 cm^{-1} as well as the region 2800-3000 cm^{-1} show, as anticipated, the typical aminodextran bands. The most prominent signals for MPNs related to the N-isobutyryl-cysteine shell protecting the gold core are expected in the region between 1800 cm^{-1} and 1200 cm^{-1}. In this region OptoDex® A also contributes to the IR spectrum. The important presence of water is indicated through the broad band above 3000 cm^{-1}. The black spectrum (a) in Figure 2-41, confirms the presence of a thick film of the photolinker polymer. Spectrum b (red) assesses the presence of MPNs with the characteristic bands labeled (1), (2), (3) and (4), which will be discussed in detail later. Spectrum c (cyan) depicts the situation after UV exposure (*ex situ*). Spectra d (dark green) and e (blue) reveal, although the highly reduced intensities, the bands evident in spectrum c (cyan). These spectra describe the final IRE modification after mild (dark green, d) and extensive water washing (blue line, e). The washing step under these conditions and the detectable presence of the MPNs is the proof that the photobonding occurred and was effective in immobilizing the nanoparticles on the surface. The illumination step deserves deeper attention. Figure 2-42 shows a difference spectrum revealing the changes upon illumination. One significant difference is remarkable in the water related absorption, in the 3600-3100 cm^{-1} wavelength region, ν_s(H-O-H) and ν_{as}(H-O-H), and around 1645 cm^{-1} δ(H-O-H). After UV exposure an important decrease of the water quantity in the thick film is registered. Note that spectra are registered after the same time, namely 30 min, of air purging. Then, the water observed in the spectra is linked to the water embedded in the dextran layer. UV illumination could cause a collapse of the dextran backbone structure with partial exclusion of absorbed water molecules.

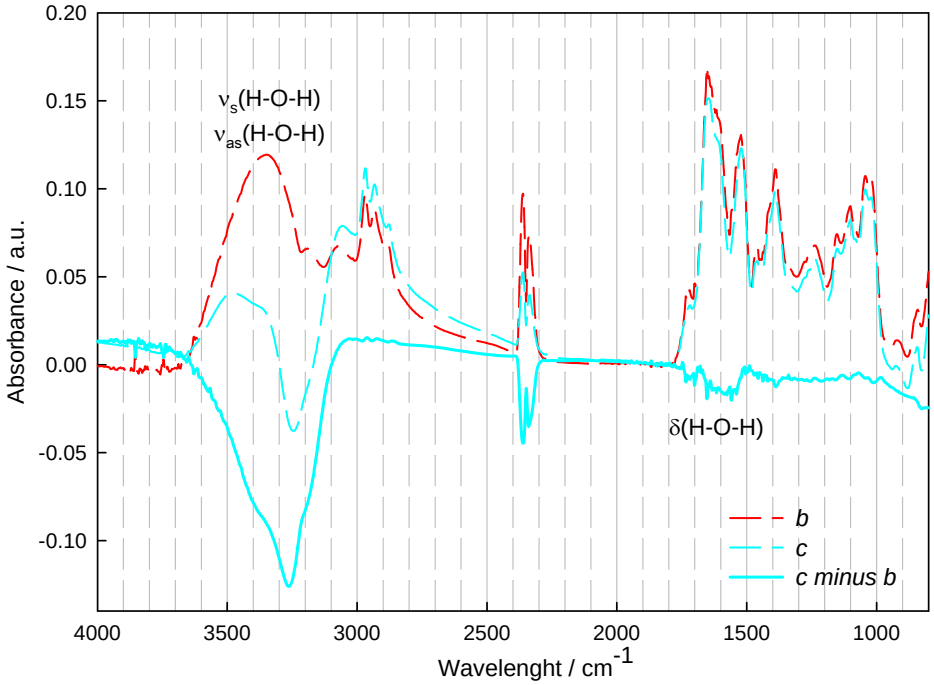

Figure 3-4. ATR spectra corresponding to N-isobutyryl-cysteine Au nanoparticles layered on OptoDex® A thick film before (b, red dashed line) and after (c, cyan dashed line) illumination. The plain cyan line results from mathematical subtraction of c minus b and describes the differences attributable to the UV light exposure. ν_s(H-O-H), ν_{as}(H-O-H) and δ(H-O-H) denote the symmetric stretching, the antisymmetric stretching and the bending mode of water. b and c refers to the actions' sequence listed in 2.7.2.1.

The water decrease detectable by ATR spectroscopy may be a consequence of the carben generation and insertion reaction: the inter glucopyranose rings cross reaction may cause a partial contraction of the thick film, with some internal pores occlusion. Figure 3-4 reveals another important point: under UV-irradiation in the presence of air, thiols can be converted into sulfoxides. The spectra give no evidence for such a reaction under our conditions. This is important because the sulfoxides are much weaker adsorber than the thiols. The difference spectrum in Figure 3-5 corresponds to the spectrum of a thick film of N-isobutyryl-L-cysteine monolayer protected gold nanoparticles (difference spectrum b minus a). It was obtained by subtracting the spectrum measured after MPN thick film casting from the one before casting, over an

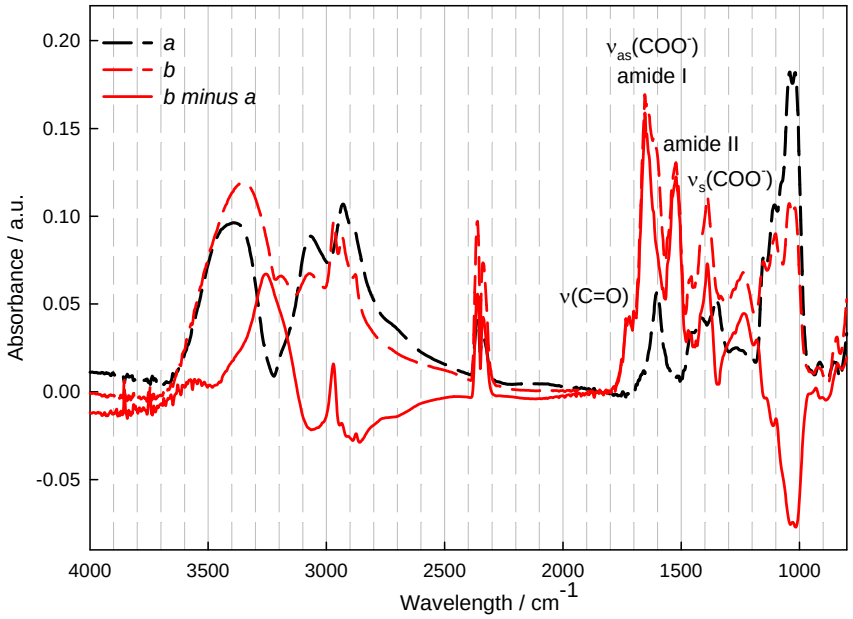

Figure 3-5. Spectrum of MPNs thick film (red solid line) as resulting from spectrum b (red dashed line, N-isobutyryl-cysteine Au nanoparticle cast and evaporated over an OptoDex® A thick film) minus spectrum a (dark dashed line, OptoDex® A thick film only). Not surprisingly the water content is bigger in spectrum b corresponding to a ranked bilayer (surface adjacent layer, OptoDex® A; superposed layer, MPNs) with a consequent increased global thickness.

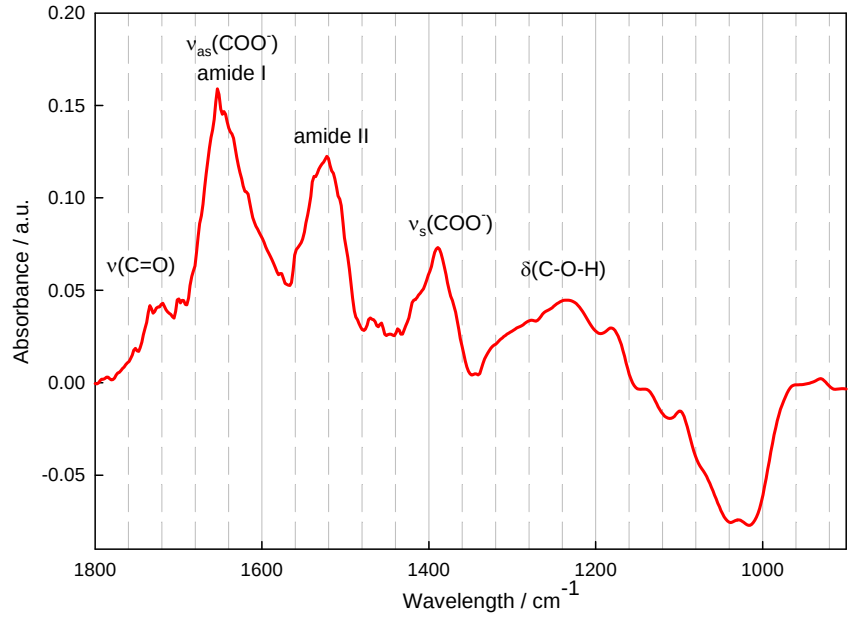

Figure 3-6. Blow up of the spectrum of N-isobutyryl-L-cysteine monolayer protected gold nanoparticles as cast as a thick film on the Optodex® A coated Ge IRE.

IRE pre-modified by OptoDex® A. Such a calculated spectrum was taken as reference to ascertain the presence on MPNs on the surface also in tiny amount. A blow up of the spectrum in the fingerprint region for N-isobutyryl-L-cysteine monolayer protected gold nanoparticles is shown in Figure 3-6. The strongest absorption in the 1680-1600 cm^{-1} wavelength region originates from the superposition of two typical absorption bands: the asymmetric carboxylate stretching mode $\nu_{as}(COO^-)$ together with the amide I mode.

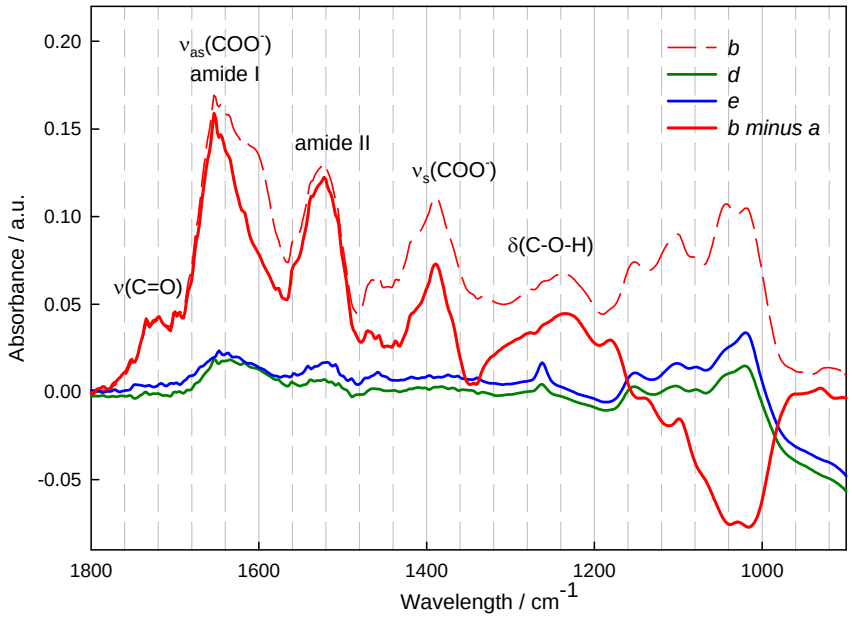

Figure 3-7. ATR spectra of N-isobutyryl-L-cysteine gold nanoparticles immobilized on the Ge IRE. Green and blue lines correspond to spectra after mild and extensive washing, respectively. The N-isobutyryl-L-cysteine gold nanoparticle finger print is evident as revealed from the comparison with the N-isobutyryl-L-cysteine gold nanoparticle thick film spectrum (red solid line). The red dashed line spectrum describes step b: OptoDex® A appears and it guides the observer to trace the weaker (in intensity) but identical (in position) bands in spectra d and e.a, b, d and e refers to the actions' sequence listed in 2.7.2.1.

The amide II mode is found at 1520 cm^{-1}. The asymmetric stretching of the carboxylate absorbs at 1395 cm^{-1} ($\nu_{as}(COO^-)$), while the C=O stretching mode band, due to the protonated acid, is found near 1720 cm^{-1}(ν(C=O)). The corresponding

bending mode due to the –OH is expected in the region between 1200 and 1280 cm^{-1}. These absorption bands correspond to the fingerprint of the N-isobutyryl-L-cysteine shell as depicted in Figure 2-1. Bands assignment is supported by the IR spectra of the deprotonated MNPs in solution, registered in transmission[12, 17], and by those of N-acetyl-L-cysteine adsorbed on gold, registered in ATR (attenuated total reflection) [31, 32].

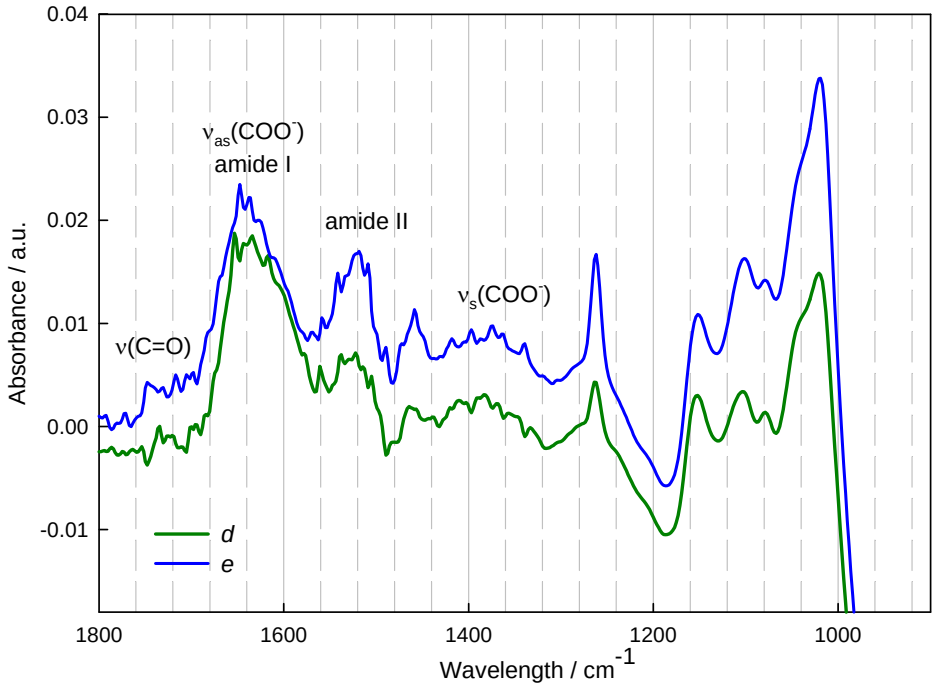

Figure 3-8. Blow up of the ATR spectrum of the N-isobutyryl-L-cysteine gold nanoparticles covalently linked on the edge on the Ge IRE via OptoDex® A thick film actinic activation. In the region comprised between 1200 cm^{-1} and 1000 cm^{-1} OptoDex® A bands are also still appreciable.

The well established ATR spectrum of N-isobutyryl-L-cysteine gold nanoparticle thick film stands as reference to decipher the ATR signals as resulting after immobilization by covalent chemical bond generation on the modified Ge IRE. In Figure 3-7, the spectra related to the completed sequence of the immobilization procedure (last two steps, d and e, green and blue line spectra) clearly show the

presence of MPNs also after UV exposure and extensive rinsing. The only way to justify the presence of such MPNs is to admit that the OptoDex® A mediated immobilization occurred successfully. A blow up of the spectra related to the grafted nanoparticle appears in Figure 3-8**.** In conclusion, the series of spectra registered, allow us to claim that N-isobutyryl-L-cysteine monolayer protected gold nanoparticle, with a size smaller than 2 nm, were successfully immobilized on a surface and detectable via ATR spectroscopy.

3.3.2. MPNs immobilization via OptoDex® A thick film (co-coating)

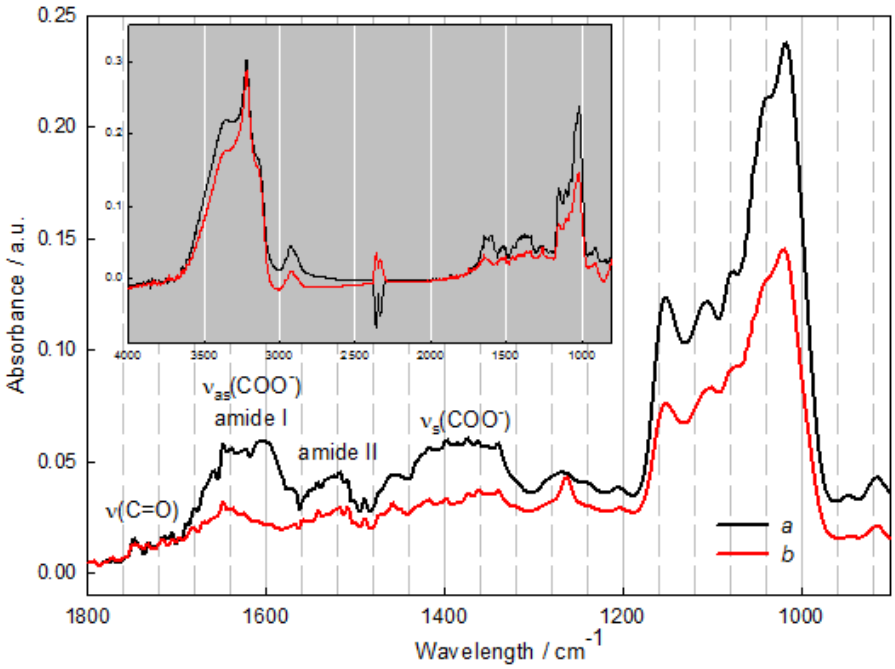

Figure 3-9. Blow-up of the spectra referring to the MPNs immobilization using the *co-coating* method. Graphic (I) depicts the surface modification as originated by the MPNs and OptoDex® A blend just cast and evaporated (black line, step a) and the same after UV exposure and extensive water rinsing (red line, step b). The photobonding occurs and typical absorptions relating to the presence of the N-isobutyryl nanoparticles are detectable. The gray window containing graphic (II) shows the two spectra in the 4000-800 cm^{-1} wavelength range.

The entire procedure leading to the immobilization of N-isobutyl-cysteine gold nanoparticles according to the *co-coating* technique can be resumed in two steps as follows:

a) OptoDex A / N-isobutyryl-cysteine Au nanoparticles blend casting, leading by evaporation to a thick Optodex® A- MPN composite film;

b) UV light exposure and extensive water rinsing.

This sequence of actions where monitored by ATR measurements as reported **in** Figure 3-9**.** The examination of the spectra before and after illumination and water rinsing demonstrates that the immobilization technique was successful.

3.3.3. MPNs immobilization *via* OptoDex® A thin film

The two technique described in the former paragraphs imply the preliminary formation of a thick layer of photolinker, namely the generation of an excess of actinic group which partially link to the surface, partially to the MPNs and partially crosslink each other or with the surrounding water molecules. The unbound part of the thick layer is important and is removed by simple water rinsing after the photobonding event. An alternative was providing a thin film of OptoDex® A, cast on the surface by physisorption. The resulting interface is a monolayer of photoactivable polymer. In this case the procedure can be described by the following segments:

a) OptoDex® A thin film physisorption on the IRE;

b) N-isobutyryl-cysteine Au nanoparticles thick film casting;

c) UV light exposure and extensive water rinsing.

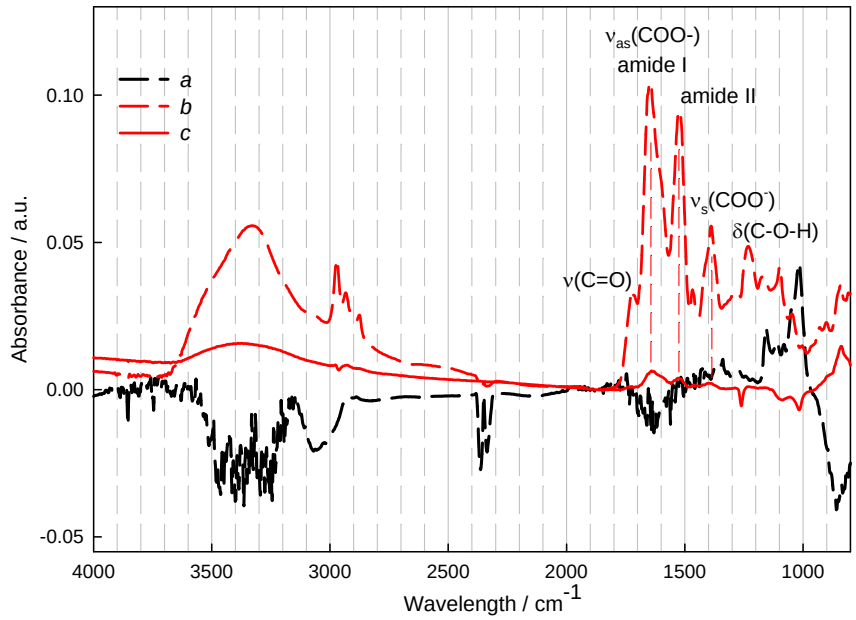

Figure 3-10. OptoDex® A thin film mediated immobilization of N-isobutyryl-L-cysteine gold nanoparticles. Spectrum a (dashed black profile) assesses the OptoDex® A physisorption. Spectrum b (red dashed line) relates to the casted MPNs and spectrum c (solid red line) depicts the surface as after UV exposure and thorough water rinsing.

Figure 3-10 reports the spectroscopic observation of this functionalization. It must be noted that for the functionalization the double cell micro fluidic system and the SBSR measuring technique was applied.The use of the flow through cell allowed the observation of the OptoDex® A physisorption in situ. For sake of economy, exceptionally for this serie of experiments an aqueous solution 0.05 mg/ml (instead of 0.1 mg/ml) of photolinker was used and the surface exposure time was consequently prolonged up to 90 min till the growth of the OptoDex® signal was complete. The SBSR technique was used with the purpose to get separated but quasi simultaneous signals for a parallel functionalization on two different macro sized zones of the IRE, namely R and S compartment areas. The results not shown, confirm that the technique allows quantitatively reproducible OptoDex® A physisorption but a slight difference is noted in terms of water content. This can be due to slight incompensation of the

large water signal in the SBSR mode. Once the formation of the OptoDex® A layer was assessed, the equal functionalization of both compartments permitted the use of the SBSR technique in its standard purpose. Only the area corresponding to the sample compartment (S) was flooded with the MPNs solution and after evaporation spectrum b (red dashed line) was registered confirming the presence of a thick layer of N-isobutyryl-L-cysteine gold nanoparticles. The water amount is related to the thickness of the MPNs layer whose homogeneity is not controllable. After UV exposure and water rinsing the MPN signals diminished significantly as expected but a detectable amount remains grafted on the surface (spectrum c, in Figure 3-10 and Figure 3-11**).**

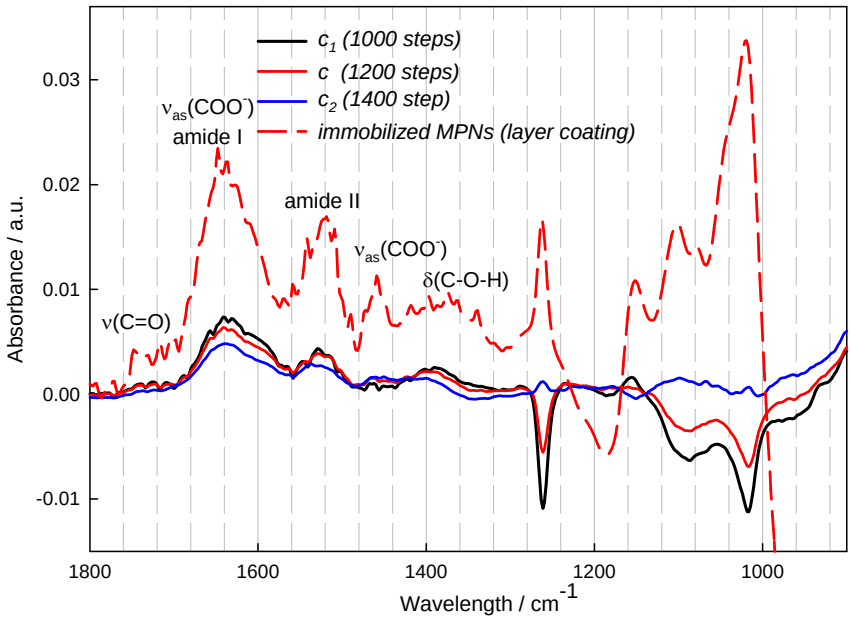

Figure 3-11. Blow up in the 1800-900 cm^{-1} wavelength range of ATR spectra describing MPNs immobilization *via* OptoDex A thin film physisorption and following UV exposure. The red dashed line refers to MPNs immobilization *via* OptoDex A thick film and serves as reference to elucidate the characteristic bands of grafted N-isobutyryl-gold-nanoparticles. Spectra c, c_1 and c_2 result from SBSR measurements at different lift positions, namely 2000-1000 (reference-sample) for spectrum c_1 (black spectrum), 2000-1200 for spectrum c (red spectrum), 2000-1400 for spectrum c_2 (blue spectrum).

A series of SBSR spectra were recorded setting different lift positions for the IR beam on the IRE, namely 1000, 1200 and 1400 steps, while keeping the same position as reference, 2000 steps. The three spectra reported in Figure 2-49 photograph the MPNs grafting on a large area, sweeping the surface comprised between 1000 and 1400 lift steps and the almost entire IRE length. Such an investigation aims to qualitatively define the homogeneity of the MPNs layer. In this perspective, it can be underline that no obvious removal of OptoDex® by the MNPs is detected.

3.3.4. Comparison of the described methods for MPNs immobilization *via* OptoDex® A

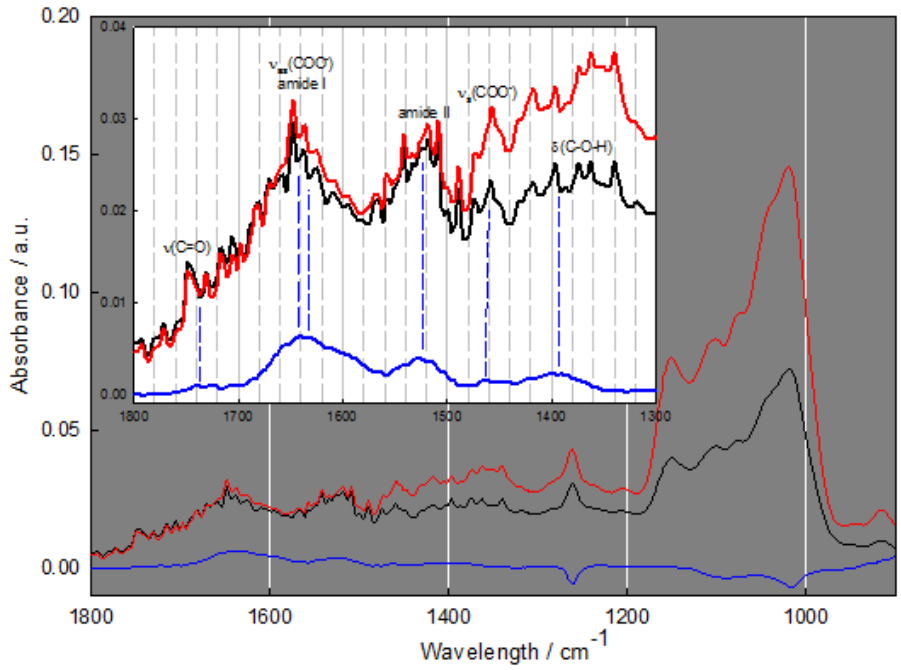

Figure 3-12. Comparison of ATR spectra referring to different MPNs immobilization methods. Thick film casting methods are described by the red spectrum (*co-coating*) and by the black spectrum (*layer coating*). The OptoDex® A presence is detectable between 1200 and 1000 cm^{-1}. The blue spectrum refers to the thin film mediated method and it has been registered in SBSR mode. The contribution due to the OptoDex® A thin film is automatically eliminated from the spectra. Graphic (II) is a blow up of the same spectra evidencing the MPNs immobilization.

In Figure 3-12 spectra for MPNs immobilization using the three described methods are grouped. A blow-up in the region containing the N-isobutyryl-L-cysteine nanoparticle fingerprint is also included. The black spectrum describes the germanium IRE as chemically modified with MPNs photobonded through the layer coating technique, casting the photolinker in a thick film. The red lined spectrum describes the germanium IRE as chemically modified with MPNs photobonded thought the co-coating technique also casting the photolinker/MPNs blend in a thick film. The blue spectrum relates to MPNs immobilized using the layer coating technique casting the photolinker polymer in a thin film. It must be noted that only the latter spectrum (blue line) has been recorded by the SBSR technique. This approach was not applicable to the thick film mediated immobilization methods. A direct comparison between thick and thin film coating techniques is in not possible because in the former methods it is not possible to separate the contribution due to the OptoDex® A. Nevertheless it is obvious that the three techniques led to chemical grafting of N-isobutyryl-cysteine on the surface. The spectra linked to the co-coating (red line) and layer coating (black line) methods - both implying the formation of a thick layer of OptoDex® A on the surface - show an equal amount of immobilized MPNs. In the same spectra, the contrary is observed for OptoDex® A: a different amount of immobilized OptoDex®A is evident from the 1200-1000 cm^{-1} region. If considering the experimental conditions, some remarks on the method effectiveness can be made. The respective starting quantities were:

I. 300 µl of 0.1 mg/ml solution of OptoDex® A, corresponding to 0.03 mg of casted OptoDex® A on the 50 x 20 mm area of the IRE, first layer (*layer coating* method).

II. 400 µl of 0.5 mg/ml solution of MPNs corresponding to 0.2 mg of cast on the 50 x 20 mm are of the IRE, second layer (*layer coating* method).

III. 300 µl of blend solution 0.2 mg/ml in OptoDex® A and 0.4 mg/ml in MPNs, corresponding to 0.03 mg of OptoDex® A and 0.06 mg on MPNs (*co-coating* method), unique layer.

These values demonstrate the higher effectiveness of the *co-coating* method: the Optodex® A starting amount are the same, the MPNs amount is 3.3 times lower and the signal intensity related to MPNs immobilized in conclusion, the same. A possible explication for the higher signal of the OptoDex® A in the case of the co-coating method is a better blending of the two components of the composite.

3.4. Exploration of monolayer protected gold nanoparticles behaviour versus aminodextran modified surface

3.4.1. Experimental section

3.4.1.1. Germanium plate modification

Pretreated Ge IRE, 1 mm thick (N = 42.5, number of internal reflections), were functionalized by OptoDex® A physisorption in situ using a Delrin® home-built liquid flow-through cell with a total volume of 0.077 mL and a gap of 250 μm between the IRE and the polished edge. The two separated compartments, R as reference and S as sample, were connected to a peristaltic pump allowing the surface flooding to get ATR time-resolved spectra monitoring the surface functionalization. Chamber S was flown for 1 hour with an aqueous solution of OptoDex® A 0.1 mg/ml and then for 20 min with pure water, meanwhile chamber R was exposed to water. These conditions were already ascertained favorable to the formation of a physisorbed OptoDex® A film (few layers). After water removal and microfluidics set-up demounting, the surface was dried by nitrogen flushing. The areas bearing the photoactive polymer were locally illuminated as described above. Polymer physisorption and irradiation concerned both sides of the IRE. The photo exposed Ge element was clamped in the flow-through cell; both chambers were flooded with water and set again in the spectrometer verifying that the same conditions as prior to exposure were established. The local functionalization corresponding to the sample compartment area (upper region, comprised from 1600 to 3000 lift steps) allowed the optimized use of the SBSR technique to follow the monolayer formation. Alternatively, IRE thin film functionalization was performed by dipping, rinsing and UV exposure as already described, to ensure a homogeneous coating. The quality of the coating was estimated by registering a reference spectrum (clean and plasma

pretreated IRE) and then a sample single channel spectrum to get the polymer film fingerprint. SBSR measurements at progressive lift steps were registered to evaluate the monolayer casting quality on a macro sized surface (20 mm x 50 mm). In both cases a weakly positive interface was created, responding to the necessity to minimize the repulsive coulomb interaction between the negatively charged MPNs and the slightly negative Ge IRE surface.

3.4.1.2. Surface exposure to MPN solution

The same Delrin® home-built liquid flow-through cell as described above was used for ATR-IR experiments monitoring interaction between the surface and MPNs. The flow-through cell can be heated or cooled, but all measurements reported here were performed at room temperature (T = 298 K). The ATR-IR cell is described in more detail elsewhere. Four different aqueous solution containing N-isobutyryl-cysteine gold nanoparticles were prepared and investigated: a) MPNs 0.5 mg/ml in pure water; b) MPNs 0.5 mg/ml in PBS 1%; c) MPNs 0.5 mg/ml in aqueous citric buffer at pH 5; d) MPNs 0.5 mg/ml in aqueous citric buffer at pH 6. The main difference between a) and b) stay in the higher ionic strength of b) due to presence of salts introduced by PBS. The pH value, which is 7.0 for a) and 7.4 for b), changed only faintly. The difference between solution c) and d) was mainly the pH value, 6 for preparation c) and 5 for preparation d).

3.4.2. ATR measurements

In-situ data acquisition. After water flooding of compartments and ascertaining the absence of air bubbles absence (water signal the same for both R and S), a series of spectra were collected to verify the baseline stability as a proof of the IRE coating quality (no polymer removal or modification). As the S compartment

started to be flooded SBSR spectra were registered. Spectra were recorded at a resolution of 4 cm^{-1}.

3.5. Results and discussion

The surface flooding by the solution containing N-isobutyryl-L-cysteine Au nanoparticle in pure water did not show any detectable interaction attributable to the MPNs with the OptoDex® A modified surface. The possible explication is that at pH 7 the nanoparticle shell decorated with carboxylic acid groups is highly protonated and simple repulsive coulomb interaction prevent any surface approach.

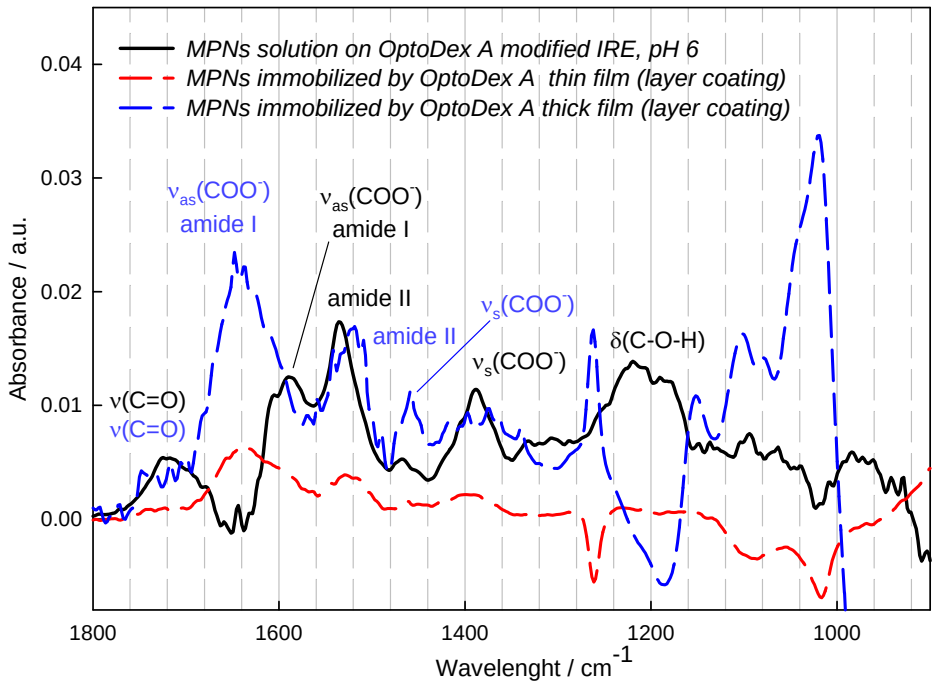

Figure 3-13. Detection by ATR spectroscopy of MPNs' spontaneous interaction with OptoDex® A modified germanium surface at pH 6.

This situation could change under the effect of increased solution ionic strength. Two solutions of the same concentration with an increased ionic strength were prepared

using PBS buffer and PBS buffer 1% as solvent and injected in the S compartment while plain buffer was run in the R compartment. Also in this case no interaction was detectable. The logical following parameter which required to be changed was the pH. Citric buffer adjusted to pH 6 was used as solvent and the solution containing MPNs led to weak but clear interaction with the OptoDex® A chemically modified surface. In Figure 3-13 the black spectrum refers to signal detected after 60 min of surface exposure. Spectra relating to immobilized MPNs are reported in the same graphic for comparison.

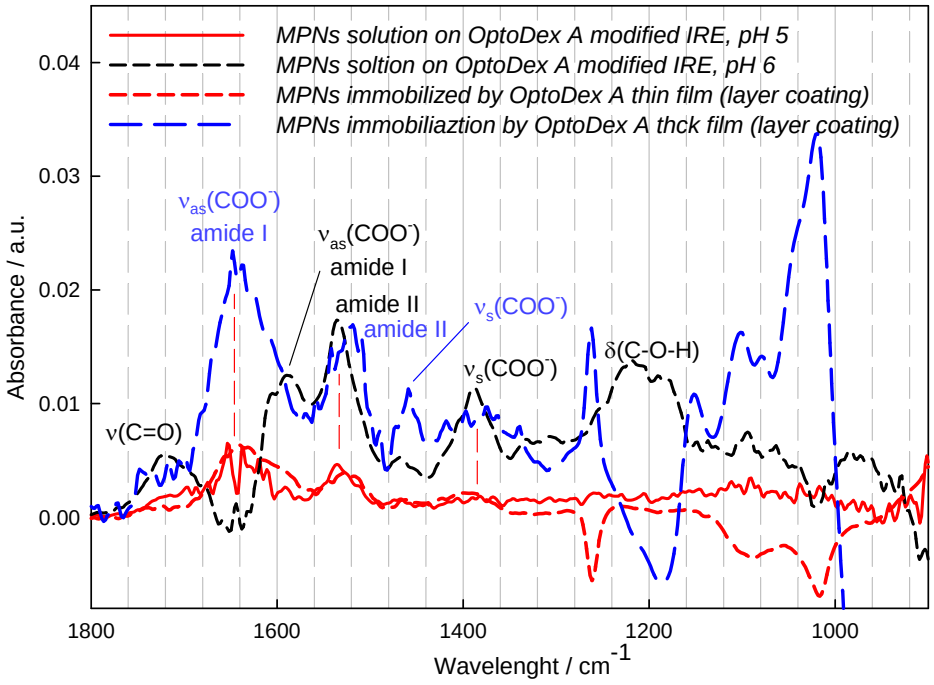

Figure 3-14. ATR spectra summarizing the detectable interactions between Au MPNs and OptoDex® A derived Ge IRE. In respect to Figure 2-51, the spectrum reporting the interaction of Au MPNs and OptoDex® A derived Ge IRE at pH 5, is added (red plain line)

The corresponding ATR spectrum (red line) is reported in Figure 3-14**.** The intensity of the signals leads to the conclusion that, at pH 5 under the described conditions, the interaction is less advantageous than at pH 6. To explain this behavior it is necessary

to consider the effect of the pH variation towards the nanoparticle and the surface. At pH 5 the particles are less negatively charged, wich diminishes the interaction with the positive surface. A shift is remarked for the carboxylic group symmetric and asymmetric stretching modes. Coherently the same is observed for amide I mode. The amide II band shifts only slightly. Particularly significant is the ν(C=O) band. For the MPNs in solution (not immobilized on the surface) at pH 6, the carboxylic groups of the protecting layer seems to be more protonated (clear signal in the black lined spectrum at about 1750 cm^{-1}). In correspondence, the bending mode absorption at 1250 cm^{-1} increases. The differences in the spectrum with respect to the immobilized MPNs may partly be due to the different interaction with the polymer in the two cases. This result inspired a further series of similar measurements using a MPNs solution at pH 5 (citric buffer adjusted to required value).

3.5.1. Transmission Electron Microscopy

The OptoDex® mediated grafting of gold N-isobutyryl-L-cysteine (AuNILC) nanoparticles was observed via ATR spectroscopy. Using the IR based spectroscopic technique, observation if focused on the organic shell of the particles, namely N-isobutyryl-L-cysteine. The high sensitivity of such a technique should not hide the limits of the same: for example surface topography is not directly accessible, even if some consideration can be drawn concerning global surface homogeneity. Also, the metal core itself of the nanoparticles does not lead to signals in the mid IR. Although no apparent reasons could support to the hypothesis of desorption of the chemisorbed organic shell, the investigation by transmission electron microscopy was performed to bring information directly linked to the gold particles on the surface. For ATR-IR, germanium optical elements were used. For TEM observation, silicon oxide coated, 300 mesh, copper grids were submitted to the process previously described and

monitored by IR spectroscopy. The two materials, germanium coated by GeO_2 and copper coated by SiO_2, can be assimilated.

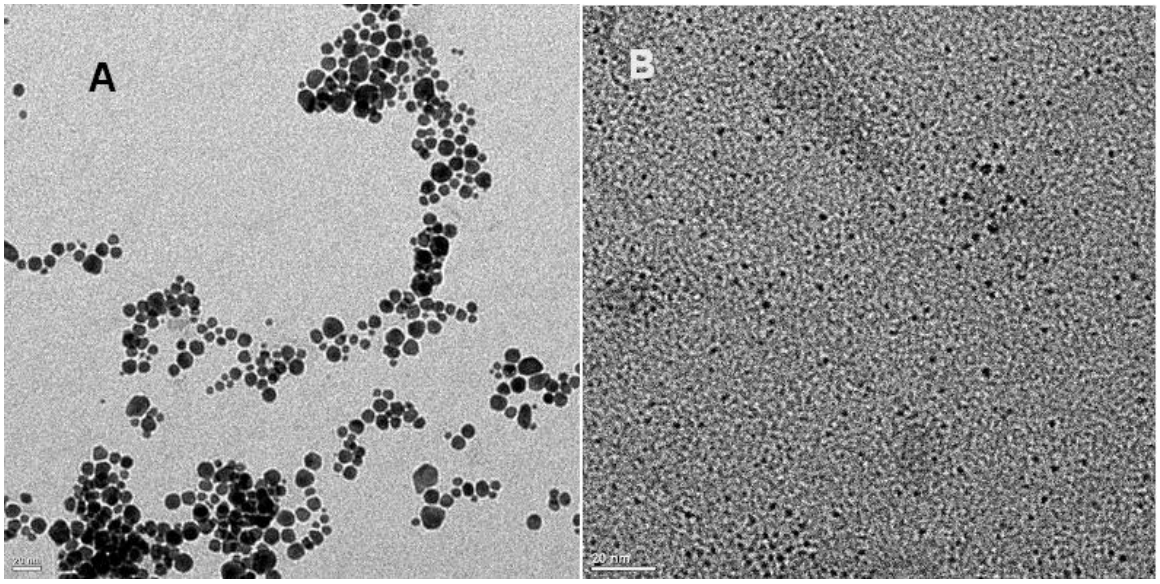

Figure 3-15. TEM images of AuNILC nanoparticle as cast on the conductive grid from aqueous medium (A). The same particles as cast from organic phase (toluene). The bar length corresponds to 20 nm. Courtesy of Cyrille Gautier[30].

The two techniques, TEM in imaging and ATR-IR in spectroscopy, result complementary. It must be noted that the same particles, as resulting from synthesis and purification were previously observed to aggregate (see Figure 3-15 (A)) following transfer to the grid from an aqueous medium. To isolate monodispersed nanoparticles as reported in Figure 3-15 (B), phase transfer in toluene was required (organic phase) before casting onto conductive support for transmission electron measurements[8, 30]. TEM images were recorded with a Philips C200 electron microscope operated at 200 kV. In the case of AuNILC MPNs grafted on the SiO_2 coated grid, the TEM sample was prepared by casting and evaporating a drop of the OptoDex® (0.1 mg/ml in water) as first layer and subsequent casting and drying a drop of AuNILC MPNs aqueous solution (0.05 mg/ml). Conditions for UV exposure at 350 cm^{-1} (time and UV source distance) were adjusted to fulfill the required energy.

Afterward, dipping in water of the sample was prolonged up to 30 min. In such conditions, AuNILC MPNs, if not covalently cross-linked to the surface, would dissolve in water. The image depicted in Figure 3-16 relates to AuNILC MPNs on a film of OptoDex®.

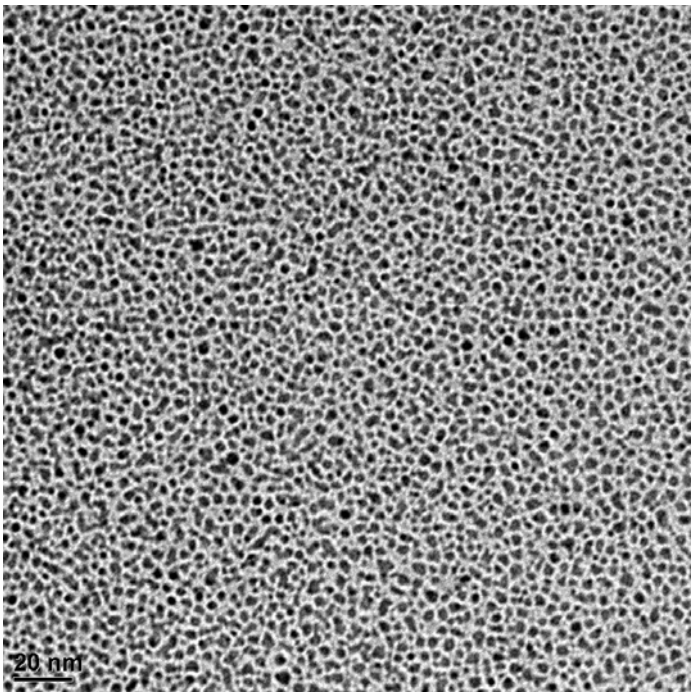

Figure 3-16. TEM images of AuNILC nanoparticle immobilized on SiO_2 coated copper grid by OptoDex® and associated Photobonding technology. The bar length corresponds to 20 nm.

The presence of gold nanoparticle is evinced confirming covalent immobilization by UV irradiation. Nanoparticles spread homogenously over a macro portion of surface and remain separated without further chemical modification[8]. Size and (mono-)dispersion correspond to data previously reported for AuNILC MPNs, as separated by gel electrophoresis and investigated by TEM[30]. A blow-up of the same grafted MPNs is reported in Figure 3-17. More precisely, on the left is reported a transmission electron microscope image. On the right, the same surface is observed in diffraction. Only one diffraction plane can be focused. Therefore only particles with

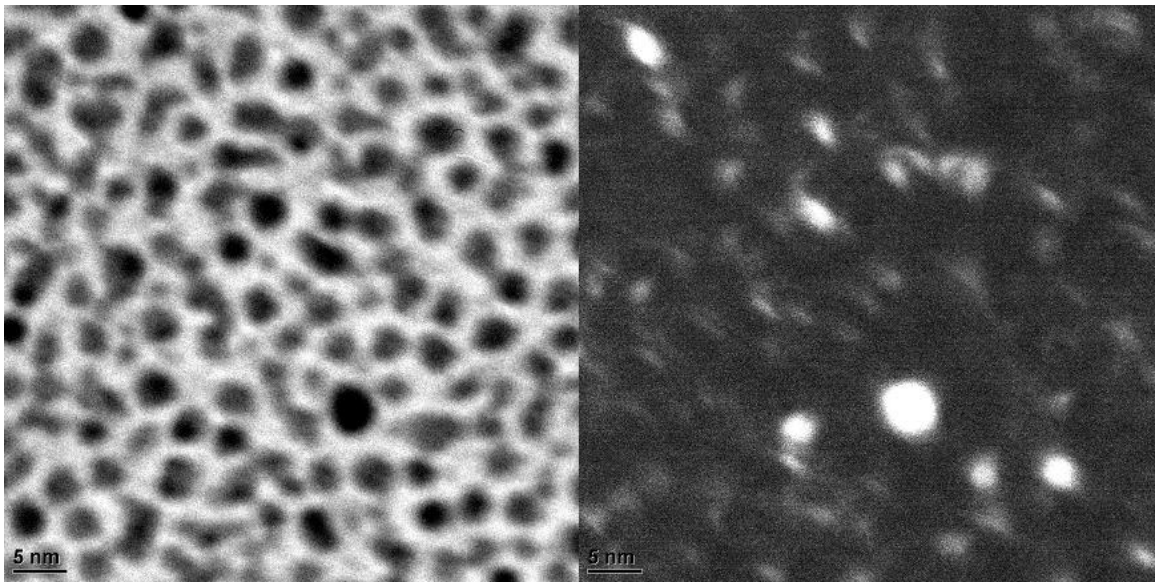

Figure 3-17. Image of AuNILC nanoparticle immobilized on SiO_2 coated copper grid by OptoDex® in transmission (left hand) and diffraction (right hand). The bar length corresponds to 5 nm.

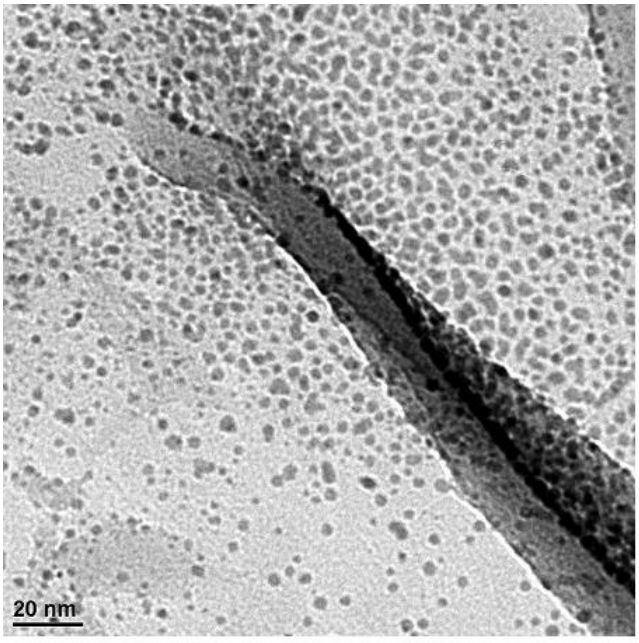

Figure 3-18. TEM image of AuNILC nanoparticles immobilized on SiO2 coated copper grid by OptoDex® in proximity of a tear caused by the thermal stress induced by the electrons beam. The bar length corresponds to 20 nm.

the right orientation are visible. The image shows clearly some diffracting gold nanoparticles at the same position as in the right picture (transmission). It must be

noted that TEM grids were cleaned and plasma pretreated before functionalization. The high hydrophilicity of the resulting support and the small surface area determined a very little quantity of respective solutions to enter in contact with interface. The local thermal stress generated by the electron beam eventually tore the film revealing conveniently its section as shown in Figure 3-18**.** Nanoparticles seem to be woven into the polymer tissue which could be assimilated to a porous gold sponge-like network. TEM observation of sample prepared by one step casting of a blend of nanoparticle and actinic polymer of the same starting concentration led to lower density of nanoparticles.

3.6. Conclusion and outlook

Covalent immobilization of gold nanoparticles on to the surface was achieved using actinic dextran based polymer as interlayer. ATR-IR spectroscopy revealed to be a sensitive method to detect monolayer capped gold nanoparticles down to 2 nm size *in situ*. The fingerprint of the organic shell was targeted. Direct information on the metal and the core size were deduced by transmission electron microscoscopy. The two techniques, both at molecular level, furnished complementary information. OptoDex® mediated nanoparticles surface grafting, in association with high precision dispensing and surface patterning, might be used to pattern nanoparticles on surfaces. Blending of suitably functionalized gold nanoparticles and dextran based polymer could also result in a convenient way to increase the sensitivity of label-free biosensing by optical waveguide techniques. The sensitivity of such devices depends on the number of selector molecules immobilized on the sensor, to which the analyte can bind and which are probed by the evanescent field. This number can be increased by mimicking a sponge. Gold is assessed as optimal interface layer for affinity based biosensors. The polymer constituent plays the role of the covalent glue to the sensor

surface, assures a biocompatible and self-passivating environment and enables the three dimensional development of the gold nanoparticle network, which allows biomolecule nesting in “pores” defined by nanoparticle cluster assembling and polymer network. The properties of the functional material can be tuned by varying the polymer / gold nanoparticle blending ratio and the nanoparticle size. Porous gold as enhancer for detection sensitivity has already been developed using electrochemical deposition of gold, which leads to a rough surface and increase of effective surface area[33]. The advantage of the described technique would be the specific addressability of any inert surface to be locally modified with porous gold by spotting three dimensional patterns. The sensitivity enhancement through nano gold sponge-like functionalization could be adapted to any existing commercially available surface plasmon resonance platforms. Furthermore, the small interstitial distance between nanoparticles could motivate to step forward conductivity measurements.

3.7. References

1. Verma, A.; Rotello, V. M., Surface recognition of biomacromolecules using nanoparticle receptors. *Chemical Communications* **2005**, (3), 303-312.

2. Elghanian, R.; Storhoff, J. J.; Mucic, R. C.; Letsinger, R. L.; Mirkin, C. A., Selective Colorimetric Detection of Polynucleotides Based on the Distance-Dependent Optical Properties of Gold Nanoparticles. *Science* **1997,** 277, (5329), 1078-1081.

3. Ghosh, S. K.; Kundu, S.; Mandal, M.; Pal, T., Silver and Gold Nanocluster Catalyzed Reduction of Methylene Blue by Arsine in a Micellar Medium. *Langmuir* **2002,** 18, (23), 8756-8760.

4. Sun, S.; Murray, C. B.; Weller, D.; Folks, L.; Moser, A., Monodisperse FePt Nanoparticles and Ferromagnetic FePt Nanocrystal Superlattices. *Science* **2000,** 287, (5460), 1989-1992.

5. Daniel, M. C.; Astruc, D., Gold Nanoparticles: Assembly, Supramolecular Chemistry, Quantum-Size-Related Properties, and Applications toward Biology, Catalysis, and Nanotechnology. *Chem. Rev.* **2004,** 104, (1), 293-346.

6. Katz, E.; Willner, I., Integrated Nanoparticle–Biomolecule Hybrid Systems: Synthesis, Properties, and Applications. *Angew. Chem. Int. Ed.* **2004,** 43, (45), 6042-6108.

7. Negishi, Y.; Takasugi, Y.; Sato, S.; Yao, H.; Kimura, K.; Tsukuda, T., Magic-Numbered Au_n Clusters Protected by Glutathione Monolayers (n = 18, 21, 25, 28, 32, 39): Isolation and Spectroscopic Characterization. *J. Am. Chem. Soc.* **2004,** 126, (21), 6518-6519.

8. Negishi, Y.; Tsukuda, T., One-pot preparation of subnanometer-sized gold clusters via reduction and stabilization by meso-2,3-dimercaptosuccinic acid. *J. Am. Chem. Soc.* **2003,** 125, (14), 4046-4047.

9. Schaaff, T. G.; Shafigullin, M. N.; Khoury, J. T.; Vezmar, I.; Whetten, R. L.; Cullen, W. G.; First, P. N.; Gutierrez-Wing, C.; Ascensio, J.; Jose-Yacaman, M. J., Isolation of Smaller Nanocrystal Au Molecules: Robust Quantum Effects in Optical Spectra. *J. Phys. Chem. B* **1997,** 101, (40), 7885-7891.

10. Templeton, A. C.; Wuelfing, W. P.; Murray, R. W., Monolayer-Protected Cluster Molecules. *Acc. Chem. Res.* **2000,** 33, (1), 27-36.

11. Brust, M.; Walker, M.; Bethell, D.; Schiffrin, D. J.; Whyman, R., Synthesis of Thiol-derivatised Gold Nanoparticles in a Two-phase Liquid-Liquid System. *J. Chem. Soc., Chem. Commun.* **1994**, 801-802.

12. Gautier, C.; Burgi, T., Vibrational circular dichroism of N-acetyl-L-cysteine protected gold nanoparticles. *Chemical Communications* **2005**, (43), 5393-5395.

13. Alvarez, M. M.; Khoury, J. T.; Shaaff, T. G.; Shafigullin, M. N.; Vezmar, I.; Whetten, R. L., Optical Absorption Spectra of Nanocrystal Gold Molecules. *J.Phys.Chem.B* **1997,** 101, 3706-3712.

14. Schaaff, T. G.; Whetten, R. L., Giant Gold-Glutathione Cluster Compounds: Intense Optical Activity in Metal-Based Transitions. *J. Phys. Chem. B* **2000,** 104, (12), 2630-2641.

15. Alvarez, M. M.; Khoury, J. T.; Schaaff, T. G.; Shafigullin, M. N.; Vezmar, I.; Whetten, R. L., Critical size in the growth of Au clusters. *Chem. Phys. Lett.* **1997,** 266, (1), 91-98.

16. Yao, H.; Miki, K.; Nishida, N.; Sasaki, A.; Kimura, K., Large optical activity of gold nanocluster enantiomers induced by a pair of optically active penicillamines. *Journal of the American Chemical Society* **2005,** 127, (44), 15536-15543.

17. Gautier, C.; Burgi, T., Chiral N-Isobutyryl-cysteine Protected Gold Nanoparticles: Preparation, Size Selection, and Optical Activity in the UV-vis and Infrared. *J. Am. Chem. Soc.* **2006,** 128, (34), 11079-11087.

18. Gautier, C.; Bieri, M.; Dolamic, I.; Angeloni, S.; Boudon, J.; Bürgi, T., Probing Chiral Nanoparticles and Surfaces by Infrared Spectroscopy. *CHIMIA International Journal for Chemistry* **2006,** 60, 777-782.

19. Bieri, M.; Gautier, C.; Bürgi, T., Probing chiral interfaces by infrared spectroscopic methods. *Phys. Chem. Chem. Phys.* **2007,** 9, 671 - 685.

20. Sigrist, H.; Mühlemann, M.; Dolder, M., Philicity of amino acid side-chains for photogenerated carbenes. *J. Photochem. Photobiol. B: Biol.* **1990,** 7, 277−287.

21. Das, J.; Zhou, X.; Miller, K. W., Identification of an alcohol binding site in the first cysteine-rich domain of protein kinase C d. *Protein Sci.* **2006,** 15, (9), 2107-2119.

22. Vodovozova, E., Photoaffinity labeling and its application in structural biology. *Biochemistry* **2007,** 72, (1), 1-20.

23. Yonzon, C. R.; Stuart, D. A.; Zhang, X.; McFarland, A. D.; Haynes, C. L.; Van Duyne, R. P., Towards advanced chemical and biological nanosensors--An overview. *Talanta* **2005,** 67, (3), 438-448.

24. Cui, Y.; Bjork, M. T.; Liddle, J. A.; Sonnichsen, C.; Boussert, B.; Alivisatos, A. P., Integration of Colloidal Nanocrystals into Lithographically Patterned Devices. *Nano Lett.* **2004,** 4, (6), 1093-1098.

25. Grunes, J.; Zhu, J.; Anderson, E. A.; Somorjai, G. A., Ethylene Hydrogenation over Platinum Nanoparticle Array Model Catalysts Fabricated by Electron Beam Lithography: Determination of Active Metal Surface Area. *J. Phys. Chem. B* **2002,** 106, (44), 11463-11468.

26. Ohshima, T.; Song, H. Z.; Okada, Y.; Akahane, K.; Miyazawa, T.; Kawabe, M.; Yokoyama, N., Precisely ordered quantum dot array formed using AFM lithography for all-optical electron spin quantum computers. P*hysica status solidi (c)* **2003,** 0, (4), 1364-1367.

27. Fischbein, M. D.; Drndic, M., CdSe nanocrystal quantum-dot memory. *Applied Physics Letters* **2005,** 86, (19), 193106.

28. Decher, G., Fuzzy Nanoassemblies: Toward Layered Polymeric Multicomposites. *Science* **1997,** 277, (5330), 1232-1237.

29. Ullman, A., Formation and Structure of Self-Assembled Monolayers. *Chem. Rev.* **1996,** 96, 1533-1554.

30. Gautier, C.; Burgi, T., Chiral Chiral N-isobutyryl-cysteine Protected Gold Nanoparticles: Preparation, Size Selection, and Optical Activity in the UV-vis and Infrared. *J. Am. Chem. Soc.* **2006,** 128, (34), 11079-11087.

31. Bieri, M.; T., B., Adsorption Kinetics, Orientation, and Self-Assembling of N-Acetyl-L-cysteine on Gold: A Combined ATR-IR, PM-IRRAS, and QCM Study. *J. Phys. Chem. B.* **2005,** 109, 22476-22485.

32. Bieri, M.; T., B., Enantiodiscrimination between an N-Acetyl-lcysteine SAM and Proline: An In Situ Spectroscopic and Computational Study. *Phys. Chem. Chem. Phys.* **2006,** 7, 514-523.

33. Bonroy, K.; Friedt, J. M.; Frederix, F.; Laureyn, W.; Langerock, S.; Campitelli, A.; Sàra, M.; Borghs, G.; Goddeeris, B.; Declerck, P., Realization and Characterization of Porous Gold for Increased Protein Coverage on Acoustic Sensors. *Anal. Chem.* **2004,** 76, 4299-4306.

Chapter 4

Dextran-based thin film coated platforms for for glycoprofiling in microarray format

4.1. Preface

The content of this chapter is related to the work carried out at CSEM, in the Surface Bioengineering laboratory, under the supervision of Dr. Hans Sigrist and Dr. Hui Gao (present address: *arrayon biotechnology*, Neuchâtel, Switzerland) within a fruitful collaboration with the Nestlé Research Center, Nestec Ltd., Switzerland. The collaboration, from the candidate point of view, fruited two major results: the willing of furthering the investigation of the dextran based polymer OptoDex® in the frame of a pure academic environment under the supervision of professor Thomas Bürgi and the redaction of the paper "Glycoprofiling with Micro-Arrays of Glycoconjugates and Lectins", accepted and published by the journal "Glycobiology", in 2005 (Angeloni *et al*)[1]. The microarray design and manufacturing, the protocol optimization for a bioactivity retention and expression in miniaturized screening tests, the manipulation of glycoproteins and lectins, including flourescence labeling, the synthesis of the neo-glycoconjugate, were performed at CSEM. The biological material to be probes in terms of glycoexpression profiling (cell extracts and expolysaccharides) was supplied by Nestlé Research Center. To support the efficacy of the *ad-hoc* tailored application in microarray format, a bacteriological challenge experimental set was carried out at Nestlé Research Center, too, under the supervision of Dr. Norbert Sprenger. To him, a special acknowledgment must be addressed for effective support, bright vision and stimulant competence sharing, also in the manuscript reaction. This chapter consists of

the cited paper's manuscript, featuring the layout used for the redaction of this thesis report. Except for the bacteriological challenge, and the biological evaluation linked to gene expression, too far from the specific competences and tasks of the candidate, it reports the work performed within the outline of candidate's PhD project.

4.2. Abstract

To facilitate deciphering the information content in the glycome, thin film-coated photoactivatable surfaces were applied for covalent immobilization of glycans, glycoconjugates or lectins in microarray formats. Ligth-induced immobilization of a series of bacterial exopolysaccharides on photoactivateable dextran (OptoDex®) coated analytical platforms (PhotoChips) allowed covalent binding of the exopolysaccharides. Their specific galactose decoration was detected with fluorescence labeled lectins. Similarly, glycoconjugates were covalently immobilized, and displayed glycans were profiled for fucose, sialic acid, galactose and lactosamine epitopes. The applicability of such platforms for glycan profiling was further tested with extracts of Caco2 epithelial cells. Following spontaneous differentiation or upon pretreatment with sialyllactose, Caco2 cells showed a reduction of specific glycan epitopes. The changed glycosylation phenotypes coincided with altered enteropathogenic *E. coli* adhesion to the cells. This microarray strategy was also suitable for the immobilization of lectins through biotin-neutravidin-biotin bridging on platforms functionalized with a biotin derivatized photoactivable dextran (OptoDex-Biotin). All immobilized glycans were specifically and differentially detected either on glycoconjugate- or on lectin arrays. The results demonstrate the feasibility and versatility of the novel platforms for glycan profiling.

4.3. Introduction

Carbohydrates (glycans) cover the surface of most if not all living cells and organisms, in the form of diverse glycoconjugates. Glycans create a landscape of recognition sites, barriers and carriers that help to control the rhythms of metabolism from conception to catabolism. Generally, glycans represent the first and crucial interface to the cell's biotic and abiotic environment, mediating recognition and

communication processes. Thus they control immunological recognition, cell-cell adhesion, pathogen attack, and protein folding and placement[2-4]. Glycans are generally assembled of diverse monosaccharide building blocks that are glycosidically linked to each other at different positions. Consequently, glycans show a high structural diversity reflecting in general functional diversity. Thus, it is a multidisciplinary challenge to decode the information content displayed by glycan structures in various biological contexts[5-7]. Lactic acid bacteria produce a wide spectrum of secreted high molecular weight exopolysaccharides (EPS). These glycans can be formed of structurally diverse building blocks. In milk processing EPS are of significant interest, because of their texturizing properties upon milk fermentation. However, they might not only contribute to structural and biofilm related properties, but also serve as 'decoy' for unwanted agents such as enterotoxins or adhesins of pathogens. Moreover, EPS might contribute to the establishment of a favorable matrix for beneficial microbial communities in natural environments such as the intestine. The surface glycosylation pattern of enterocytes changes during intestinal development. Most prominently there is a shift from a high sialic acid to high fucose displaying phenotypes (for review see *Biol-N'garagba and Louisot[8]).* Concurrently, the enterocyte microbial crosstalk is likely affected by such changes, leading to changed bacterial community structures and resistance or vulnerability of the host to pathogen insults. EPS and intestinal surface glycosylation patterns obviously encode information implicated in physiological and ecological processes. Deciphering this information content is thus an important prerequisite for an educated selection and design of strategies to promote either protection from unwanted noxious agents or promote wanted beneficial microbes. One route to facilitate decoding efforts is the establishment of analytical platforms for robust and high density display of glycan structures. Recent years have seen increasing needs for such platforms to investigate

protein-carbohydrate interactions and specifically to identify ligands and test specificities of bacterial, plant and animal lectins (for review see Drickamer and Taylor[9]; Wang[10]). Different types of microarray platforms were described for oligosaccharide, glycan, glycolipid, glycoprotein and glycoconjugate display with most approaches based on non-covalent bonding[5, 7, 11-15]. Characteristics of the different platforms for glyco-profiling were recently reviewed (Feizi et al.[16]). Microarray based platforms in microformats are of particular interest, because they require little sample quantities, allow high density sample display and provide reliable assay sensititvity.

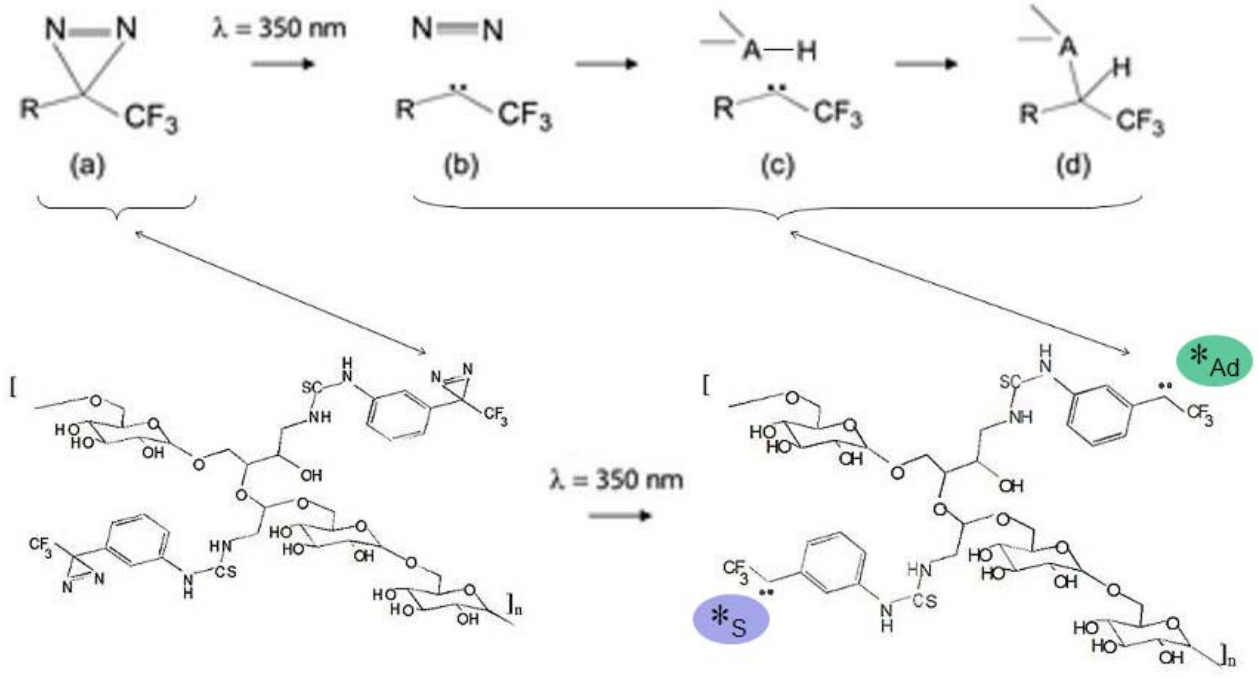

Figure 4-1. Reaction mechanism of light induced covalent immobilization of bio/molecules on a surface. Aryl-trifluoromethyl-diazirines (a), photoactivated at 350 nm generate highly reactive carbenes and release molecular nitrogen (N2) (b). Carbenes spontaneously undergo insertion reactions (c) and form covalent bonds with the surface,*S, and/or adsorbed bio/molecules, *Ad (d). Lower half of panel illustrates dextran derivatized with the photoactivateable aryl-trifluoromethyl-diazirines.

Microarray platforms have an exceptional content capacity and permit the identification and quantification of thousands of molecules in one single experiment. Despite the exorbitantly high theoretical number of possible molecular glycan configurations, the actual number of different glycan structures found in nature is likely only a minute fraction. For endogenous mammalian glycan structures it is estimated to be in the range of 5009. Thus, having an appropriate surface at hand it is envisageable to display all natural glycan structures on a single microarray. Here we present the use and applications of versatile microarray platforms based on dextran-coated glass slides (PhotoChips) suitable for (i) covalent glycan and (ii) glycoconjugate immobilization, and for (iii) ligand mediated bridging of functionlized biomolecules such as lectins or oligosaccharides on OptoDex-Biotin platforms. The dextran-based polymer OptoDex® used, is derivatized with aryl-trifluoromethyl-diazirine groups[17-19]. Upon illumination, aryl-trifluoromethyl-diazirine groups form reactive carbenes (Figure 4-1), which eventually react with any vicinal molecule to form covalent bonds[20, 21]. Expectedly, this approach leads to covalent linkage of any molecule of interest to any surface of interest in one step. In combination with other functional groups such as biotin, the photoactivateable dextran polymer yields a higly versatile tool for surface (bio)engineering. The presented results show the feasibility of biomolecule binding to such microarray platforms and illustrate the versatility of the microarray based tools with different applications.

4.4. Results

4.4.1. Exopolysaccharide microarray.

Bacterial exopolysaccharides (EPS) from seven different lactic acid bacteria were covalently immobilized in microarray format aiming at the screening of functionally displayed glycan structures. To this end, the seven EPS of known structures were

dissolved in water and printed onto PhotoChips. Upon illumination, the aryl-trifluoromethyl-diazirine groups formed reactive carbenes and covalently linked the EPS to the dextran surface in one step. The structures of the repeating molecular features of the EPS are shown (Figure 4-2), together with the respective PNA (peanut agglutinin) and MAA (*Maackia amurensis* agglutinin) binding profiles. PNA bound preferentially to the EPS structure of *L. bulgaricus* 291 harboring a β-D-Galp-(1-4)-β-D-Glcp- side chain (Figure 4-3 E,H), and also bound to the *L. helveticus* 59 EPS with a β-D-Galp-(1-6)-α-D-Glcp- side chain (Figure 4-3,H). PNA did not bind to EPS with branches of single α- or β-Gal moieties or with terminal Gal in the furanose form (Figure 4-3 A,B,D,F,G,H). Equally, the sialic acid specific lectin MAA did not bind to any of the presented EPS structures. Therefore, PNA bound preferentially to β-Gal residues on EPS, when they are spaced by a Glc from the EPS backbone (Figure 4-2). These results illustrate the specific ligand binding of PNA lectin and, more importantly in the context of this investigation, show the feasibility of EPS immobilization on microarrays for functional screening and identification of the epitopes displayed on unknown EPS structures. Thus, bacterial EPS structures displayed in microarray formats can in the future be screened for their ability to serve as ‘decoy’ for viruses, and microbial adhesins and toxins.

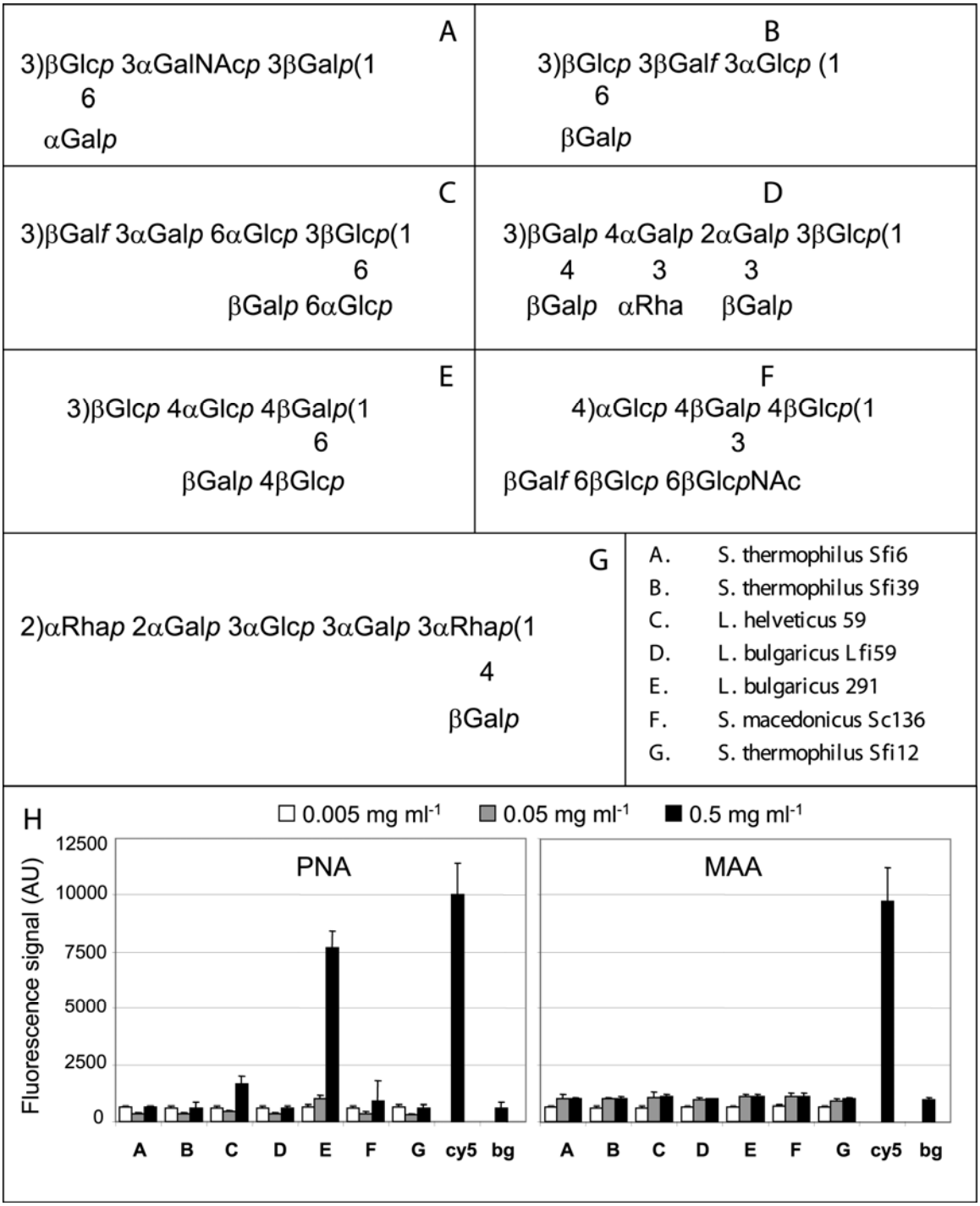

Figure 4-2. Structures of the EPS repeating unit from different lactic acid bacteria (A-G) as dubbed in the figure, and detection of different concentrations of immobilized EPS by the lectins PNA and MAA (negative control) (H). Cy5-OptoDex (Cy5) is an internal fluorescent standard and 'bg' indicates the measured background values. Mean signals and standard deviations are shown.

4.4.2. Glycoprotein microarray characteristics.

As for glycans, a series of reference glycoproteins were immobilized covalently in microarray formats, taking again advantage of the carbene reaction. Resulting glycoprotein microarrays were probed with fluorophore conjugated lectins to demonstrate feasibility of differential glycan profiling. Figure 2-59 depicts the detection of 5 glycoconjugates together with BSA as control protein with 6 different plant lectins. All tested lectins primarily recognized specific glycan structures as predicted from their respective binding specificities (Table 4-1).

Acronym	***Full name***	***Glycan recognized***	***Control protein/ glycoconjugate***
PNA	Peanut agglutinin	Gal-β-1,3-GalNAc-R Gal-R	asialofetuin OptoDex-lactose
UEA	*Ulex europaeus* agg.	Fuc-α-1,2-Gal-R	2FL-BSA
TPA	*Tetragonolobus purpureas* agg	Fuc-R	2FL-BSA
SNA	*Sambucus nigra* agg.	SA-α-2,6-Gal-R	fetuin, transferrin
MAA	*Maackia amurensis* agg.	SA-α-2,3-Gal-R	fetuin
DSA	*Datura stramonium* agg.	Gal-β-1,4-GlcNAc-R GlcNAc-R	asialofetuin asialofetuin

Table 4-1. Known glycan recognition specificities of plant lectins used in this study. Data complied from datasheets of respective lectins.

All lectins showed excellent signal to background ratios. Virtually no binding to the BSA control protein was detected with either lectin (Figure 2-59). MAA recognized glycans displayed on fetuin as predicted and to a much lower extent on asialofetuin. The latter might be due to incomplete desialylation (Figure 4-3 A). PNA recognized best glycans displayed on asialofetuin, and also recognized lactose and 2'fucosylated

lactose linked to BSA (Figure 4-3A). The former two results are expected from the known PNA ligand specificity.

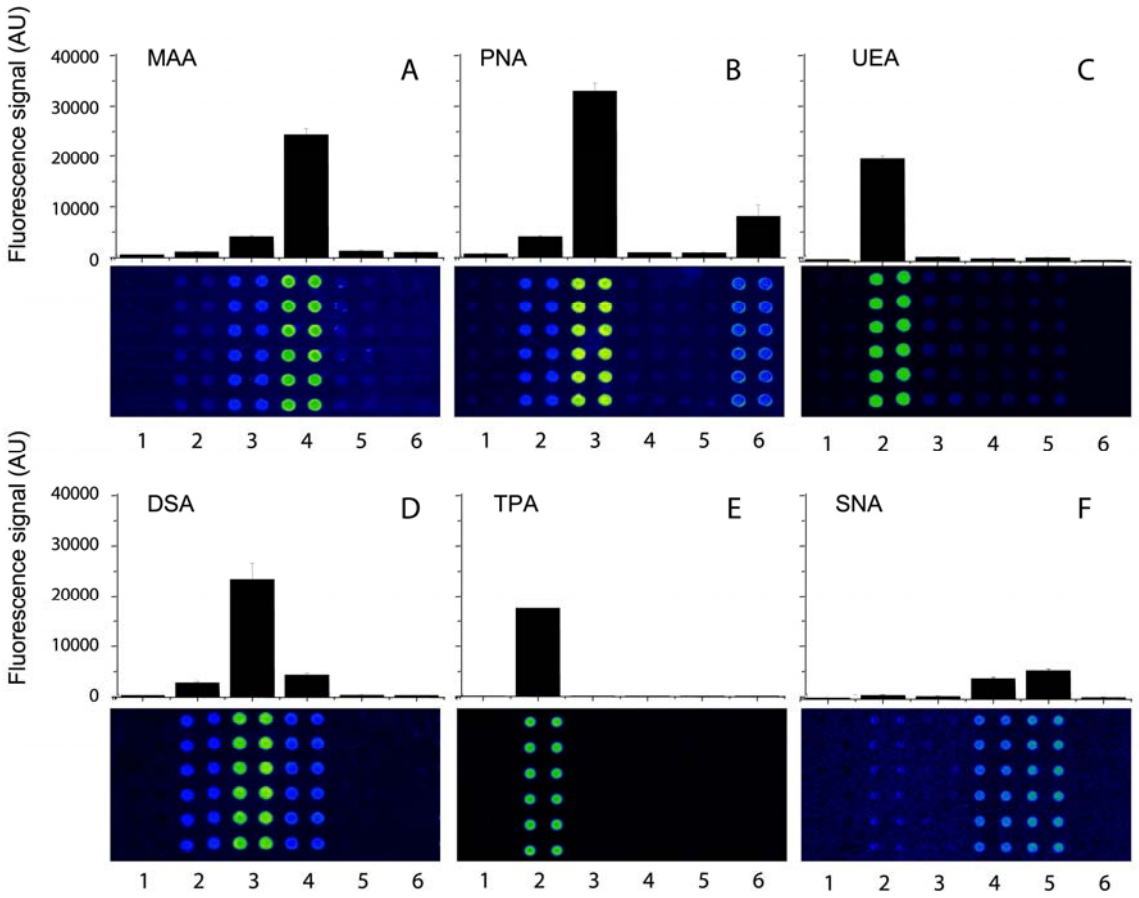

Figure 4-3. Printed BSA (1), reference glycoproteins 2'fucosyllactose-BSA (2), asialofetuin (3), fetuin (4), transferrin (5), and the neo-glycoconjugate OptoDex-lactose (6) detected by lectins MAA (A), PNA (B), UEA (C), DSA (D), TPA (E) and SNA (F). The lower panel of each figure shows the actual spot image, false colored with yellow, green, blue in the order of decreasing signal intensity. Mean signals and standard deviations are shown.

UEA (Ulex europaeus agglutinin) and Tetragonobolus lectin (TPA) bound only to fucosylated lactose (Figure 4-3CE). DSA (Datura stramonium agglutinin) showed preferred binding to asialofetuin as predicted, but also measurable binding to fetuin and fucosylated lactose (Figure 4-3 D). Finally, SNA (Sambucus nigra agglutinin) recognized transferrin and fetuin (Figure 4-3 F), which terminally expose α-2,6 linked sialic acid residues.

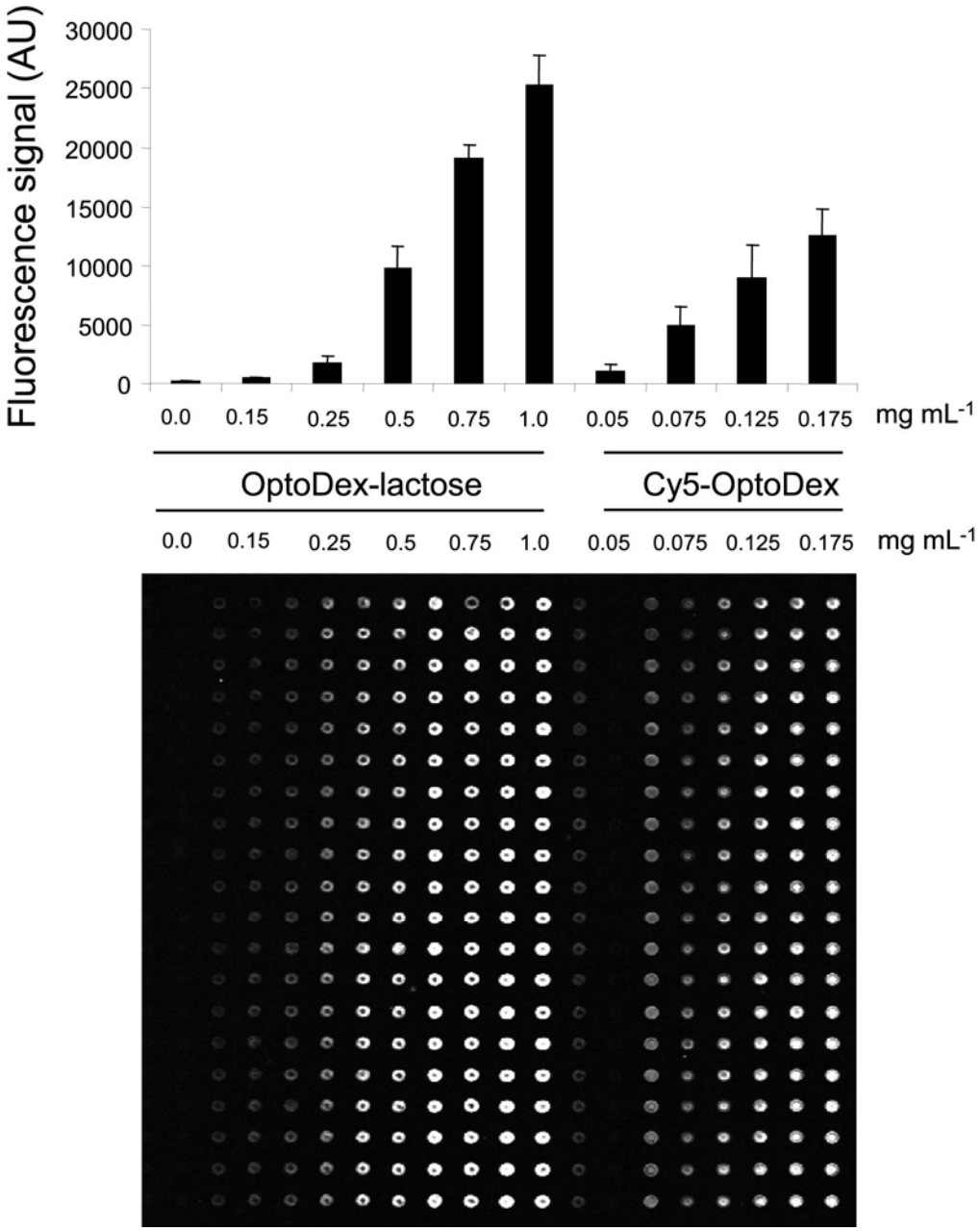

Figure 4-4. Dilution series of OptoDex-Lactose detected by fluorescent lectin PNA (Cy5-PNA) together with fluorescent OptoDex® (Cy5-OptoDex). Indicated print solution concentrations are in mg/ml. The lower half shows the actual recognized spots of the array with decreasing signal intensities. Mean signals and standard deviations are shown.

The presented findings indicate that glycoprotein display and respective glycan profiling on PhotoChips are (i) possible.

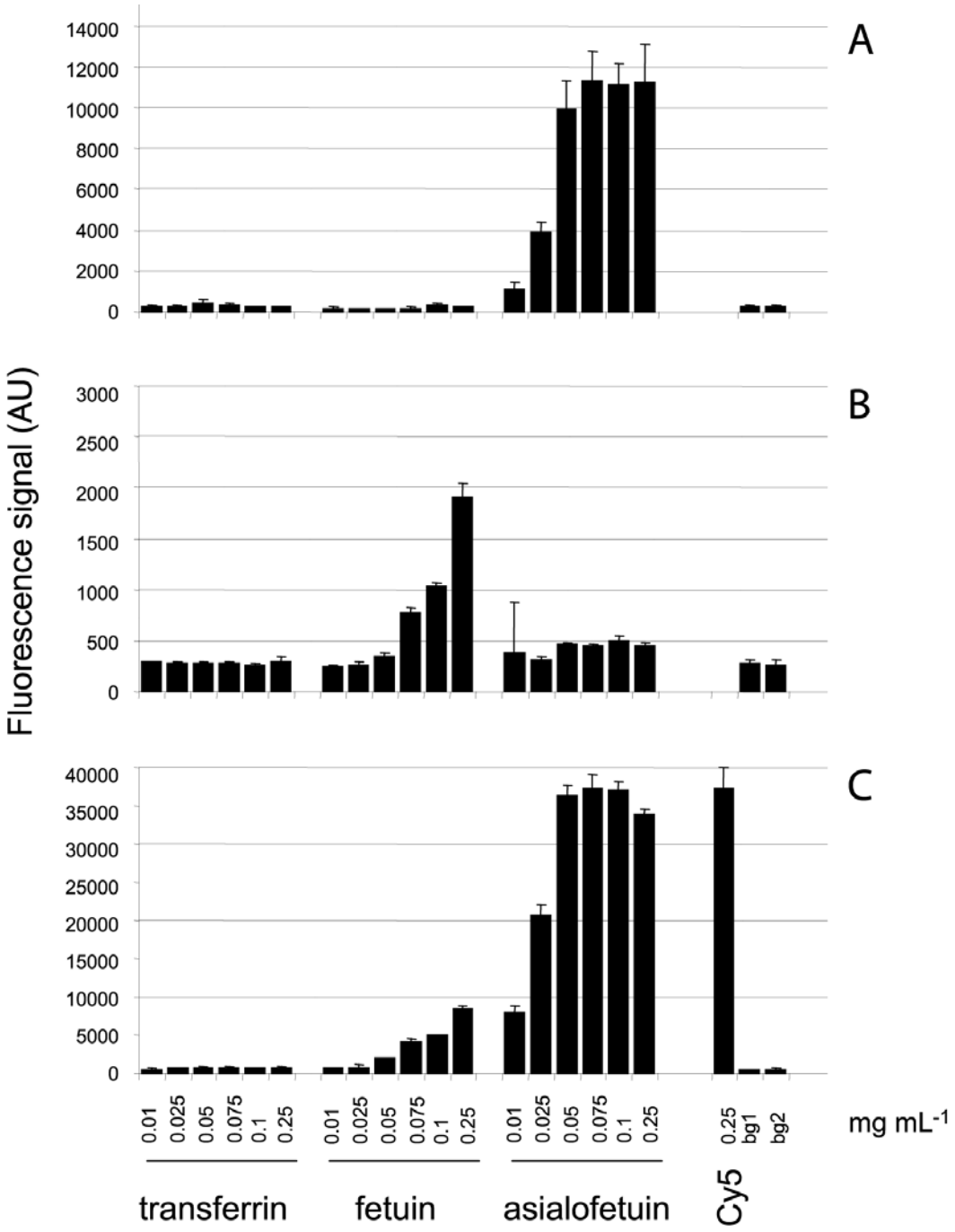

Figure 4-5. Dilution series of glycoproteins detected by fluorescent lectins PNA (A), MAA (B), and DSA (C). Cy5-OptoDex (Cy5, C) was printed as an internal reference (0.25 mg/ml). Amounts indicated are in mg/ml.'bg1' indicates background inside the array grid, 'bg2' indicates background outside the array grid (indicating the efficiency of unspecific binding suppression). Mean signals and standard deviations are shown.

Glycan arrays yield (ii) appreciable signal-to-noise ratios, and (iii) quantifiable differential glycan profiles. The display of oligosaccharide structures in the form of neo-glycoconjugates (e.g. 2'fucosyllactose on BSA, lactose on dextran) represents a facile approach allowing for covalent oligosaccharide immobilization on PhotoChips. Different concentrations of OptoDex-Lactose (a photactivable dextran based neoglycoconjugate (Caelen et al[19], Chevolot at al[22]), were immobilized on PhotoChips to assess signal quantitation, glycoconjugate binding capacities and detection limits. The displayed glycans were detected and quantified with the fluorescence labeled lectin PNA. The response is dose dependent (Figure 4-4) and does not reach saturation at the concentrations used. Linearity of response is best achieved at print solution concentrations between 0.5 and 1 mg/ml. The detection limit is somewhere below 0.25 mg/ml print solution dispensed, corresponding to about 12 pg probe molecule applied per spot. In parallel, a dilution series of fluorophore-conjugated dextran was printed and quantified. The results showed linearity of the recorded fluorescence signal and demonstrated that the surface binding capacitiy did not saturate at the concentrations used. Moreover, the experiments illustrated good spot-to-spot reproducibility. Similarly, different concentrations of reference glycoproteins were printed and their glycans were detected and quantified with specific lectins (Figure 4-5). PNA and DSA detection of asialofetuin showed saturation (Figure 4-5 A,C) at 2.5 pg asialofetuin applied (50 pl of 0.05 mg/ml), and the detection limit was below 0.5 pg per spot. Detection of fetuin-linked glycans with MAA did not saturate at the concentrations employed, and the detection limit was around 2.5 pg (Figure 4-5 B). The results suggest either that fetuin can be immobilized at still greater amounts (> 12.5 pg) than asialofetuin (2.5 pg), or more likely, the results reflect the different binding affinities between MAA, DSA and PNA. For DSA and PNA, response linearity is best achieved at asialofetuin print solution concentrations between

0.01 and 0.05 mg/ml. For MAA, linearity of response is attained with fetuin print concentrations between 0.075 and 0.25 mg/ml. The above used reference glycoproteins were selected to serve as positive controls when assaying glycoprotein arrays.

4.4.3. Application: Glycan profiling of model cell extracts.

Extracts of Caco-2 intestinal cells were arrayed and immobilized on PhotoChips to test the applicability of the glycoprotein microarray platform for glycan profiling.

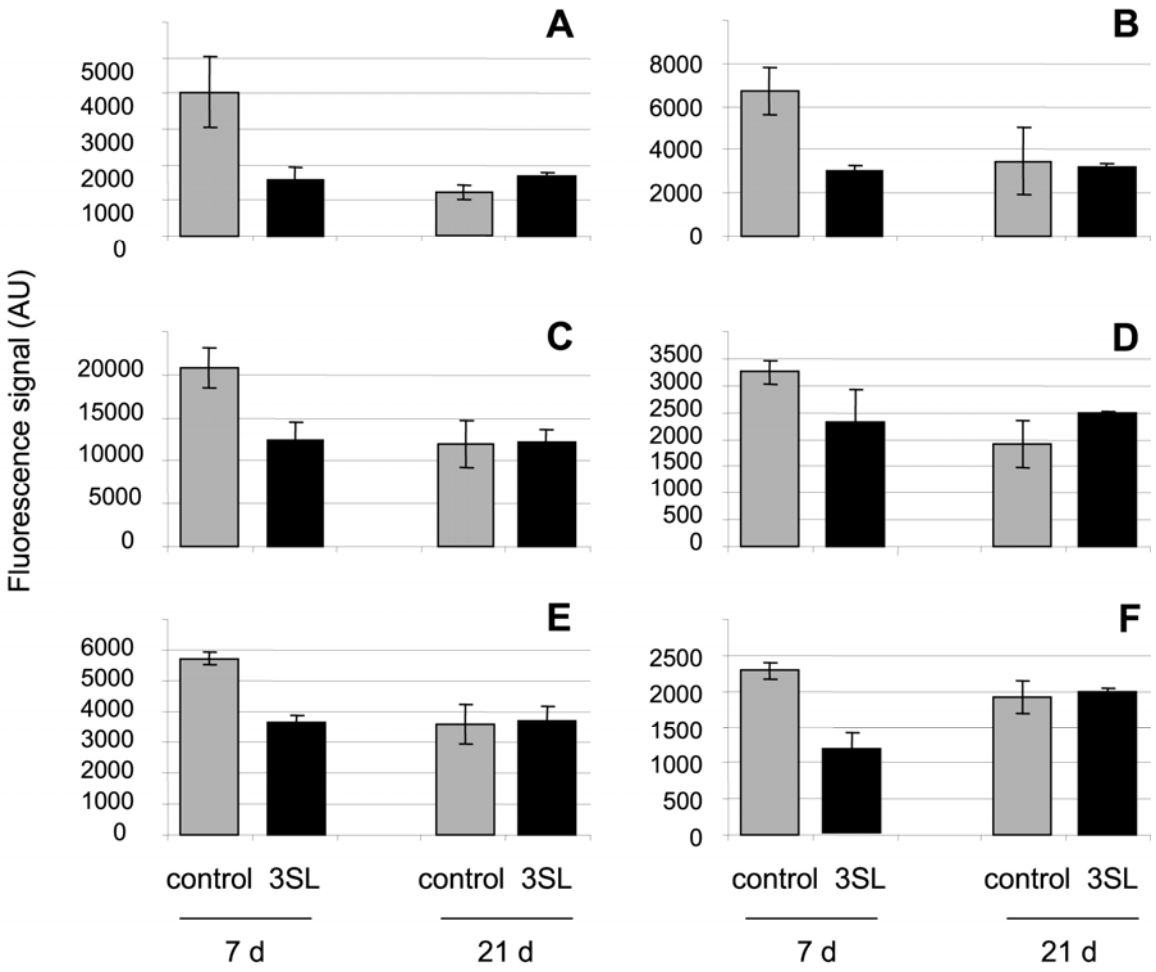

Figure 4-6. Glycan display profiles of mock treated control and 3'sialyllactose (3SL) treated cells at 7 d and 21 d in culture. (A), sialic acid linked α-2,3 detected by MAA; (B), sialic acid linked α-2,6 detected by SNA; (C), fucose linked α-1,2 detected by UEA; (D), fucose detected by TPA; (E), galactose detected by PNA; (F), lactosamine detected by DSA. Error bars indicate standard deviations (N=2).

Displayed glycans were profiled and quantified using a series of plant lectins (Figure 4-6). Caco-2 cells at 7 days post-seeding (i.e. non-differentiated) were compared with cells grown for 21 d (i.e. differentiated), either mock-treated or treated with 3'sialyllactose for 48 h prior to harvest. Relative glycan expression levels recognized by MAA (i.e. α-2,3 linked sialic acid) decreased most prominently between the 7 and 21 d cultured cells (Figure 4-6 A). Further, lower glycan expression in 21 d as compared to 7 d cultured cells was also found for α-2,6 linked sialic acid containing glycans seen by SNA, fucose containing glycans seen by UEA, and TPA and galactose ending glycans seen by PNA (Figure 4-6 B- E). In contrast, glycan moieties targeted by DSA (i.e. lactosamine) did not markedly change over time (Figure 6F). Interestingly, 3'sialyllactose treatment of 7 d cultured cells moved the expression of glycans seen by MAA, SNA, UEA, TPA, and PNA from elevated levels down to levels comparable to those found for mock-treated 21 d cultured cells (Figure 6 A-E). Thus, α-2,3 and α-2,6 linked sialic acid residues diminished together with fucose and galactose moieties. Gene expression levels of sialyltransferases responsible for the formation of α-2,3 linked sialic acids were monitored (data not shown). The results showed that 3'sialyllactose treated - as compared to mock-treated 7 d cultured cells - reduced expression levels of *ST3Gal-I* (2.5x), *-II* (2x), and *–IV* (5x). *ST3Gal-III*, *-V*, and *-VI* were not affected. Thus, reduction of MAA detected glycans was reflected by a reduction in respective gene expression levels. Additionally, cell extracts were spotted manually onto nitrocellulose membranes for lectin staining and signal quantification (data not shown). The results confirmed the observation made using the microarray platform: cell glycosylation phenotypes changed with increasing culture time and responded to oligosaccharide addition to the growth medium. This conclusion is further supported by the following finding. Lactosamine containing glycans recognized by DSA showed lower expression levels in 7 d cultured cells upon

treatment with 3'sialyllactose as compared to mock-treated cells, while levels were equally high in 7 d and 21 d control cells and 21 d 3'sialyllactose-treated cells (Figure 4-6 F). Seven d cultured Caco-2 cells apparently sensed the presence of 3'sialyllactose in the growth medium and responded by changing glycan expression profiles, while 21 d cultured cells did not respond to the oligosaccharide treatment.

4.4.4. Bacterial challenge.

To evaluate the significance of the observed glycan changes in the context of bacterial-epithelial cell crosstalk, 3'sialyllactose-, lactose-, and mock-treated cells were challenged with an enteropathogenic E. coli (EPEC). Total bacterial adherence to such pretreated cells was monitored (Figure 4-7). About 10

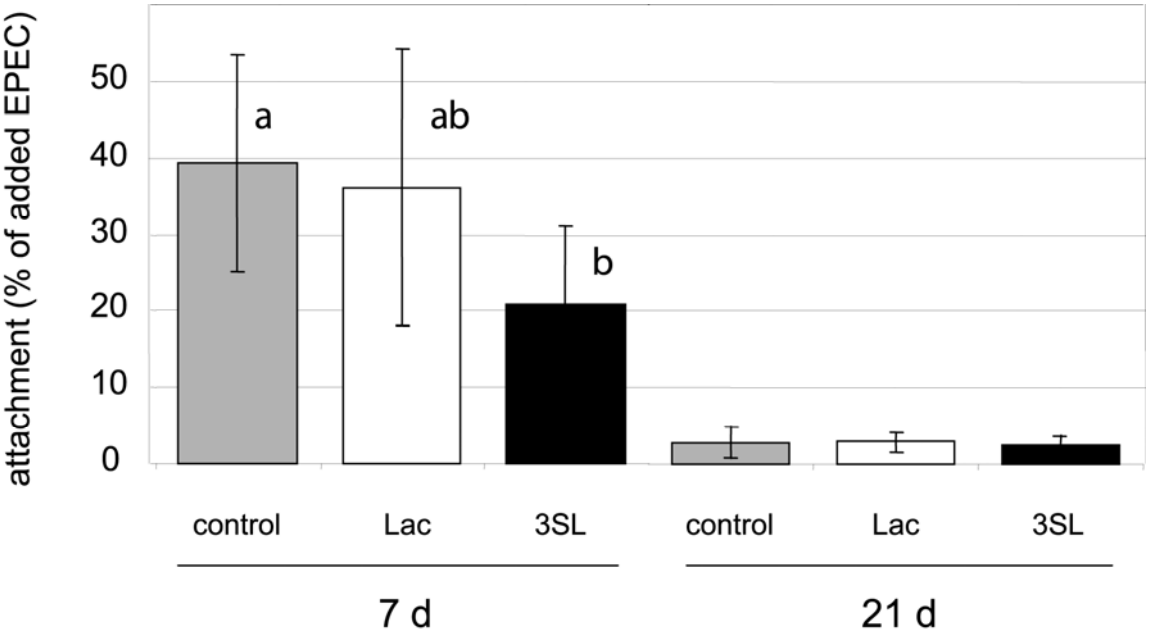

Figure 4-7. EPEC challenge of Caco2 cells grown 7 d and 21 d which were either mock pretreated (control), lactose (lac) or 3'sialyllactose (3SL) pretreated and washed before bacterial challenge. Error bars indicate standard deviations (N=6). Statistical analysis was done using unpaired t-test, P value 0.0265.

times more bacteria attached to 7 d cultured cell (ca. 40 % of added bacteria) as compared to 21 d cultured cells (ca. 3 % of added bacteria). Upon pretreatment of 7 d cultured cells with 3'sialyllactose and subsequent washing of the cells, EPEC

adherence was reduced to about 50 % as compared to the lactose- or the mock-treated control cells (Figure 4-7). This was seen in an EPEC adherence reduction from 35 to 40 % of added bacteria to about 20 %. EPEC adherence to 21 d cultured cells either mock-, lactose- or 3'sialyllactose-pretreated, was indifferent and, as mentioned above, reduced by about 90 % as compared to 7 d cultured mock-treated control cells. The reduced EPEC adherence to 21 d as compared to 7 d cultured cells coincided with lower glycan expression levels as determined by lectin based glycan profiling described above.

4.4.5. Lectin microarray.

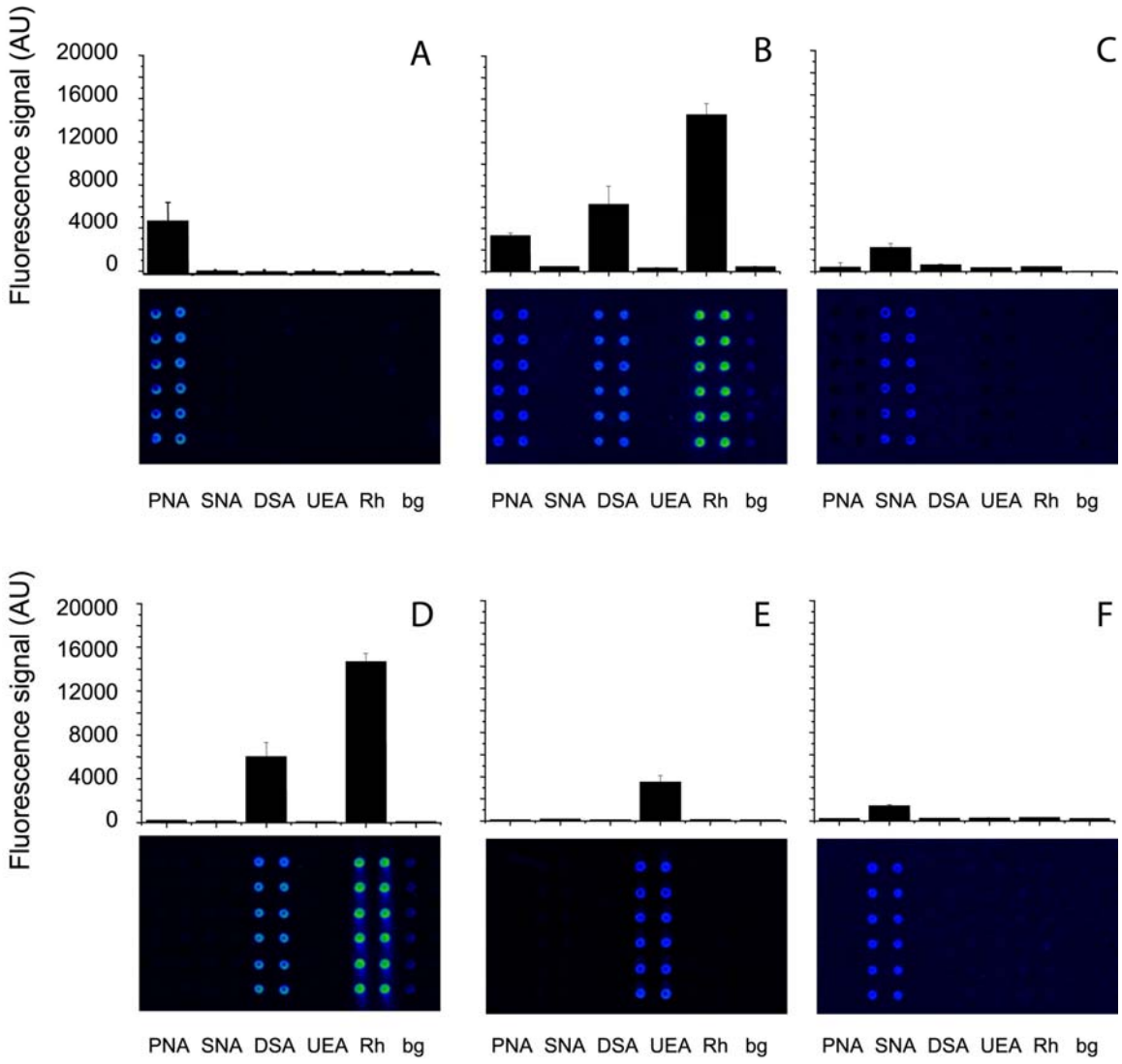

Figure 4-8. Lectin microarray probed with Cy5-OptoDex-Lactose (A), Cy3-Asialofetuin (B), Cy5-fetuin (C), Cy3-lactosamine-BSA (D), Cy5-2'fucosyllactose-BSA (E), and Cy5-transferrin (F). Rh: rhodamine and biotin double-labeled dextran as internal standard (detectable using the Cy3 scanning set-up), bg: background. Mean signals and standard deviations are shown.

To further explore the application range of the OptoDex® based platforms for microarraying, in particular the OptoDex-Biotin platform, 4 plant lectins were immobilized through a biotin-neuravidin-biotin bridge and probed with fluorophore labeled glycoconjugates (Figure 4-8). Differential glycan profiles were detected with the immobilized lectins. OptoDex-Lactose bound primarily to immobilized PNA,

asialofetuin to DSA and, to a lesser extent, to PNA, fetuin to SNA, lactosamine-BSA to DSA, 2'fucosyllactose-BSA to UEA and transferrin to SNA (Figure 8). Signal-to-noise ratios were comparable to, and as good as for the glycoprotein arrays. Homogeneous lectin binding to individual spots was achieved upon addition of glycerol or a mock protein such as BSA to the print solution. The lectin array technology complements antibody arrays, previously shown to be functional upon immobilization on PhotoChips and diverse functional platforms[23]. Hybrid lectin/antibody arrays may serve as profiling tools, not only for glycan expression but also for the detection of specific immunoreactive markers.

4.5. Discussion

The insight that glycan structures are of key importance for numerous biological processes in health and disease lead to the recent need for the development of high-throughput platforms for analysis of glycan information content. Thus, the last years have seen increasing numbers of studies reporting the development and use of microarray based glycan display platforms[16]. Mono- and oligosaccharides were covalently linked to gold or modified glass and plastic surfaces and thus became accessible for functional carbohydrate protein interaction measurements[15, 24, 25]. Further, nitrocellulose and polystyrene coated surfaces were reported suitable platforms for microarray format display of biomolecules such as neoglycolipids[5], glycoproteins and glycans[26]. However, as for microtiter plate based display of biomolecules, such as glycoproteins, these nitrocellulose and polystyrene based platforms rely on non-covalent adsorptive immobilization. Here we described the use of PhotoChips and OptoDex-Biotin platforms for covalent and ligand-mediated immobilization of biomolecules on microarray formats. Procedures related to PhotoChips enabled single-step covalent immobilization of (i) bacterial glycans, (ii)

reference glycoproteins and neoglycoconjugates, and (iii) cell extracts. Further, OptoDex-Biotin platforms allowed for bridging biotinylated lectins through neutravidin. All mentioned immobilized biomolecules remained biologically active and allowed on-array functional protein-carbohydrate interaction measurements. Differential recognition profiles were in accordance with the available structural and compositional information on the profiled reference compounds. The microarray investigations presented here extend the versatility of the above mentioned nitrocellulose and polystyrene surfaces for glycoconjugate and glycan display. PhotoChips allow for direct covalent biomolecule immobilization through reactive carbenes, and OptoDex-Biotin platforms enable neutravidin mediated display of biotinylated biomolecules[17, 18, 23]. It is worth noting that all dextran based platforms are hydrophilic and suppress nonspecific binding. The dextran network provides a stabilizing environment for biomolecules and increases the surface for biomolecule display. All features are essential for reliable detection of biological interactions. The one-step covalent immobilization of unmodified biomolecules on PhotoChips is a most direct immobilization approach. It is highly valuable for glycan immobilization, the binding of high molecular weight neoglycoconjugates and glycoproteins. Although this study focuses on the immobilization and arraying of glycoproteins and bacterial EPS, it is equally foreseeable to covalently crosslink *via* the photoactivateable dextran other glycan preparations, such as those derived from plant, fungal and bacterial cell walls. Direct covalent immobilization of lipid- or polyacrylamide-linked neoglycoconjugates[27, 28] has been demonstrated with nitrocellulose coated surfaces[5, 16]. Oligosaccharide immobilization presented here, required pre-coupling to proteins, e.g. 2'fucosyllactose-BSA, or to dextran, e.g. OptoDex-Lactose. Alternatively, oriented immobilization *via* biotin/neutravidin allowed for functional on-array protein-carbohydrate recognition. To this end, dual functionalized dextran was chosen

having photoactivateable groups in combination with biotin. With increasing numbers of immobilization techniques it should be interesting and important to perform comparative glycan-protein interaction studies using differently immobilized glycans to assess the influence of the immobilization protocol and the platforms on the interaction analysis[16, 29]. For lectins, direct crosslinking through the photoactivatable carbenes was attempted and lectins could be bound to the surface. However, carbohydrate binding activity was lost in this approach. This was likely due to structural rearrangements of the oligomeric lectins. On the other hand, biotin-neutravidin-biotin bridging yielded functional lectin arrays. In the future, these lectin microarrays might be combined with array of antibodies[18, 23] to have at hand microarrays specifically designed to assess the physiological status of cells or tissues. To apply the dextran platform for microarray based glycan quantification, cell extracts of intestinal model cells were printed and covalently linked on PhotoChips. Displayed glycans were profiled and quantified with plant lectins. As known for intestinal surface glycosylation occurring during development[8], cell lines changed glycosylation phenotypes depending on the time in culture or differentiation status, respectively. Most prominently, α-2,3 linked sialic acid epitopes diminished from 7 d to 21 d in culture, which reflects a similar pattern as observed *in vivo* during development. Interestingly, treatment of 7 d cultured cells with the oligosaccharide 3'sialyllactose led to decreased glycosylation as compared to mock treated cells of the same time in culture. For α-2,3-linked sialyic acids, this reduction correlated with a reduced gene expression level for respective genes *ST3Gal-I, –II* and *–IV*, while the other *ST3Gal* genes were not affected. In summary, such 3'sialyllactose treated 7 d cultured cells showed glycosylation patterns similar to 21 d cultured control cells. The only exceptions were lactosamine epitopes, which were reduced upon oligosaccharide treatment of 7 d cultured cells, but which remained unaltered over time in mock-

treated controls. Pretreatment of 7 d cultured cells with 3'sialyllactose led to about 50 % reduction of enteropathogenic *E. coli* adhesion as compared to lactose or mock-pretreated cells. The reduced adherence correlated with reduced sialic acid and lactosamine epitopes. Both, sialic acid and lactosamine epitopes were previously proposed to play a key role in EPEC adherence to CHO cells[30]. Further, lactosamine moieties were also shown to alter EPEC localized adherence phenotype[31, 32]. Considering, a scenario with lactosamine as key player might be valid for the 7 d cultured cells. However, another mechanism should come into play to explain the overall reduced EPEC adherence to 21 d as compared to 7 d cultured cells, because (i) lactosamine levels were comparable between the mock-treated 7 d and 21 d cultured cells, and (ii) total EPEC adherence was much lower to 21 d cultured cells as compared to 7 d cultured and 3'sialyllactose pretreated cells. Future studies will elaborate the connection between the expressed sialylated and lactosamine displaying glycans on the cells and the adherence of EPEC. To this end, it might be envisaged to perform on-array adhesion analysis using bacteria or potentially viral particles. For mammalian cells, however, the ca. 150 μm spot diameter of the herein presented microarray platform might be limiting as compared to another recently presented glycan array that was exploited for cell adhesion studies[33].

4.6. Materials and methods

4.6.1. Biomolecule preparation.

Lectins for Cy3 or Cy5 labeling were purchased from Sigma: Peanut agglutinin (PNA), *Ulex europaeus* I lectin (UEA), *Maackia amurensis* agglutinin (MAA), *Sambucus nigra* agglutinin (SNA), *Datura stramonium* agglutinin (DSA), and *Tetragonolobus purpureas* agglutinin (TPA). Biotinylated lectins were purchased from Vector Laboratories (Burlingame, CA): biotinylated Peanut agglutinin (biotin-

PNA), biotinylated *Sambucus nigra* agglutinin (biotin-SNA), biotinylated *Datura stramonium* agglutinin (biotin-DSA), biotinylated *Ulex europaeus* lectin (biotin-UEA). Rhodamine and biotin double-labeled dextran was a product of Molecular Probes (Leiden, The Netherlands). PhotoChips and OptoDex-Biotin platforms were obtained from CSEM, Switzerland. Control glycoproteins were either purchased from Sigma (transferrin, fetuin, asialofetuin, bovine serum albumin (BSA) or from Dextra Laboratories (2'fucosyllactose-BSA, lactosamine-BSA). OptoDex-Lactose was prepared by derivatizing amino-group functionalized OptoDex® with mono(lactosylamido)-mono(succinimidyl)suberate (Pierce, Ill). The reaction product was purified by gel filtration. Caco-2 cells were seeded at a concentration of 100'000 cells/ml and grown at 37°C (10% CO_2) in Dulbecco's-MEM containing 3.7 g/L $NaHCO_3$; 1 g/L D-glucose, fetal bovine serum (FBS) (#2-01F00-1, 10% for Hep-2 and 20% for Caco-2 cells), 200 mM glutamine (GibcoBRL #25030-024) and penicillin/streptomycin (10000 IU/ml-10000 UG/ml, GibcoBRL #15140-114). Cells were grown for up to 21 days before harvest. Cell cultures were treated with medium without FBS or with the same medium supplemented either with lactose or 3'sialyllactose at concentrations of 2 mg/ml. Cells were treated for 2 days prior to harvesting and treatments were renewed after 1 day. For extraction, cells were washed in PBS, scraped from the culture wells and collected in microcentrifuge tubes. Cells from one well of a 6-wells plate were resuspended in 0.5 ml PBS supplemented with protease inhibitors (Complete™, Roche, Switzerland). Cell extracts were homogenized by successive passing through a 25-gauge syringe needle. Homogenized extracts were frozen on dry ice and kept at - 80°C until printing. Just before printing, samples were homogenized again as before. Bacterial EPS were isolated and prepared according to a standard protocol (Stingele et al., 1996). Briefly, proteins were removed from spent culture supernatants by trichloracetic acid (TCA) precipitation

(20 % (v/v) final TCA). After protein removal by centrifugation, EPS were precipitated upon addition of acetone (final 50 % (v/v)). Precipitated EPS were recovered in water, and the solution was adjusted to pH 7 before dialysis against water for 24 h. After removal of insoluble material, EPS were freeze-dried. Before printing EPS were dissolved in PBS at a concentration of 0.5 mg/ml.

4.6.2. Biomolecule immobilization.

PhotoChips and OptoDex-Biotin platforms in slide formats were used as analytical platforms. Upon printing as detailed below, the arrayed platforms were illuminated for 4 min with high power ultraviolet lamp (1000 W) at 365 nm (11 mW/cm^2). After rinsing, OptoDex-Biotin platforms were incubated with neutravidin (0.05 mg/ml) in PBS for 30 min at ambient temperature. Biomolecules were arrayed with a pin-and-ring printer (Affymetrix Arrayer 417™), applying ca. 50 pl per spot, which gave an average spot diameter of ca. 150 μm. Print automation was supported by the instrument specific Affymetrix 417™ Arrayer Software. PhotoChips with printed biomolecules were irradiated as described above to effect covalent probe molecule immobilization. After photobonding the surfaces were rinsed with PBS containing 1% BSA (once), PBS/Tween 20 (3 times), PBS (3 times) and deionized water (3 times). Biotinylated lectins were prepared in HEPES buffer supplemented with divalent ions (Mg^{++}, Mn^{++}, Ca^{++}; 1 mM each) and BSA (0.5 mg/ml) for printing. Printed slides were incubated for 10 min before rinsing them with TBS complemented by Tween-20 (0.05%; TBS-Tween) and free biotin (0.5 mg/ml) for 10 min. Thereafter, slides were rinsed once each with TBS- Tween, TBS and deionized water. All processes related to platform handling, printing and photoimmobilization were carried out in a dedicated clean room. Prepared microarrays were vacuum-sealed and stored at 4°C (lectin arrays) or –20°C until used.

4.6.3. Array probing.

Cyanine reagents (Cy5 or Cy3) either monofunctional or bisfunctional were used for fluorescence labeling of target biomolecules according to manufacturer's instructions (Amersham Biosciences). For lectin labeling, free dye was removed by size exclusion chromatography on prepacked PD10 columns pre-equilibrated with TBS buffer at pH 7.2 supplemented with divalent ions (Mg++, Mn++, Ca++; 1 mM each, TBS+) at room temperature. Labeled samples were stored at 4°C in the dark. Refrigerated platforms with arrayed biomolecules were allowed to warm to room temperature for at least 30 min before rehydration. To this end, slides were sequentially rinsed for 5 min each in PBS-BSA (1% w/v), PBS-Tween 3 times, deionized water. Thereafter, a frame was applied to the slides (Gene Frame®, ABgene, 65 µl) to generate an incubation chamber around the printed spots. Fluorescence labeled lectins were diluted to a final concentration of 0.02 mg/ml in TBS+ buffer complemented by blocking reagent (final 10 % (v/v), Roche, Switzerland). Each slide was incubated with 65 µl lectin medium for 30 min at room temperature in the dark. Thereafter, slides were rinsed for 5 min each with PBS-BSA (1% (w/v)), PBS-Tween 3 times, PBS 3 times and deionized water. Slides were air dried and kept in the dark before fluorescence reading. For lectin arrays on OptoDex-Biotin platforms, all incubations were carried out in TBS+ buffer. Incubation- and rinsing steps were as described above, however slides were not allowed to dry before the final wash. Microarrays were read using a gene array scanner (Affymetrix 428™Array Reader) and signals were quantified using the ImaGene™ software package (Biodiscovery, Inc, USA).

4.6.4. Cell culture and bacterial challenge.

Caco-2 cells were seeded and treated as described above. Before bacterial challenge, Caco-2 cells were washed 2 times with PBS. EPEC strain E2348/69 was grown overnight at 37 °C without shaking in BHI supplemented with 10 μCI/ml ^{3}H–thymidine (Pharmacia). Bacteria were washed in PBS and adjusted to an OD_{600} of 0.1 in PBS. Fifty μl of bacterial solution were added to 1 ml DMEM without FBS, and then applied onto pretreated and washed Caco2 cells in 12-well plates. Two hours later, cells were washed 2 times with PBS. Cells were lysed with 0.5 ml 0.5 N NaOH. Thereafter, scintillation cocktail was added and radioactivity counted in a scintillation counter. An aliquot of labeled bacteria was kept to determine total counts added to the cells in order to calculate the % of adherent bacteria. Mean bacterial attachment (N=6) and SEM are presented.

4.7. Acknowledgements

The authors are grateful to Peter Duncan for fruitful discussions and critical reading of the manuscript, to John Newell and Ingrid Klenner for excellent technical help, to Luisa Lopes for help with statistical analysis and to Laure Jolly for help with the bacterial EPS. This work was in part supported by the Swiss Commission for Technology and Innovation (CTI).

4.8. References

1. Angeloni, S.; Ridet, J. L.; Kusy, N.; Gao, H.; Crevoisier, F.; Guinchard, S.; Kochhar, S.; Sigrist, H.; Sprenger, N., Glycoprofiling with Micro-Arrays of Glycoconjugates and Lectins. *Glycobiology* **2005,** 15, (1), 31-41.

2. Varki, A., Biological roles of oligosaccharides: all of the theories are correct. *Glycobiology* **1993,** 3, (2), 97-130.

3. Karlsson, K. A., Microbial recognition of target-cell glycoconjugates. *Curr. Opin. Struct.Biol.* **1995,** 5, (5), 622-635.

4. Bertozzi, C. R.; Kiessling, L. L., Chemical Glycobiology. *Science* **2001,** 291, 2357-2364.

5. Fukui, S.; Feizi, T.; Galustian, C.; Lawson , A. M.; Chai, W., Oligosaccharide microarrays for high-throughput detection and specificity assignments of carbohydrate-protein interactions. *Nat. Biotechnol.* **2002,** 20, 1011-1017.

6. Gabius, H.; André, S.; Kaltner, H.; Siebert, H., The sugar code: functional lectinomics. *Biochim. Biophys. Acta* **2002,** 1572, 165-177.

7. Nam, M. J.; Madoz-Gurpide, J.; Wang, H.; Lescure, P.; Schmalbach, C. E.; Zhao, R.; Misek, D. E.; Kuick, R.; Brenner, D. E.; Hanash, S. M., Molecular profiling of the immune response in colon cancer using protein microarrays: occurrence of autoantibodies to ubiquitin C-terminal hydrolase L3. *Proteomics* **2003,** 3, 2108-2115.

8. Biol-N'garagba, M.; Louisot, P., Regulation of the intestinal glycoprotein glycosylation during postnatal development:role of hormonal and nutritional factors. *Biochimie* **2003,** 85, 331-352.

9. Drickamer, K.; Taylor, M. E., Glycan arrays for functional glycomics. *Genome Biology* **2002,** 3:, (12).

10. Wang, D., Carbohydrate microarrays. *Proteomics* **2003,** 3, 2167–2175.

11. Qian, X.; Metello, S. J.; Choi, I. S.; Wu, H.; Liang, M. N.; Whitesides, G. M., Arrays of self-assembled monolayers for studying inhibition of bacterial adhesion. *Anal.Chem.* **2002,** 74, 1805-1810.

12. Seong, S. Y.; Choi, C. Y., Current status of protein chip development in terms of fabrication and application. *Proteomics* **2003,** 3, 2176-2189.

13. Templin, M. F.; Stoll, D.; Schwenk, J. M.; Potz, O.; Kramer, S.; Joos, T. O., Protein microarrays: Promising tools for proteomic reasearch. *Proteomics* **2003,** 3, 2155-2166.

14. Espina, V.; Mehta, A. I.; Winters, M. E.; Calvert, V.; Wulfkuhle, J.; Petricoin III, E. F.; Lance, L. A., Protein microarrays: Molecular profiling technologies for clinical specimens. *PROTEOMICS* **2003,** 3, (11), 2091-2100.

15. Schwarz, M.; Spector, L.; Gargir, A.; Shtevi, A.; Gortler, M.; Altstock, R. T.; Dukler, A. A.; Dotan, N., A new kind of carbohydrate array, its use for profiling anti-glycan antibodies, and the discovery of a novel human cellulose-binding antibody. *Glycobiology* **2003,** 13, 749-754.

16. Feizi, T.; Fazio, F.; Chai, W.; Wong, C. H., Carbohydrate microarrays — a new set of technologies at the frontiers of glycomics. *Curr. Opin.in Struct. Biol.* **2003,** 13, (5), 637-645.

17. Barié, N.; Rapp, M.; Sigrist, H.; Ache, H. J., Covalent photolinker-mediated immbilization of an intermediate dextran layer to polymer-coated surfaces for biosensing applications. *Biosensors & Bioelectronics* **1998,** 13, 855-860.

18. Gao, H.; Kislig, E.; Oranth, N.; Sigrist, H., Photolinker-polymer-mediated immobilization of monoclonal antibodies, $F(ab')_2$ and F(ab') fragments. *Biotechnol. Applied. Biochem.* **1994,** 20, 251-263.

19. Caelen, I.; Gao, H.; Sigrist, H., Protein Density Gradients on Surface. *Langmuir* **2002,** 18, 2463-2467.

20. Liu, M. T. H., Chapter 7-9. In *Chemistry of Diazirines*, Liu, M. T. H. E., Ed. CRC Press, Boca Raton, FL.: 1987; p 160.

21. Sigrist, H.; Collioud, A.; Clémence, J. F.; Gao, H.; Luginbühl, R. R.; Sänger, M.; Sundarababu, G., Surface immobilization of biomolecules by light. *Optical Engineering* **1995,** 34, (8), 2339-2348.

22. Chevelot, Y.; Martins, J.; Milosevic, N.; Léonard, D.; Zeng, S.; Malissard, M.; Berger, E. G.; Maier, P.; Mathieu, J.; Crout, D. H. G.; Sigrist, H., Immobilization on Polystirene of Diazirine

Derivatives of Mono- and Disaccharides: Biological Activities of Modified Surfaces. *Bioorganic & Medicinal Chemistry* **2001,** 9, 2943-2953.

23. Gao, H.; Guinchard, S.; Crevoisier, F.; Angeloni, S.; Sigrist, H., Microarrays and Surface Engineering for Bioanalysis. *Chimia* **2003,** 57, 651-654.

24. Houseman, B. T.; Mrksich, M., Carbohydrate Arrays for the Evaluation of Protein Binding and Enzymatic Modification. *Chem.Biol.* **2002,** 9, (4), 443-454.

25. Park, S.; Shin, I., Fabrication of Carbohydrate Chips for Studying Protein-Carbohydrate Interactions. *Angew.Chem.Int.Ed.* **2002,** 41, 3180-3182.

26. Willats, W. G.; Rasmussen, S. E.; Kristensen, T.; Mikkelsen, J. D.; Knox, J. P., Sugar-coated microarrays: a novel slide surface for the high-throughput analysis of glycans. *Proteomics* **2002,** 2, 1666-1671.

27. Feizi, T.; Childs, R. A., Neoglycolipids:probes in structure/function assignments to oligoscchiarides. *Methods Enzymol.* **1994,** 242, 205-217.

28. Bovin, N., Neoglycoconjugates: trade and art. *Biochem.Soc.Symp.* **2002**, 143-160.

29. Leteux, C. M.; Stoll, M. S.; Childs, R. A.; Chai, W.; Vorozhaikina, M.; Feizi, T., Influence of oligosaccharide presentation on the interactions of carbohydrate sequence-specific antibodies and the selectins: Observations with biotinylated oligosaccharides. *J. Immunol. Methods* **1999,** 227, (1-2), 109-119.

30. Vanmaele, R. P.; Finlayson, M. C.; Armstrong, G. D., Effect of enteropathogenic Escherichia coli on adherent properties of Chinese hamster ovary cells. *Infect. Immun.* **1995,** 63, 191-198.

31. Cravioto, A.; Tello, A.; Villafan, H.; Ruiz, J.; del Vedovo, S.; Neeser, J., Inhibition of localized adhesion of enteropathogenic Escherichia coli to HEp-2 cells by immunoglobulin and oligosaccharide fractions of human colostrum and breast milk. *J.Infect.Dis.* **1991,** 163, 1247-1255.

32. Vanmaele, R. P.; Heerze, L.; Armstrong, G. D., Role of lactosyl glycan sequences in inhibiting enteropathogenic Escherichia coli attachment. *Infect. Immun.* **1999,** 67, 3302-3307.

33. Nimrichter, L.; Gargir, A.; Gortler, M.; Altstock, R. T.; Shtevi, A.; Weisshaus, O.; Fire, E.; Dotan, N.; Schnaar, R. L., Intact cell adhesion to glycan microarrays. *Glycobiology* **2004,** 14, (2), 197-203.

Chapter 5

Conclusions and Outlook

The straight, non-invasive, bio-compatible and bio-active light driven immobilization of a portfolio of sugar tethered composites in microarray format led to the acknowledgment of the photobonding technology as suitable tool to harvest information in the wide domain of carbohydrates-proteins classification and function deciphering[1-5]. The results described in chapter 4 convincingly show the efficacy and versatility of the light induced surface anchoring by carbene insertion of glycans. But besides experimentally recognizing the positive effect, the mechanism behind it was not completely elucidated. Questions remained concerning the reasons sustaining OptoDex® A as the best photolinker to fit the task as a surface soft glue. The acquired know-how gave evidence that OptoDex® A revealed in most cases the desirable photolabile fixing agent for the explored glycans, except for the immobilization of lectins for which the best way was found in the mediation of OptoDex® Biotin. Recall that OptoDex® A is a dually derived dextran based polymer: it displays actinic aryldiazine as primary function and amines as second derivatization. The latter remain available onto the surface to eventually encourage a classical chemical coupling or a pre-photoexposure interaction. The tendency, before this study, was to attribute the efficacy of OptoDex®A to its friendly behavior towards the bio-probe. The work done during this thesis highly evidenced the role of amines in regulating the dextran – surface interaction. The charge driven physisorption, also in presence of such a small charge density, sounds as a novel perspective to look at the dextran surface

modification. The almost hundred per cent effectiveness of the photobonding mechanism when mediated by a thin physisorbed layer of OptoDex® A, is outstanding. Moreover amines were demonstrated to play a crucial role in the interaction with the oxydril groups of the plasma pre-treated surface, definitely stressing the importance of such treatment as cleanliness provider and oxydril generator (under the investigated conditions). The ionic strength can be used to tune the film thickness. Immobilization on the surface of monolayer protected gold nanoparticles could contribute to the engineering of gold nanostructures that shorten the distance between plasmonic devices and bio applications[6], eventually taking advantage of carbohydrates micro-patterning[7, 8] and the passivating properties of dextran[9]. Topical surface dispensing, structured surfaces and engineered nano-objects as well as bio-hybrids, fabricated through bottom-up designed metal or semiconductor core structures, together with the state-of-the art of nanolithography, represent some outlooks, which give best significance to the presented thesis work[10].

5.1. References

1. Pilobello, K.; Krishnamoorthy, L.; Slawek, D.; Mahal, L., Development of a Lectin Microarray for the Rapid Analysis of Protein Glycopatterns. *ChemBioChem* **2005,** 6, (6), 985-989.

2. Manimala, J. C.; Roach, T. A.; Li, Z.; Gildersleeve, J. C., High-Throughput Carbohydrate Microarray Analysis of 24 Lectins. *Angew. Chem. Int. Ed.* **2006,** 45, 3607 –3610.

3. Culf, A. S.; Cuperlovic-Culf, M.; Ouellette, R. J., Carbohydrate Microarrays: Survey of Fabrication Techniques. *OMICS: A Journal of Integrative Biology* **2006,** 10, (3), 289-310.

4. Ito, Y.; Yamauchi, T.; Uchikawa, M.; Ishikawa, Y., Photoimmobilized array of panel cells for assay of antibodies. *Biomaterials* **2006,** 27, 2502-2506.

5. Pohl, N. L., Array methodology singles out pathogenic bacteria. *Nat Chem Biol* **2006,** 2, (3), 125-126.

6. Xu, F.; Persson, B.; Lofas, S.; Knoll, W., Surface plasmon optical studies of carboxymethyl dextran brushes versus networks. *Langmuir* **2006,** 22, (7), 3352-3357.

7. Carroll, G. T.; Wang, D.; Turro, N. J.; Koberstein, J. T., Photochemical Micropatterning of Carbohydrates on a Surface. *Langmuir* **2006,** 22, 2899-2905.

8. Hu, M.; Chen, J.; Li, Z.-Y.; Au, L.; Hartland, G. V.; Li, X.; Marquez, M.; Xia, Y., Gold nanostructures: engineering their plasmonic properties for biomedical applications. *Chem. Soc. Rev.* **2006,** 35, (11), 1084-1094.

9. Martwiset, S.; Koh, A. E.; Chen, W., Nonfouling characteristics of dextran-containing surfaces. *Langmuir* **2006,** 22, (19), 8192-8196.

10. Mark, S. S.; Bergkvist, M.; Yang, X.; Teixeira, L. M.; Bhatnagar, P.; Angert, E. R.; Batt, C. A., Bionanofabrication of metallic and semiconductor nanoparticle arrays using S-layer protein lattices with different lateral spacings and geometries. *Langmuir* **2006,** 22, (8), 3763-3774.

Aknowledgemets

La toile de cette thèse est tissée par les fils des actions inspirées et des idées élégantes, ainsi que du soutien des nombreuses personnes qui, au bon moments et aux bons endroits, ont fait la différence.

"I can't go on, I'll go on". (Samuel Barclay Beckett, in Three Novels, The Unnamable, 1954)

My deepest feeling of gratitude goes to Thomas Bürgi. Under his guidance and supervision I could accomplish my thesis's work, and this represented a "second chance" and probably last chance to conclude my work. I was not a young student anymore when we met, and I had the beautiful chance to feel I was learning something far away from my previously acquired competences. He was able, in his special silent and effective way, to first blaze the trail and then to follow me. He provided scientific and human support, and instilled enthusiasm.

My appreciation goes to Thomas Ward, my mentor. He never gave up in encouraging me to resume my thesis and has finally become the internal voice I could not ignore any more. With his straight attitude he always reminded me that the results I was looking for could be obtained only by putting myself out of my comfort zone.

I thank the CSEM, who decided to fund this work and to support me and this fruitful collaboration during crucial years of my life.

I thank Hans Sigrist who accepted to review my thesis as an external expert on the committee, as a last step of a long scientific collaboration which was the hidden start of this thesis work, as well as the team of *arrayon* biotechnology.

I thank Guy Voirin, for reviewing my thesis as an external expert on the committee; he showed generous personal investment in a task that he inherited from Rino Kunz
I thank my colleagues from the office at University: Marco Bieri, Cyrille Gautier, Igor Dolamic, Julien Boudon, Natallia Stalkovick, Ranja Afshar., Joel Mannin, Marie Jo Breguet. I could not imagine more precious mates to share this part of my life together.
Je remercie le service de chimie et le service de conciergerie de l'institut de Chimie pour leurs présences précieuses, ils mettent à disposition une infrastructure solide sur laquelle on peut compter.
I thank my colleagues from CSEM. With some among them I prepared the "mental platform" for this thesis work and with all of them today I deeply share the pleasure of new competences and new life's opportunities. Thanks to Martha Liley for always being attentive in recognizing competencies and valorizing them.
Thanks to Norbert Sprenger and Nestlé Research Center in Lausanne, Switzerland for inspiring and granting part of this work.
Thanks to my friends who shared my enthusiasm, supported me, also when they do not fully understand what it was all about.
I thank Anouck, who supported and understood.
Thanks to my parents and my sister, for giving me among many things also the logistic support necessary to work on my thesis and to simultaneously and audaciously nurture growing up of my son.
Thanks my husband, for his love and his indestructible confidence in me and estimation of my capacities.
Thanks to my son, who was able to render me his mother, while I struggled with the existential questions that arise during a thesis work.

Curriculum Vitae

SILVIA ANGELONI SUTER, SILVIA.ANGELONI@CSEM.CH

RUE DE LA PERRIERE 2, 2000 NEUCHATEL, SWITZERLAND - TEL. +41 78 682 32 34

Present occupation

From 2007/01 **R&D Engineer** in the BioMEMS sector, Division of Nanotechnology and Life Science of CSEM SA, Centre Suisse d'Electronique et de Microtechnique (non-profit, private company, 350 employees), Neuchâtel, Switzerland. Major R&D field of interaction: in vitro barrier biological models, nanoparticles screening, surface chemistry design for biosensing.

2001-2004 **R&D Engineer** in the Surface Bioengineering team, Division of Nanotechnology and Life Science of CSEM SA. Major R&D field of interaction: biotechnology industry. Extension of a novel surface functionalization technology in the domain of glycomics. Investigate new possible applications, and new surface biochemical models.

From 2004 -2006 In parallel, according to the academic acknowledgement of the specific research line developed in the past years, CSEM currently funded an *ex novo* project in collaboration with the University of Neuchâtel (Surface Spectroscopy and NanoSciences group lead by Professor Thomas Bürgi) based on ATR (Attenuated Total Reflection) Spectroscopy for polymer surface interaction investigation at molecular level. The project lead to the redaction of this manuscript for the application to the PhD degree.

Professional experience

1999-2001 Scientific collaborator and PhD candidate, group of Professor Carlo Floriani, Institute of Analytical and Mineral Chemistry, University of Lausanne, Switzerland. Worked in the field of coordination chemistry, synthesis of macrocycle complexes and their metalloderivaties, halted because of "force majeure", details available upon request.

Assistant with teaching responsibilities for weekly chemistry laboratory sessions, supervising Geology, Biological Sciences and Medicine undergraduate students. Supervisor Prof. C. Buenzli, Institute of Analytical and Mineral Chemistry, University of Lausanne, Switzerland.

1997-1998 **Researcher** in the laboratories of department of Chemistry of the University “La Sapienza”, Rome, Italy, in the domain of metallorganic chemistry. Supervisor Prof. Claudio Ercolani, research topic:”Synthesis, structure and properties of tetrakis(selenodiazole)porphyrazine metallocomplexes”.

1998 September Collaboration for data processing of magnetic susceptivity measures at CNR (National research Center), Montelibretti, Rome, Italy. Supervisor Dr. G. Rossi.

1994-1997 Production manager in the Azienda Agricola Areddia s.r.l., Campoverde, Latina, Italy, a

farm of 45000 m^2 of greenhouses, with 30 permanent employees and an annual turnover of 2 million Euro. Role included the management of purchases, the planning of space and time allocation for growth and sale of plants, as well as the supervision of employees.

Education

2007 **PhD thesis finalization**, manuscript submitted

1999 Italian State Exam authorizing to exercise the free profession of Chemical Engineer / qualifying to work as a freelance Chemical Engineer, final mark 84/100 (Abilitazione all'esercizio della libera professione, **Esame di Stato**).

1998 **Master of Science in Chemistry**, organico-biological specialization, University "La Sapienza", Rome, Italy, final mark 108/110. (Laurea in Chimica, indirizzo organico-biologico).

1989 High school certificate, Istituto M.Massimo di Roma, Italy, final mark 60/60. (**Maturità Classica**, gives access to Italian universities).

Specialiation courses

2005 September **Introduction to Special techniques in FTIR ATR spectroscopy,** Prof. Urs Fringeli University of Vienna, Austria.

2000 September **Metal ions in biological systems**, summer workshop in inorganic chemistry, organized by the University of Berne, Switzerland.

2000 March-June **Industrial applications of coordination chemistry**, Prof. H. Mimoun, Firmenich, S.A., La Plaine, Geneva, Switzerland

1999 September **Advanced materials: crystal engineering and properties**, summer workshop in inorganic chemistry, organized by the University of Geneva, Switzerland.

1999 March-June **Coordination chemistry in industrial oxidation processes**, Prof. H. Mimoun, Firmenich, S.A., La Plaine, Geneva, Switzerland.

Technical and scientific knowledge

In the last years, focus on photolinker mediated surface immobilization of glycans and establishment of handling protocols and manufacture procedures of such bio-molecule microarrays. From previous experience, basic practice of NMR, FT-IR, UV-VIS, measure of magnetic susceptivity, practice in the dry box use and synthesis procedure under nitrogen and argon atmosphere for oxygen and humidity sensitive products. Recently acquired high experience in molecular *at* or *near interface* investigation using FTIR-IR spectroscopy (ATR, Attenuated Total Reflection Infrared spectroscopy).

Other information

Languages English and French fluent, Italian mother tongue.

Computer literacy Proficient in use of office applications, to present and communicate results (technical and scientific reports)

Administrative details Italian citizen, 38 years old, married to a Swiss citizen, permit C. One child, 30 months old.

List of Publications

Gautier, C., Bieri, M., Dolamic, I., Angeloni, S., Boudon, J. and Bürgi, T., Probing Chiral Nanoparticles and Surface by Infrared Spectroscopy. Chimia 2006, 60 (11), 777-782

Angeloni, S., Ridet, J.L., Kusy, N., Gao, H., Crevoisier, F., Guinchard, S., Kochhar, S., Sigrist, H. and Sprenger, N., Glycoprofiling with Micro-Arrays of Glycoconjugates and Lectins. Glycobiology 2005, Vol 15(1), 31-41.

Gao, H., Guinchard, S. Crevoisier, F., Angeloni, S. and Sigrist, H., Microarray and surface engineering for bio-analysis. Chimia 2003, Vol 57, 651-654.

Angeloni, S., Bauer, E., Ercolani, C., Popkova, I., Stuzhin, P., Tera(selenodiazole)porphyrazines. 2: Metal complexes with Mn(II), Co(II), Ni(II) and Zn(II). J. of Porphyrins and Phtalocyanines 2001, Vol 5 (12), 881-888.

Angeloni, S. and Ercolani, C., New classes or porphyrazine macrocycles with annulated heterocyclic rings. J. of Porphyrins and Phtalocyanines 2000, Vol 4 (5), 474-483.

Gao, H., Crevoisier, F., Caelen, I., Angeloni, S , Guinchard, S. Sigrist, H., Sprenger, N., Jolly, L., Kusy, N., Kochhar, S., Protein-Arrays and Glyco-Array. In Biosurf IV, Spatial Organization and Dynamics of Biomolecules and Cells at Surfaces, Swiss Federal Institute of Technology 2001, Lausanne, Switzerland 20-21 September (poster).

Gao, H., Guinchard, S, Crevoisier, F., Angeloni, S., Sigrist, H., Functional PhotoChip Platforms: In Chips to Hits Conference 2002, Philadelphia, USA October 27-31 (poster).

Angeloni, S, Gao, H., Crevoisier, F., Sigrist, H., Sprenger, N., Ridet, J.L., Jolly, Kochhar, S. Covalent-bonded Carbohydrate Microarrays for Recognition and Profiling. In Annual Conference of the American Society for Glycobiology 2002, Boston MH, USA 9-12 November (poster)

Angeloni, S, Chai-Gao, H., Crevoisier,F., Guinchard, S., Neumayer, J., Sigrist, H., Ridet, J.L., Kochhar, S., Sprenger, N., arrayon® PhotoChips – A novel approach for Glycoconjugate and Cell Extract Profiling. In MipTec International Conference and Exhibition on Drug Discover 2003, Basel, Switzerland 12–15 May(poster).

Gao, H., Angeloni, S , Crevoisier, F., Caelen, I., , Guinchard, S. Sigrist, Surface Bioengineering for Microanalytics and Biomaterials. In Biosurf V - Functional Polymeric Surfaces in Biotechnology 2003, ETH Zürich, Switzerland 25-26 September (poster).

Gao, H., Angeloni,S., Crevoisier, F., Guinchard, S, Sigrist, H.;Surface Bioengineering for Microanalytics and Biomaterials. In MipTec European Conference and Exhibition on enabling technologies for Drug Discovery 2004, Basel 3–6 May (poster).

« .....Et la conscience du déschirement porte en elle le désir d'harmonie.……donner à nos gestes, à nos pensées, la continuité de l'avant-nous et de l'après-nous est une chose en la quelle je crois. »

I. CALVINO*, Un heremite à Paris*